

©2009

Kaya Ghosh

ALL RIGHTS RESERVED

Identification of Proteins of the Infectious Apparatus of *Encephalitozoon cuniculi*

By

KAYA GHOSH

A Dissertation submitted to the

Graduate School-Newark

Rutgers, The State University of New Jersey

in partial fulfillment of the requirements for the degree of

Doctor of Philosophy

Graduate Program in Biological Sciences

written under the direction of

Professor Ann Cali

and approved by

Newark, New Jersey

October 2009

ABSTRACT OF THE DISSERTATION

Identification of Proteins of the Infectious Apparatus of *Encephalitozoon cuniculi*

By KAYA GHOSH

Dissertation Director:
Professor Ann Cali

The microsporidia are a diverse phylum of obligate intracellular parasitic protists that infect all major animal groups and have been recognized as emerging human pathogens for which few chemotherapeutic options currently exist. These organisms infect every tissue and organ system, causing significant pathology especially in immune-compromised populations. The microsporidian spore employs a unique infection strategy in which its contents are virtually injected into a host cell via the polar tube, an organelle that lies coiled within the resting spore but erupts with a force sufficient to pierce the plasma membrane of its host cell. It appears that this process is driven by a dramatic osmotic swelling within the spore just prior to germination, which is resisted by the spore wall until the moment of polar filament eruption. Neither the means by which this rapid influx of water across the hydrophobic cell membrane might be supported, nor the molecular structural basis for the elasticity of the polar tube or the tensile strength of the spore wall is well understood. However, the recent sequencing of the genome of human-pathogenic species *Encephalitozoon cuniculi* has enabled the adoption of genomic and proteomic approaches to address these problems. In the first part of this project, an aquaporin-like gene from this organism (*EcAQP*)

was cloned and the protein subjected to standard functional tests in a heterologous *Xenopus* oocyte swelling assay. Increased water-permeability and localization of *EcAQP* to the plasma membrane of transfected oocytes demonstrated the functionality of this gene, suggesting a mechanism for water flux in germinating spores. The second part of this project employed a shotgun-proteomic strategy to identify novel structural components of the microsporidian infectious apparatus. Mass spectrometry of insoluble fractions of spore lysate identified over fifty candidate proteins, many of which were immunolocalized *in situ*. As a result, novel components of the mitosome, the developing spore wall, and a heretofore unrecognized filamentous network within the lumen of the parasitophorous vacuole were putatively identified. Thus the work described herein generates insights regarding the biochemical events and molecular structural components involved in the infectious process of these unique intracellular pathogens.

Preface

I would like to extend heartfelt thanks to my mentor, Dr. Ann Cali. Were it not for her unwavering support and belief in me, this work would not have been possible. I have learned so much about the microsporidia and parasitology in general from her, as she is a natural born teacher whose enthusiasm for the subject is easily communicable. In addition, I have enjoyed being her teaching assistant for several years, especially during the Fall semester when she teaches her parasitology course. I look forward to our keeping in touch and my gaining her unique perspective on future research endeavors.

I am extremely grateful to Dr. Louis Weiss of Albert Einstein College of Medicine, who welcomed me as a volunteer in his laboratory almost five years ago and has been the best, most supportive co-mentor anyone could ever ask for since. In his research laboratory where multiple kinds of parasite abound, I have learned more science than I thought possible in a few years' time and have been inspired by his breadth of knowledge on both parasitology and molecular biology. I would also like to thank him for his generosity in enabling me to attend scientific conferences and especially a summer parasitology course, which was utterly life-changing (in a good way). The years I have spent in his lab have truly been a pleasure and a privilege, and I look forward to upcoming collaborations.

A big thank you to my in-lab colleagues, both at Rutgers and Einstein, whose help and advice on my project have been invaluable. At Rutgers, Cyrilla Pau's

kind technical assistance enabled me to finally obtain the EM data I was after for two years. Dr. Peter Takvorian's sharing of his experiences regarding immunoEM have also been very useful. I would also like to thank all the members of the molecular parasitology group at Einstein, especially Drs. Boume Bouzahzah, FNU Nagajyothi, Yanfen Ma, and Huan Huang, whose proximity to my lab bench exposed them to my frequent appeals for advice, especially at the beginning when I was just learning molecular biology techniques. Their patience and generosity in sharing their know-how means a lot to me. I am also grateful to Dr. Mahalia Desruisseaux for Western Blotting advice and general nutritional support, Dazhi Zhao for helping me with retroorbital mouse bleeds, and to Vicki Braunstein for advice regarding cell culture issues. In addition, I am very glad to have the friendship and support of all the people in the lab.

Collaborations with several other scientists and colleagues have been instrumental in accomplishing this work as well. I would like to thank Dr. Thomas MacDonald and Sean McBride for their collaboration during the first phase of this work which required use of the *Xenopus* oocyte system; Dr. Ruth Angeletti and Eddie Nieves of the Laboratory for Macromolecular Analysis and Proteomics, whose excellent advice regarding sample fractionation and expertise in mass spectrometry made the second, proteomic phase of this work possible; and Frank Macaluso, Leslie Gunther-Cummins, Juan Jimenez, and Geoff Perumal of the Analytical Imaging Facility for microscopy-related advice and assistance, which was key in obtaining difficult EM data.

I am also very fortunate to have such a helpful and supportive Dissertation Committee. From Rutgers, I would like to thank Dr. David Kafkewitz, who is doubly generous to have also served on my qualifying committee, and Dr. Nihal Altan-Bonnet, who I have had the pleasure of getting to know over the past year, for serving on my Committee. I am also grateful to Dr. John Chan of Einstein for taking the time and effort to serve on my committee. I have benefited from having their suggestions and perspective regarding my project.

Last but not least, I want to thank my family and friends for sharing my happiness when things have gone well and being a source of comfort and encouragement during more difficult patches. Without the lifelong love, support, and guidance of my mother and father, Urmil and Syamal Ghosh, I would have had no foundation to undertake a project of this magnitude. The love and camaraderie of my brother, Andrew Ghosh, have also been a wellspring of joy and good humor. In addition, I am lucky to have friends like Gail Bayarin and Millie Mejia, who have encouraged me throughout and just been a lot of fun when necessary. Finally, I want to thank Philipp Henrich for his love, patience, encouragement, acceptance of my flaws, and critical reading of the manuscript.

In memory of my grandfather

Dr. Basudeb DasSarma

Chemist

January 1, 1923 – November 16, 2007

Table of Contents

Title Page	i
Abstract of the Dissertation	ii
Preface	iv
Table of Contents	viii
List of Tables	xiii
List of Illustrations	xiv
1 INTRODUCTION	1
1.1 The Microsporidia	2
1.2 Modern approaches to understanding the microsporidian spore	8
2 FUNCTIONAL CHARACTERIZATION OF THE PUTATIVE AQUAPORIN FROM <i>ENCEPHALITOZOON CUNICULI</i>	16
2.1 INTRODUCTION	17
2.2 MATERIALS AND METHODS	20
2.2.1 Parasites	21
2.2.2 Cloning and expression of EcAQP in <i>Xenopus</i> oocytes	21
2.2.3 Oocyte swelling assays	22
2.2.4 Expression of EcAQP in <i>Escherichia coli</i>	23
2.2.5 Purification of fusion protein, immunization of mice, and evaluation of serum by immunoblot	24
2.2.6 Immunolocalization of EcAQP in <i>Xenopus</i> oocytes	25
2.2.7 Sequence analysis	26
2.3 RESULTS	27

2.3.1 Functional characterization of <i>EcAQP</i>	28
2.3.2 Sequence analysis and phylogenetic construction	30
2.3.4 Production of antiserum to <i>EcAQP</i>	32
2.3.5 Immunolocalization of <i>EcAQP</i> in <i>Xenopus</i> oocytes	33
2.4 DISCUSSION	34
3 PROTEOMICS-BASED IDENTIFICATION AND CHARACTERIZATION OF NOVEL PROTEINS OF THE INFECTIOUS APPARATUS OF <i>ENCEPHALITOOZON CUNICULI</i>	39
3.1 INTRODUCTION	40
3.2 MATERIALS AND METHODS	45
3.2.1 Culturing of microsporidia to maximize spore yield and ensure purity	46
3.2.2 Fractionation of spores	
3.2.3 Digestion and Proteomic tandem mass spectrometry (MS/MS) analysis of spore lysate fractions	48
3.2.3.1 DTT-solubilized material	48
3.2.3.2 DTT-insoluble material	50
3.2.4 Bioinformatic analysis of selected proteins	53
3.2.4.1 BLAST similarity search	53
3.2.4.2 <i>in silico</i> predictions of biochemical attributes	53
3.2.5 Amplification of genes from microsporidian genomic DNA and gel-purification of PCR products	54
3.2.6 Cloning genes into bacterial expression vector and transformation and screening of cloning host strain	60
3.2.7 Expression, detection, and purification of microsporidian proteins	60

3.2.7.1 Evaluation of expression by SDS-PAGE and Immunoblot	61
3.2.7.2 Confirmation of identity of recombinant ECU10_1500 by MALDI-TOF mass spectrometry	62
3.2.7.2.1 In-gel digestion	62
3.2.7.2.2 MALDI-TOF mass spectrometry	63
3.2.7.2.3 Peptide mass fingerprinting	64
3.2.8 Immunization of mice	64
3.2.9 Evaluation of sera by immunoblot	65
3.2.10 Immunolocalization of hypothetical protein “hits” <i>in situ</i>	66
3.2.10.1 Immunofluorescence microscopy	66
3.2.10.2 Correlative light–immunolectron microscopy	67
3.3 RESULTS	69
3.3.1 Purity of parasites harvested from culture	70
3.3.2 Results of LC-MS/MS experiments	70
3.3.3 Amplification of microsporidian genes	81
3.3.4 PCR-screening and sequencing of recombinant pET-41 Ek/LIC vector colonies	81
3.3.5 Evaluation of heterologous expression of proteins	82
3.3.5.1 SDS-PAGE and immunoblots	82
3.3.5.2 MALDI-TOF mass spectrometry/peptide mass fingerprinting of recombinant ECU10_1500	86
3.3.6 <i>In silico</i> predictions of biochemical attributes	88
3.3.7 Evaluation of mouse antisera by immunoblot	89

3.3.8 <i>In situ</i> immunolocalization of hypothetical proteins	92
3.3.8.1 Immunofluorescence microscopy	92
3.3.8.1.1 Nuclear/perinuclear hypothetical proteins	93
3.3.8.1.2 Cytoplasmic proteins	93
3.3.8.1.3 Other intracellular proteins	94
3.3.8.1.4 Peripheral proteins	95
3.3.8.1.5 Vacuolar	95
3.3.8.1.6 Non-specific and non-reactive antisera	96
3.3.8.2 Correlative light/immunoelectron microscopy	109
3.4 DISCUSSION	113
3.4.1 Efficacy and efficiency of methods	114
3.4.1.1 PCR amplification of hypothetical genes of <i>Enc. cuniculi</i>	114
3.4.1.2 Cloning into prokaryotic vector	115
3.4.1.3 Protein expression and purification	116
3.4.1.4 Antisera production	124
3.4.2 <i>In situ</i> immunolocalization of hypothetical proteins	128
3.4.2.1 Nuclear/perinuclear hypothetical proteins	130
3.4.2.2 Cytoplasmic proteins	131
3.4.2.3 Other intracellular proteins	133
3.4.2.4 Peripheral proteins	134
3.4.2.5 Cytoplasmic proteins	135
3.4.3 Conclusion	138
4 FINAL CONCLUSIONS AND FUTURE STUDIES	143

BIBLIOGRAPHY	150
APPENDICES	165
Appendix 1: Figure 1.1	166
Appendix 2: Figure 1.2	167
Appendix 3: Figure 1.3	168
CURRICULUM VITA	169

List of Tables

Table 3.1 Primers and PCR conditions for amplification of hypothetical <i>Enc. cuniculi</i> genes	55-59
Table 3.2. Proteins identified by LC-MS/MS of fractionated <i>Enc. cuniculi</i> spore lysate	71-72
Table 3.3. Detection of peptides for selected hypothetical genes and polar tube and spore wall proteins identified by LC-MS/MS	73-80
Table 3.4. Observed peptide mass fingerprint of expressed recombinant ECU10_1500 protein.	88
Table 3.5 Summary of results for hypothetical <i>Enc. cuniculi</i> genes.	140-142

List of Illustrations

Figure 1.1. Generalized life cycle of the microsporidia.	3
Figure 1.2. The microsporidian spore.	9
Fig 1.3. Germination process of the microsporidia.	11
Figure 2.1. <i>EcAQP</i> -injected <i>Xenopus laevis</i> oocyte swelling assay.	29
Figure 2.2. Swelling of <i>EcAQP</i> oocytes is not inhibited by HgCl ₂ .	29
Figure 2.3. An unrooted phylogenetic tree of aquaporins (AQP) including <i>EcAQP</i> .	31
Figure 2.4. Alignment of <i>EcAQP</i> , human AQPs 1 (accession no. NP_932766), 2 (NP_000477), and AQP A of <i>Dictyostelium discoideum</i> (BAA85158).	32
Figure 2.5. Expression of recombinant <i>EcAQP1</i> -GST and <i>EcAQP2</i> -GST.	33
Figure 2.6. Heterologous expression of <i>EcAQP</i> in <i>Xenopus laevis</i> oocytes.	34
Fig. 3.1. Workflow for treatment of <i>Enc. cuniculi</i> lysate.	52
Figure 3.2. Verification of purity of microsporidia cultured <i>in vitro</i> .	70
Figure 3.3. PCR-amplified hypothetical <i>Enc. cuniculi</i> genes.	81
Figure 3.4. Screening of transformed <i>E. coli</i> colonies for <i>Enc. cuniculi</i> inserts.	82
Figure 3.5. Representative results of expression of <i>Enc. cuniculi</i> genes evaluated by SDS-PAGE.	83-84
Figure 3.6. Representative results of expression of <i>Enc. cuniculi</i> genes evaluated by immunoblot.	85
Figure 3.7. MALDI-TOF mass spectrum for ECU10_1500-GST fusion protein.	87

Figure 3.8. Biochemical attributes of expressed vs. non-expressed proteins.	89
Fig. 3.9. Immunoblots of mouse antisera to hypothetical <i>Enc. cuniculi</i> proteins.	91
Fig. 3.10. Immunofluorescence localization of ECU07_0400	97
Fig. 3.11. Immunofluorescence localization of ECU03_1010	97
Fig. 3.12. Immunofluorescence localization of ECU05_0140	98
Fig. 3.13. Immunofluorescence localization of ECU08_0420	98
Fig. 3.14. Immunofluorescence localization of ECU02_0150	99
Fig. 3.15. Immunofluorescence localization of ECU03_0430	99
Fig. 3.16. Immunofluorescence localization of ECU09_1080	100
Fig. 3.17. Immunofluorescence localization of ECU04_1480	100
Fig. 3.18. Immunofluorescence localization of ECU07_0640	101
Fig. 3.19. Immunofluorescence localization of ECU09_0270	101
Fig. 3.20. Immunofluorescence localization of ECU09_1010	102
Fig. 3.21. Immunofluorescence localization of ECU09_0280	102
Fig. 3.22. Immunofluorescence localization of ECU10_1070 and comparison to SWP1	103
Fig. 3.23. Immunofluorescence localization of ECU10_1500 in <i>Enc. cuniculi</i>	104
Fig. 3.24. Immunofluorescence localization of ECU10_1500 in <i>Enc. cuniculi</i> : three focal planes of the same parasitophorous vacuole.	104
Fig. 3.25 Immunofluorescence localization of ECU10_1500 in <i>Enc. hellem</i> : deconvolved Z-stack	105
Fig. 3.26. Immunofluorescence localization of ECU10_1500 in <i>Enc. hellem</i> : Rotated montage of a 3D-reconstruction of a deconvolved Z-stack	106

Fig. 3.27. Immunofluorescence localization of ECU06_1560	107
Fig. 3.28. Immunofluorescence localization of ECU09_0500	107
Fig. 3.29. Representative nonspecific immunofluorescence staining patterns of antisera to recombinant hypothetical <i>Enc. cuniculi</i> proteins	108
Fig. 3.30. Representative non-reactive antiserum.	108
Fig. 3.31. Immunolocalization of ECU10_1500 in <i>Enc. hellem</i> -infected host culture by silver-enhanced correlative light/immunoEM microscopy, plate 1.	110
Fig. 3.32. Immunolocalization of ECU10_1500 in <i>Enc. hellem</i> -infected host culture by silver-enhanced correlative light/immunoEM microscopy, plate 2.	111

CHAPTER 1

Introduction

1.1 The Microsporidia

The phylum Microsporidia, a group of obligate intracellular parasitic protists, contains over 1200 species representing nearly 150 genera (Garcia, 2002; Weiss, 2001). Infections have been reported in every major animal group, from other protists to vertebrates (including humans), and in every tissue type and most organ systems (Franzen and Muller, 2001). While there is much diversity among their life cycles, morphology, and physiology, all microsporidia produce a resistant spore which is capable of extruding its internal polar filament and thereby inoculating its contents into a nearby host cell. Unique in structure and function, the spore with its polar filament and anterior attachment complex is the uniting feature of the phylum (Cali and Takvorian, 1999).

The life cycles of the microsporidia are variable and often complex, sometimes involving sexual reproduction, vertical and horizontal transmission, alternate hosts, or more than one type of life cycle and spore in a given host (Cali and Takvorian, 1999). Nonetheless, the microsporidian life cycle can be divided into three phases (Cali and Takvorian, 1999), depicted in Fig. 1.1. Phase I, the infective/environmental phase, begins with the spore, and is followed by its release from the host into the environment and its encounter with conditions suitable for polar filament eversion. Phase II, the proliferative phase, begins if and when the spore everts its polar filament in the vicinity of a suitable host cell, allowing the sporoplasm (the spore cytoplasm) to travel through the now hollow polar tubule into the host cell cytoplasm, or in some cases, the host cell nucleus. Growth, division, and development of the parasite eventually lead to its

commitment to spore formation, which marks the beginning of Phase III, the sporogonic phase. This stage contains sporonts, which divide at least once to form sporoblasts, the cells that undergo metamorphosis to form spores.

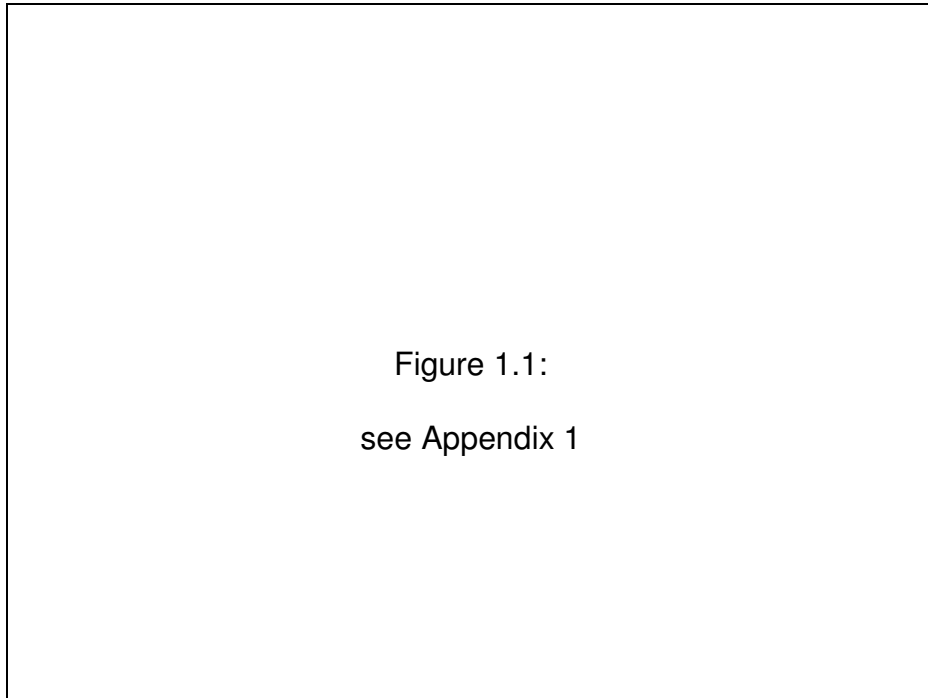


Figure 1.1. Generalized life cycle of the microsporidia. The microsporidian life cycle occurs in three phases (clockwise from top): the extracellular, infective spore; an intracellular proliferative phase; and another intracellular sporogonic phase in which the commitment to spore formation ensues (reprinted from Cali and Takvorian, 1999).

Prior to the pandemic of AIDS, microsporidia received most of their attention as parasites of a variety of animals of agricultural importance (e.g., beneficial and pestilent insects, fish, and fur-bearing animals) and animals used in laboratory research (e.g., rabbits, rodents, and primates) (Wittner and Weiss, 1999; Wasson and Peper, 2000). Microsporidia have also been employed as biological control agents of insect pests, the most notable example being

Nosema locustae, a commercially available microsporidian insecticide for use against grasshoppers on rangelands (Henry and Oma, 1981).

Since the mid-1980s, microsporidia have been increasingly implicated as agents of human disease, especially in their capacity as opportunistic parasites of AIDS patients (Cali, 1991; Weiss, 2001). Over 400 cases had been reported by 1994 (Weber et al., 1994), and recent diagnostic surveys have revealed infection rates between 2 and 70% in HIV-infected populations (Weber et al., 1994; Wittner and Weiss, 1999). They have also caused infections in other immunosuppressed individuals, such as organ transplant recipients and patients undergoing chemotherapy (e.g., Metge et al., 2000, Sax et al., 1995; reviewed in Franzen and Muller, 2001). To date, 14 identified and at least two indeterminate species of Microsporidia have been found to infect humans, representing eight genera including *Microsporidium*, a taxon reserved for species of indeterminate assignment (Didier and Weiss, 2006). In HIV-positive patients, the most common clinical manifestation is chronic diarrhea and wasting due to enteric infection, but the spectrum of disease due to these pathogens is broad and includes hepatitis, peritonitis, keratoconjunctivitis, sinusitis, bronchitis, pneumonia, cystitis, nephritis, myositis, encephalitis and other cerebral infections, and, rarely, urethritis, prostatic abscess, tongue ulcer, bone infection, and cutaneous infection (Franzen and Muller, 2001).

While microsporidia have been reported to cause pathology in immunocompromised individuals, gastrointestinal and ocular infection have also been reported in immunocompetent patients, especially in travelers to and

residents of underdeveloped countries, and contact lens wearers, respectively (Desportes-Livage and Bylen, 1998). Indeed, the high seroprevalence of anti-microsporidian antibodies revealed by surveys of immunocompetent individuals (Bergquist et al., 1984, van Gool et al., 1997) suggests that microsporidiosis in the general population may be common but self-limiting or asymptomatic (Weiss, 2001). While transmission of microsporidia to humans has not been specifically documented, there is evidence that infections can occur by multiple routes (enumerated in Weiss, 2001) including waterborne, respiratory, sexual, congenital, zoonotic transmission, and in ocular infection by traumatic inoculation into the cornea. Because of the probable risk of environmental transmission, the U.S. Environmental Protection Agency included these organisms on its two most recent Candidate Contaminant Lists CCL-1 and -2 in 1998 and 2005, respectively; these actions identify the microsporidia as pathogens that may require regulation under the Safe Drinking Water Act. They have also been named to the Category B list of biodefense pathogens by the National Institutes of Health (NIH).

The microsporidia have also attracted considerable attention due to their enigmatic status within Eukarya. Because they are eukaryotes but lack typical mitochondria and Golgi apparatus, the prevailing hypothesis at one time was that microsporidia along with diplomonads (e.g., the intestinal parasitic flagellate *Giardia*) represented primitive eukaryotes, similar to the type of cell that according to endosymbiotic theory might have accepted the first mitochondrial symbiont (Cavalier-Smith, 1991). The unusual ribosomes of microsporidia, which

are closer to those of prokaryotes in size and have 16S RNAs shorter than those of both eukaryotes and prokaryotes (Vossbrinck et al., 1987; Weiss et al., 1992), were interpreted as further evidence for this view. Early phylogenetic analysis of the rRNA of *Vairimorpha necatrix*, an entomopathogenic species, and of elongation factor 1-alpha and elongation factor 2 sequences (Kamaishi et al., 1996a,b) was also used to support the notion that microsporidia are “early” eukaryotes (Vossbrinck et al., 1987). In addition, some microsporidian genomes are exceedingly small (reviewed in Metenier and Vivares, 2001); that of *Enc. intestinalis* is 2.3 megabase pairs, the smallest of any eukaryotic organism and smaller than most bacteria. Despite the fact that genome size is not considered a good indicator of evolutionary relationships, as there is considerable overlap between and logarithmic variation within taxa, and correlation with and probable selection by cell size and rate of cell division (Cavalier-Smith, 2005), their especially diminutive genomes likely contributed to the perception of these organisms as “primitive”.

In the past decade or so, molecular and genetic evidence has converged to suggest a close relationship between Microsporidia and Fungi, effectively shelving the amitochondriate, “early eukaryote” theory (reviewed in Lee et al., 2008; Keeling and Fast, 2002). Early phylogenetic evidence linking these organisms to the so-called primitive eukaryotes now seems to be a methodological artifact of ‘long branch attraction’ of microsporidia to the base of the phylogeny (Keeling and Fast, 2005). The presence of Golgi- and ER-associated enzyme systems (Takvorian and Cali, 1994, 1996) and heat shock

proteins (Germot et al., 1997), which are typically mitochondrially associated, have been reported; this information suggests that microsporidia possess true Golgi and that they only secondarily lack mitochondria, respectively. In fact, the presence of a mitochondrial remnant, or “mitosome” (termed by Katinka et al., 2001), has now been demonstrated in several microsporidia (Williams et al., 2002; Burri et al., 2006). Multiple groups have conducted phylogenetic analyses of several genes including α - and β -tubulin (Edlind et al., 1994; Keeling, 2003; Keeling et al., 2000) and RNA polymerase II (Hirt et al., 1999), indicating that microsporidia are either derivatives or close relatives of the Fungi. While uncertainty about the nature of this relationship continued, genome-wide synteny in the *sex* and other loci with microsporidia and the basal zygomycete fungal lineage strongly supports an origin of the microsporidia from within the fungi (Lee et al., 2008). Long-observed morphological characters such as the absence of centrioles, retention of the nuclear membrane during karyokinesis, and chitinous spore wall (see Cali and Takvorian, 1999) perhaps reflect the fungal origin of these organisms as well. As a result of these observations, the microsporidia were accorded phylum status in a recently constructed phylogeny of the Fungi by a diverse assemblage of sixty-some fungal taxonomists (Hibbett et al., 2007), although general uncertainty regarding traditional basal fungal lineages such as the zygomycota precluded more specific placement. Considering that the first identified microsporidian was classified upon discovery within the fungi (Nageli, 1857), it is ironic that their affinity to this group is being reaffirmed only presently.

1.2 Modern approaches to understanding the microsporidian spore

Despite their increasing recognition as emerging human pathogens and the accompanying scholarly interest in their biology, highly effective and safe treatments do not yet exist for all of the microsporidia which infect humans (Costa and Weiss, 2000). Notably, the most prevalent microsporidian in AIDS patients (Bryan and Schwartz, 1999), the gastrointestinal parasite *Enterocytozoon bieneusi*, is relatively unsusceptible to albendazole, a commonly deployed therapeutic agent against other human-infecting microsporidia (Costa and Weiss, 2000). While other treatments such as fumagillin and polyamine analogs are being developed (reviewed in Costa and Weiss, 2000; Alvarado et al., 2009), the diversity of human-infecting species is an additional imperative for the investigation of novel drug targets in the microsporidia. These efforts have naturally focused on the spore, the infectious stage of these organisms.

The microsporidian spore is a curious cell that typically appears by light microscopy as an ovoid or pyriform body just a few micrometers long with a birefringent wall (Vavra and Larsson, 1999), depicted schematically in Fig 1.2. When activated, the slender polar tube, whose diameter in many species approaches the limit of resolution of the light microscope, extends from the apical end a distance tens of times the length of the spore. A posterior vacuolar inclusion can sometimes be seen in live preparations of resting spores, but this is difficult in human-pathogenic species which tend to be small, measuring between one and four micrometers in length (Franzen and Muller, 2001). While hints of additional cytological features may be revealed by Giemsa staining of fixed

specimens, the unique morphology of the spore was only fully appreciated in the latter half of the 20th century with the application of transmission electron microscopy (TEM). Several peculiar organelles were revealed, depicted schematically in Fig 1.2 below. The entire cell is encased in a thick wall comprised of an electron-dense exospore and an electron-lucent endospore, which lie just external to the plasma membrane. At the apical end of the spore is the anchoring disk, from which the polar filament appears to emanate before assuming the conformation of rows of coils within the cytoplasm. Abutting the anchoring disk is the polaroplast, a system of flattened and tubular sacs composed of vesicular material, and at the opposite end of the spore is the posterior vacuole. Both the polaroplast and posterior vacuole swell during spore activation, and were hypothesized as early as 1963 to play initiatory roles in extrusion of the polar tube (Lom and Vavra, 1963; Keohane and Weiss, 1999; Vavra and Larsson, 1999).

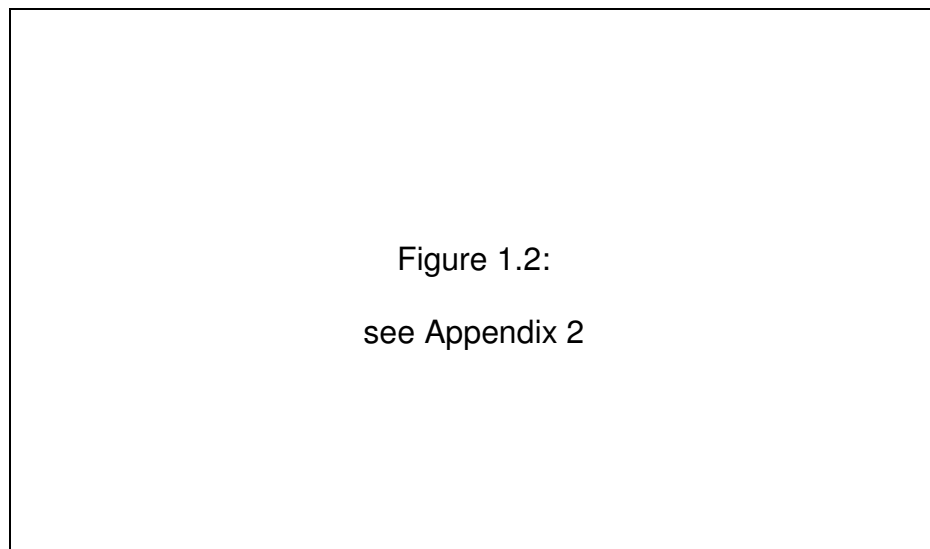


Figure 1.2. The microsporidian spore. Several unique organelles are contained within this diagnostic life cycle stage (reprinted from Keeling and Fast, 2002).

The simultaneous eversion of the polar filament and extrusion of the polar tube was metaphorically described by Ohshima in 1937 as “reversing a finger of a glove” (Ohshima, 1937). TEM and video microscopy studies have since revealed this to be a complicated process in which the polar tube erupts from the relatively thin-walled apical end of the spore, followed by passage of the sporoplasm through the tube and its appearance as a droplet at the distal end of the extruded polar tube (reviewed in Xu and Weiss, 2005). This process is schematically depicted in Fig. 1.3. During this process, the polar tube displays remarkable flexibility and dynamics: its diameter can increase two- to four-fold to accommodate sporoplasm passage, its length is increased two- to three-fold relative to the internal polar filament in the resting spore, and it even appears to change direction at its tip. If the sporoplasm is deposited in or near a suitable host cell, the host is effectively parasitized and the proliferative phase of the life cycle begins.

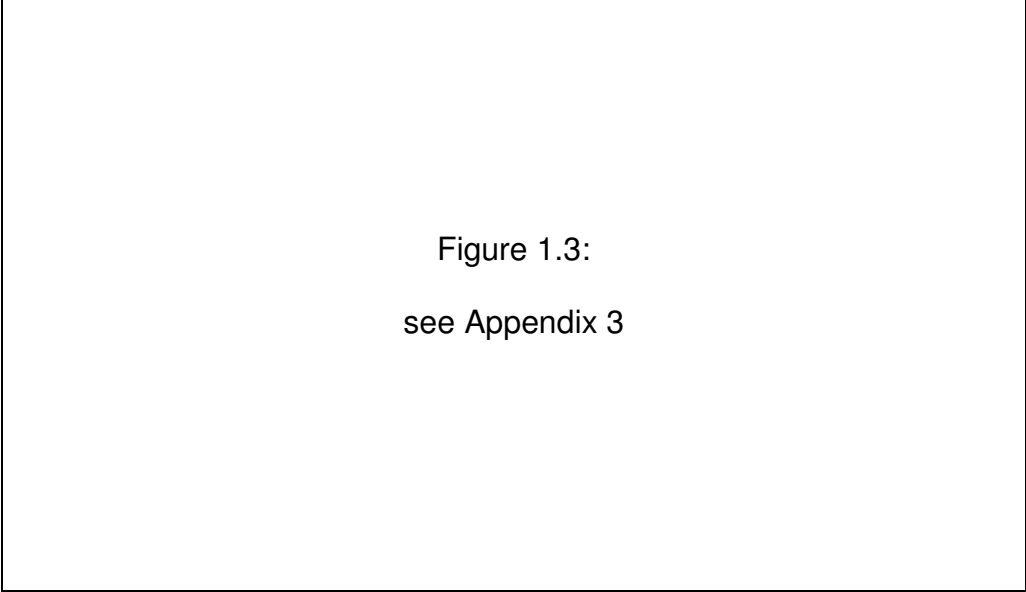


Figure 1.3:
see Appendix 3

Fig 1.3. Germination process of the microsporidia. The polar filament everts, or turns inside out as it is extruded, forming a hollow polar tube through which the sporoplasm travels, leaving behind an empty spore wall. (Figure modified from Keeling and Fast, 2002)

While extrusion of the polar tube is the most recognizable event in the infectious process of these organisms, the profound requisite reorganization of cellular structure implies that this dramatic process is the culmination of a cascade of intrasporal biochemical events. Moreover, the necessity of preventing unproductive extrusion virtually guarantees that these preceding steps are regulated by environmental signals. Indeed, spore germination is widely viewed to occur in four phases (discussed in Xu and Weiss, 2005): (1) activation, in which the first steps of the biochemical cascade are set into motion in response to an appropriate germination stimulus; (2) increase in intrasporal osmotic pressure, which generates the force necessary to rupture the spore wall and initially drive polar filament eversion; (3) eversion of the polar filament; and (4) passage of the sporoplasm through the polar tube.

Because microsporidia are emerging pathogens and are not an experimentally facile host-parasite system, none of these steps are particularly well understood. However, empirical studies by several investigators in the field have allowed the formation of several hypotheses with broad support among microsporidiologists. Regarding the first step of germination, data from many studies (reviewed in Xu and Weiss, 2005) indicate that stimuli for spore activation vary according to species. These include subjection to shifts in pH, dehydration followed by rehydration, various cations, anions, or calcium ionophores, mucins, hydrogen peroxide, and low dose ultraviolet radiation. Inhibitory stimuli include various salts, low physiological salt concentrations, silver ions, gamma and ultraviolet radiation, high temperatures, inhibitors of calcium flux, calmodulin inhibitors, and cytoskeleton disruptors. The long list of potentiators and inhibitors for spore activation likely reflect the diversity of hosts and environments in which microsporidian spores are found.

Because it is more difficult to discern the intracellular events within the spore, only a few theories have been proposed to explain the increase in osmotic pressure that precedes polar filament eversion. The best-supported and most widely accepted theory is based on the generation of an osmotic gradient by the hydrolysis of trehalose, a disaccharide of glucose, to glucose (Undeen, 1990; Undeen and Vandermeer, 1994). Trehalose levels have been shown to be decreased and glucose levels increased in extruded spores of *Anncaliia* (syns. *Brachiola*, *Nosema*) *algerae* (Undeen and Vandermeer, 1994). It is thought that the preceding events of spore activation cause a disintegration of intrasporal

compartments which otherwise sequester trehalose from its degradative enzyme, trehalase, and that the resulting increase in solute concentration in the spore causes an influx of water and concomitant swelling of the polaroplast and posterior vacuole. Trehalose breakdown has been shown to drive an osmotic gradient in the rice blast fungus *Magnaporthe grisea*, causing an increased turgor pressure which allows the fungus to burst through the cuticle of its plant host (de Jong et al., 2007). Because the flow of polar molecules such as water across the plasma membrane is energetically limited, it is likely that there exist special provisions in the spore to support the osmotic influx during activation. One possibility that has been considered is that microsporidia possess aquaporins (AQPs), a recently described family of integral membrane proteins that facilitate osmosis (Verkman and Mitra, 2000). This possibility is experimentally addressed in Chapter 2 and comprises the first half of this dissertation.

The second aim of this project was to identify novel structural components of the infectious apparatus of these organisms, especially the polar tube and spore wall. To date, the handful of component proteins across the microsporidia that have been identified (Xu and Weiss, 2005) lack homology to any known protein or conserved functional domain among characterized proteins. A better appreciation of the molecular composition of these structural components of the spore is essential for understanding the later stages of germination including polar filament eversion and intratubular passage of the sporoplasm. The flexibility and dynamics exhibited by the polar tube during the process of extrusion and the tensile strength exhibited by the spore wall during activational

swelling are necessarily emergent properties of the molecular makeup of the polar tube and spore wall, respectively. Thus, the second half of this dissertation was to identify and characterize novel proteins of these special organelles in the spore; this work is described in Chapter 3.

The Microsporidia are a large group of organisms for which divergence at the biochemical and molecular level will in all likelihood continue to be revealed. However, for the sake of coherence and expediency, it was necessary to focus on one or two model species for this dissertation work. Of the human-infecting microsporidia, the genus *Encephalitozoon* is of particular public health importance (Franzen and Muller, 2001), as it contains three species that have been demonstrated to cause human infections: *Enc. cuniculi*, *Enc. hellem*, and *Enc. intestinalis*. These species cause pathology in a wide range of tissues including the gut, liver, genito-urinary system, peritoneum, bone, skin, respiratory sinuses, lungs, brain, and ocular conjunctiva (Franzen and Muller, 2001; Didier and Weiss, 2006). *Enc. cuniculi* and *hellem* are so closely related that they may be considered sister species; they are in fact indistinguishable by light and electron microscopy (Didier et al., 1991). Due to morphological differences, *Enc. intestinalis* was originally placed in the genus *Septata* within the family Encephalitozoonidae (Cali et al., 1993) but was renamed congenerically on the basis of molecular data (Hartskeerl et al., 1995). *Enc. cuniculi* was chosen here as the primary organism of study, as it is easily propagated in cell culture (Visvesvara, 2002) and is the best-studied microsporidian in cell biological and immunological contexts (Khan et al., 2001), and its sister species *Enc. hellem*

was also investigated in Chapter 3. In addition, the *Enc. cuniculi* genome was sequenced in a landmark project in 2001 (Katinka et al., 2001). The availability of this data has inaugurated a new era in microsporidology in which genomic and proteomic strategies to characterize the infectious apparatus of these organisms are now feasible.

CHAPTER 2

Functional characterization of the putative aquaporin of *Encephalitozoon cuniculi*

This work has been published in:

Ghosh, K., Cappiello, C.D., McBride, S.M., Occi, J.L., Cali, A., Takvorian, P.M., McDonald, T.V., Weiss, L.M., 2006a. Functional characterization of a putative aquaporin from *Encephalitozoon cuniculi*, a microsporidia pathogenic to humans. *International Journal for Parasitology* 36, 57.

Ghosh, K., Takvorian, P.M., McBride, S.M., Cali, A., Weiss, L.M., 2006b. Heterologous expression of an *Encephalitozoon cuniculi* aquaporin in *Xenopus* oocytes. *J Eukaryot Microbiol* 53 Suppl 1, S72-73.

2.1 INTRODUCTION

The mechanism of spore germination has long been of interest to microsporidian researchers, and naturally it has been suggested that inhibition of this process would constitute an effective anti-microsporidian therapy (Keohane and Weiss, 1999). Germination stimuli are variable (Undeen and Epsky, 1990), but are postulated (reviewed in Keohane and Weiss, 1999) to result in cleavage of the disaccharide trehalose into glucose and its metabolites, producing an increase in intrasporal pressure and osmotic swelling that leads to extrusion of the polar filament. The diversity of this phylum has led to the consideration of an additional theory for the osmotic gradient generation in which the posterior vacuole is a site for fatty acid breakdown to H_2O_2 , which is then converted by catalase to H_2O and O_2 (Findley et al., 2005). In either case, because water flux across the lipid bilayer is limited, it has been suggested that microsporidia may possess aquaporins (AQPs) (Frixione et al., 1997), integral membrane channel proteins that facilitate osmosis (Agre and Kozono, 2003; Verkman and Mitra, 2000). This suspicion was bolstered by the observation that germination of *Anncaliia* (syns. *Brachiola*, *Nosema*) *algerae* spores is inhibitable by mercury salts, which inhibit aquaporin function (Agre and Kozono, 2003; Yang, 2000). Further evidence suggesting the presence of AQPs in microsporidia surfaced with the sequencing of the genome of *Encephalitozoon cuniculi*, a human-pathogenic species, and identification of an “aquaporin-like protein” sequence by Katinka et al. (2001).

Since the discovery of AQPs in the early 1990s by Peter Agre and colleagues (Preston et al., 1992), aquaporin biology has become an increasingly popular field, garnering Agre the Nobel Prize in Chemistry in 2003, and generating insights into their function, structure, physiology, and molecular mechanisms of conductance (King et al., 2004; Verkman and Mitra, 2000; Agre and Kozono, 2003). These proteins are the major constituent of the major intrinsic protein (MIP) superfamily (Johanson and Gustavsson 2002), which facilitate water and small solute flux across the plasma membrane. The MIPs also contain glycerol facilitators. A search of the protein databases (Entrez – National Center for Biotechnology Information) reveals that hundreds of AQPs or putative AQPs have been identified, from each of the three domains of life. AQPs are divided into two phylogenetically and functionally distinct groups (reviewed in Heymann and Engel, 1999): the classic, or orthodox AQPs, which are permeable to water, and the aquaglyceroporins, which are also permeable to glycerol and other small solutes. They are thought to exist natively as a homotetramer, with each 26-34 kDa monomer forming its own pore (Verkman and Mitra, 2000). An “hourglass model” has been posited for the shape of the monomer (Jung et al., 1994), in which six transmembrane domains surround the pore, formed in part by two canonical NPA motifs. Water-selectivity is thought to be by size-exclusion and electrostatic-repulsion (de Groot and Grubmuller, 2001, Tajkhorsid et al., 2002, reviewed in Agre and Kozono, 2003).

This portion of the work was undertaken to functionally characterize the putative *Enc. cuniculi* AQP protein in a standard heterologous *Xenopus* oocyte

expression system (Wagner et al., 2000) and to generate reagents for its immunolocalization, in view of its potential role in the infection process of these parasites. The current degree of scholarly interest in AQPs is advantageous in that it may inform the search for appropriate therapeutics directed against these proteins in microsporidia.

2.2

MATERIALS AND METHODS

2.2.1 Parasites

Enc. cuniculi was cultured in RK13 cells (rabbit kidney cells CCL37; American Type Culture Collection, Rockville, Md.) at 37 °C and 5% CO₂. Infected RK13 cells were maintained in continuous culture in minimum essential medium supplemented with 7% heat-inactivated FCS, 1% penicillin–streptomycin and 1% amphotericin B (Fungizone; Invitrogen, Carlsbad, CA) and subpassaged every week by trypsin-EDTA treatment (Invitrogen, Carlsbad, CA). Spores were harvested from culture medium twice weekly.

2.2.2 Cloning and expression of *EcAQP* in *Xenopus* oocytes

Genomic DNA was isolated from disrupted spores of *Enc. cuniculi* by SDS and proteinase K treatment and homogenization, followed by phenol–chloroform extraction, as previously described (Keohane et al., 1998). Recognition sites for the restriction enzymes *Xma* I and *Xba* I were engineered onto the N- and C-termini, respectively, of *EcAQP* (GenBank accession no. NP_586002), by PCR-amplification of genomic DNA. PCR was performed using *Pfx* DNA polymerase and 15 µM of each primer (primers, restriction sites are underlined: 5'GGACCTCCCGGGGATGACCAGAGAGACATTGAAG3' (forward), 5'GACCCTCTAGACTAAAAGCTGAGCTTGTACAG3' (reverse)); DNA was amplified for 35 cycles (45 s denaturation at 94 °C, 45 s annealing at 40 °C and 60 s extension at 60 °C). The amplicon was cloned into the *Xma* I–*Xba* I multiple cloning site of the pGEM-HE *Xenopus* expression vector (Liman et al., 1992) by *Xma* I–*Xba* I digestion and mutual ligation of the amplicon and vector, yielding

pGEM-HE-*EcAQP*. *Escherichia coli* strain DH5 α was subsequently transformed by pGEM-HE-*EcAQP*; large-scale plasmid purification from ampicillin-screened colonies was accomplished by the HiSpeed Kit (Qiagen, Valencia, CA). Identity of pGEM-HE-*EcAQP* was confirmed by restriction digestion analysis and by sequencing. pGEM-HE-*EcAQP* was linearized downstream of the 3' untranslated region (UTR) by digestion with the restriction enzymes *Sph* I or *Nhe* I. cRNA was generated in vitro by the mMessage mMachine kit (Ambion, Austin, TX) as per manufacturer's instructions using T7 RNA polymerase, nucleotide phosphate (NTP), 7-methyl-guanosine cap analog, and RNase-inhibitor. *Xenopus laevis* maintenance and surgical oocyte removal were performed as previously described (Mak and Foskett, 1994). Defolliculated stages V and VI oocytes were injected with 55 ng in 37 nL of pGEM-HE-*EcAQP* mRNA or 37 nL water (controls). Oocytes were incubated in isoosmotic ND96 buffer/pyruvate (96 mM NaCl, 2 mM KCl, 1.8 mM CaCl₂, 1 mM MgCl₂, 5 mM HEPES, 2.5 mM pyruvate, pH 7.6) at 16°C for 4–6 days, adding fresh buffer after 3 days.

2.2.3 Oocyte swelling assays

Swelling assays were conducted at room temperature in plastic 96-well culture plates. For measurement of water permeability, oocytes were transferred to hypotonic source of ND96/pyruvate (1:3 diluted ND96 buffer/0.83 mM pyruvate) or, if indicated, pre-incubated for 5 min in isoosmotic ND96/pyruvate +0.1, 1, 10, 200 μ M, or 1 mM HgCl₂ and then transferred to hypotonic ND96/pyruvate + HgCl₂. For measurement of solute conductivity, oocytes were transferred to

ND96/pyruvate where 65 mM NaCl had been replaced with 130 mM glycerol or urea. Swelling was video-monitored every 3 s with a Zeiss SV11 dissecting microscope (Zeiss, Göttingen, Germany) at 66× magnification, and a Retiga 1300 digital camera and IPLab software (Scanalytics, Fairfax, VA). Image analysis was accomplished with ImageJ software (National Institutes of Health, US; URL: <http://rsb.info.nih.gov.proxy.libraries.rutgers.edu/ij/>) by converting images to binary and treating the oocyte as a growing sphere whose volume could be inferred from its cross-sectional area. Water permeability (P_f , cm/s) was calculated based on the first 60 s of the assay and according to the following equation: $P_f = \{ [V_0] [d(V/V_0)/dt] \} / \{ (S)(V_w)(osm_{in} - osm_{out}) \}$; V_0 and S are the initial volume and surface area of each individual oocyte, respectively; $d(V/V_0)/dt$, the relative volume increase per unit time; V_w , the molecular volume of water (18 cm³/mol); and $osm_{in} - osm_{out}$, the osmotic gradient between the inside and outside of the oocyte (140×10⁻⁶ mol/cm³). Solute conductivity was inferred from $d(V/V_0)/dt$. Water permeabilities and swelling rates were statistically compared with the Student's t-test (two-tailed).

2.2.4 Expression of *EcAQP* in *Escherichia coli*

PCR primers 5'-CCGGAATTCATGACCAGAGAGACATTG-3' (forward) and 5'-CCGCTCGAGCTAGCCAGAAGGCGTAGGC C-3' (reverse) were used to engineer the restriction sites *EcoRI* and *XhoI* (underlined) onto the N-terminus and amino acid residue 125, respectively, of *EcAQP* using *Pfx*DNA polymerase and pGEM-HE-*EcAQP* to produce *EcAQP1*. DNA was amplified for 25 cycles

(15 s denaturation at 94 °C, 30 s annealing at 55 °C, and 60 s extension at 68 °C). A second PCR was performed under identical conditions to engineer restriction sites for *EcoRI* and *XhoI* onto amino acid residue 125 and the C-terminus, respectively, of *EcAQP* (5'-CCGGAATTCTCTCCGTTTGGAGGAGAC-3' [forward], 5'-CCGCTCGAGCTAAAGCTGAGCTTGTAC-3' [reverse]), to produce *EcAQP2*. *EcAQP1* and *EcAQP2* were cloned into pGEX-4T1 (GE Healthcare Bio-Sciences, Piscataway, NJ) yielding *EcAQP1*-pGEX-4T1 and *EcAQP2*-pGEX-4T1. *Escherichia coli* Rosetta strain was transformed by these constructs and fusion protein expression was induced by 0.1 mM isopropyl- β -D-thiogalactopyranoside for 13 h at 18 °C. The bacterial cells were centrifugally pelleted from culture and frozen at -80 °C.

2.2.5 Purification of fusion protein, immunization of mice, and evaluation of serum by immunoblot

Bacterial lysates were produced by thawing the bacterial cell pellets on ice in PBS with 1 mg/ml lysozyme and Complete Protease Inhibitor Cocktail (Roche Applied Science, Indianapolis, IN) followed by sonication. The crude lysate was treated by 1% Triton-X 100 and 5 μ g/ml DNase and RNase for 30 min at 4 °C and centrifuged at 25,000 g for 25 min. The supernatant was reserved and the pellet was further treated by 1.5% N-lauroylsarcosine, 25 mM triethanolamine, and 1 mM EDTA (pH 8.0) for 20 min at room temperature followed by centrifugation at 25,000 g for 25 min (Sambrook and Russell 2001). Fusion proteins were then purified from the pooled supernatants by affinity chromatography using

glutathione sepharose 4B and the glutathione S-transferase (GST) tag was then cleaved by thrombin (GE Healthcare Bio-Sciences). Following SDS-PAGE, fusion protein expression was evaluated by immunoblot using anti-GST antibody (1:1,000 dilution).

For the production of polyclonal antibody to *EcAQP*, Balb/c mice were injected intradermally with 5 µg of purified *EcAQP1* and *EcAQP2* using TiterMax Gold (CytRx Corp., Norcross, GA) adjuvant and serum was collected 30 days post-injection. A 1:1,000 dilution of serum was used as the primary antibody in an immunoblot of lysates of fusion protein-expressing bacteria.

2.2.6 Immunolocalization of *EcAQP* in *Xenopus* oocytes

Oocytes were fixed in 0.5% glutaraldehyde and 2% paraformaldehyde in 0.1 M cacodylate buffer. Oocytes were cryoprotected in increasing concentrations of sucrose in 0.1 M cacodylate buffer (7.5%, 15%, and 30% w/v) and 0.88 M sucrose overnight before being plunge frozen in 2-methyl-butane cooled in liquid nitrogen. Twenty-micrometer-thick sections were cut with a Reichert cryostat at -30°C. Sections were blocked for non-specific binding in 10% normal goat serum, 1% bovine serum albumin in PBS-Tween-20, and incubated with a 1:20 dilution of anti-*EcAQP* 1/2 for 1 h at 32°C and FluoroNanogold-anti-mouse Fab'-Alexa Fluor® 488 (a generous gift from Nanoprobes Inc., Yaphank, NY) for 30 min at 32°C. Sections were mounted on slides and examined using a Zeiss Axiovert 200 inverted microscope equipped with epifluorescence.

2.2.7 Sequence analysis

The BLAST program (Altschul et al., 1997) was used to search the databases for proteins similar to *EcAQP*. The Biology Workbench (URL: <http://workbench.sdsc.edu/>) was employed for Kyte–Doolittle hydropathy analysis (Kyte and Doolittle, 1982; Pearson and Lipman, 1988; Pearson, 1990), transmembrane segment prediction (Persson and Argos, 1994), CTREE phylogenetic construction (algorithm and program: The Biology Workbench, David J. States), and multiple protein sequence alignment (Felsenstein, 1989; Higgins et al., 1992; Thompson et al., 1994).

2.3

RESULTS

2.3.1 Functional characterization of *EcAQP*

Mean swelling rates of *EcAQP*- and water-injected oocytes in hypotonic medium are plotted in Fig. 2.1; only 1 min of *EcAQP* swelling is plotted due to bursting of some oocytes between 1 and 2 min (data not shown). At 1 min, *EcAQP* oocytes swelled on average $8.0 \pm 0.8\%$, compared with $1.8 \pm 0.2\%$ for water-injected control oocytes; at 2 min, control oocytes had only swelled $3.4 \pm 0.35\%$. Endogenously expressed AQP 3 (Schreiber et al., 2000) as well as osmosis across the lipid bilayer may account for swelling of control oocytes. The osmotic permeability, P_f , of *EcAQP* oocytes, $87 \mu\text{m/s}$, differed significantly ($p \ll 0.001$) from that of controls ($19 \mu\text{m/s}$) (Fig. 2.1, inset). Osmotic permeability of HgCl_2 -treated and -untreated *EcAQP* oocytes did not differ significantly for any of the tested HgCl_2 concentrations (Fig. 2.2). Conductivities of *EcAQP* oocytes to glycerol ($1 \times 10^{-4} \pm 6 \times 10^{-5} \text{ d}(V/V_0) \cdot \text{s}^{-1}$) and urea ($3 \times 10^{-4} \pm 6 \times 10^{-5} \text{ d}(V/V_0) \cdot \text{s}^{-1}$) did not differ significantly from those of control oocytes.

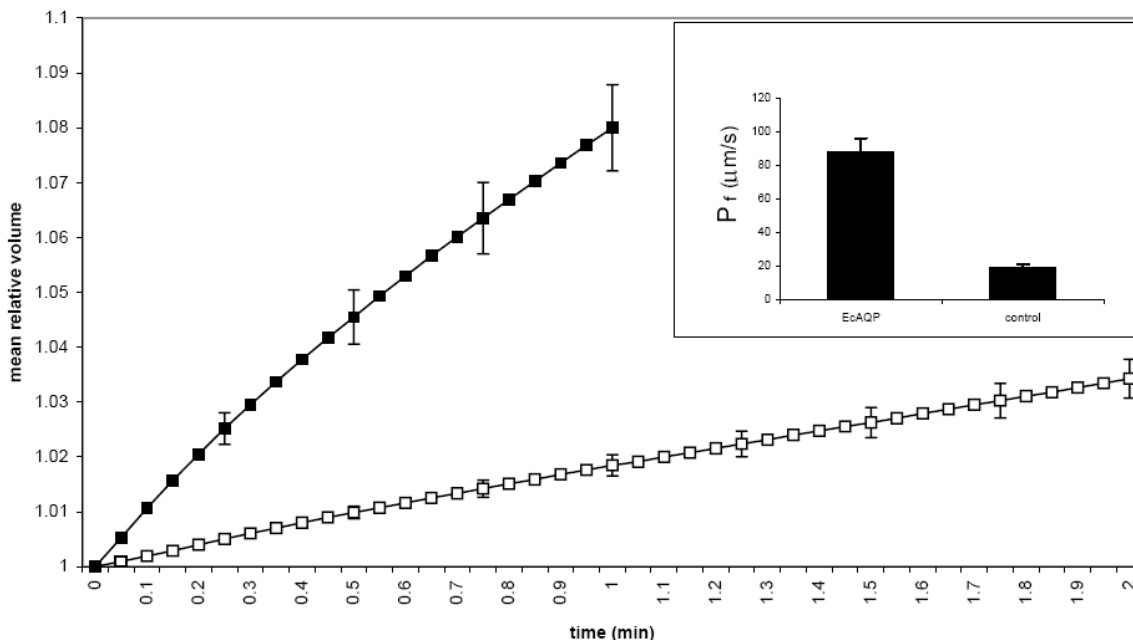


Figure 2.1. *EcAQP*-injected *Xenopus laevis* oocyte swelling assay. After 1 min, *EcAQP*-injected oocytes had swelled an average of 8.0 vs. 1.8% water-injected controls. Inset: Altered water permeability ($P < 0.001$) of *EcAQP*-injected oocytes ($87.3 \pm 8.6 \mu\text{m/s}$; $n=12$) vs. water-injected ($19.3 \pm 2.0 \mu\text{m/s}$; $n=15$). Legend: closed marker/bar, *EcAQP*-injected; open marker/bar, water-injected. (Mean \pm S.E.M; for clarity, error bars are only displayed every 15 s).

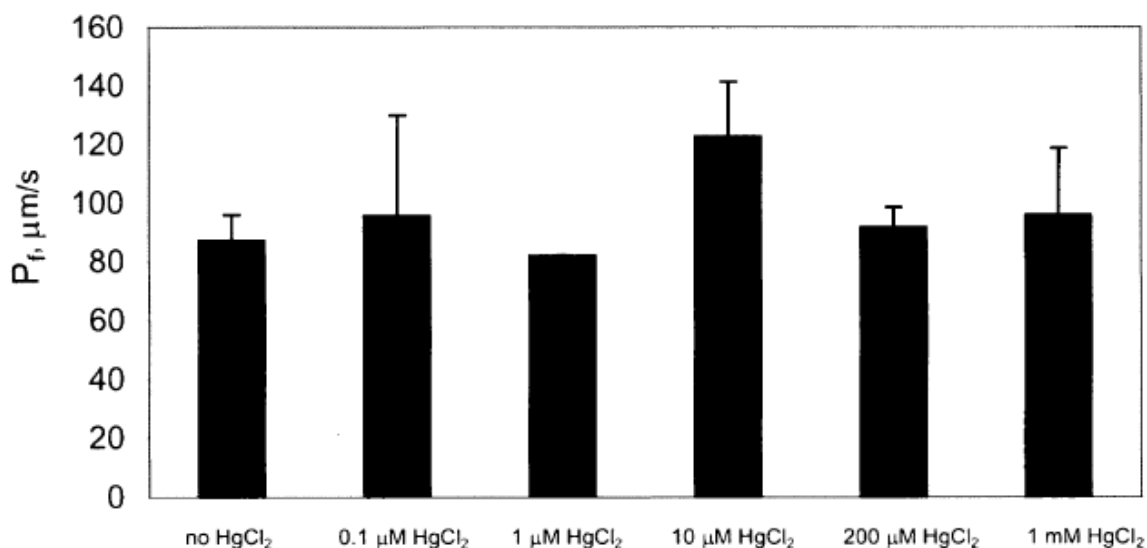


Figure 2.2. Swelling of *EcAQP* oocytes is not inhibited by HgCl_2 . Permeability differences between HgCl_2 -treated and -untreated oocytes were not significant (where $n > 1$) for all tested concentrations (0.1 μM , $n=2$; 1 μM , $n=1$; 10 μM , $n=5$; 200 μM , $n=4$; 1 mM, $n=2$; untreated, $n=12$).

2.3.2 Sequence analysis and phylogenetic construction

Kyte–Doolittle hydropathy analysis reveals *EcAQP* to be a highly hydrophobic protein, as would be expected for an aquaporin; six transmembrane segments are predicted (residues 13–37, 42–68, 79–107, 131–157, 180–208 and 222–250). Comparison of *EcAQP* with existing proteins in the databases using BLAST revealed AQP A of *Dictyostelium discoideum* to be the most similar (26% identity) among named, characterized proteins; among human aquaporins, AQP 2 was the closest match (24% identity). In an unrooted phylogenetic construction of *EcAQP*, human AQPs 0–9, and AQPs from several parasitic protists, two plants, and a yeast (Fig. 2.3), *EcAQP* clusters neither with the orthodox AQPs, which conduct only water (AQPs 0, 1, 2, 4–6), nor with the water- and solute-conducting aquaglyceroporins (AQPs 3, 7 and 9). Instead it branches closely with two other protist AQPs, one of which is an orthodox AQP of *Trypanosoma cruzi* (Montalvetti et al., 2004) while the other is an aquaglyceroporin of *Toxoplasma gondii* (Pavlovic-Djuranovic et al., 2003), and with an orthodox AQP from the yeast *Saccharomyces cerevisiae* (Laize et al., 2000). Alignment of *EcAQP* with human AQP 1 (Fig. 2.4) demonstrates the presence within *EcAQP* of the two NPA motifs believed to line the AQP aqueous pore (Jung et al., 1994), and the absence of the cysteine residue aligned with C189 of AQP 1, which is believed to confer mercury-sensitivity to AQP 1 (Preston et al., 1993).

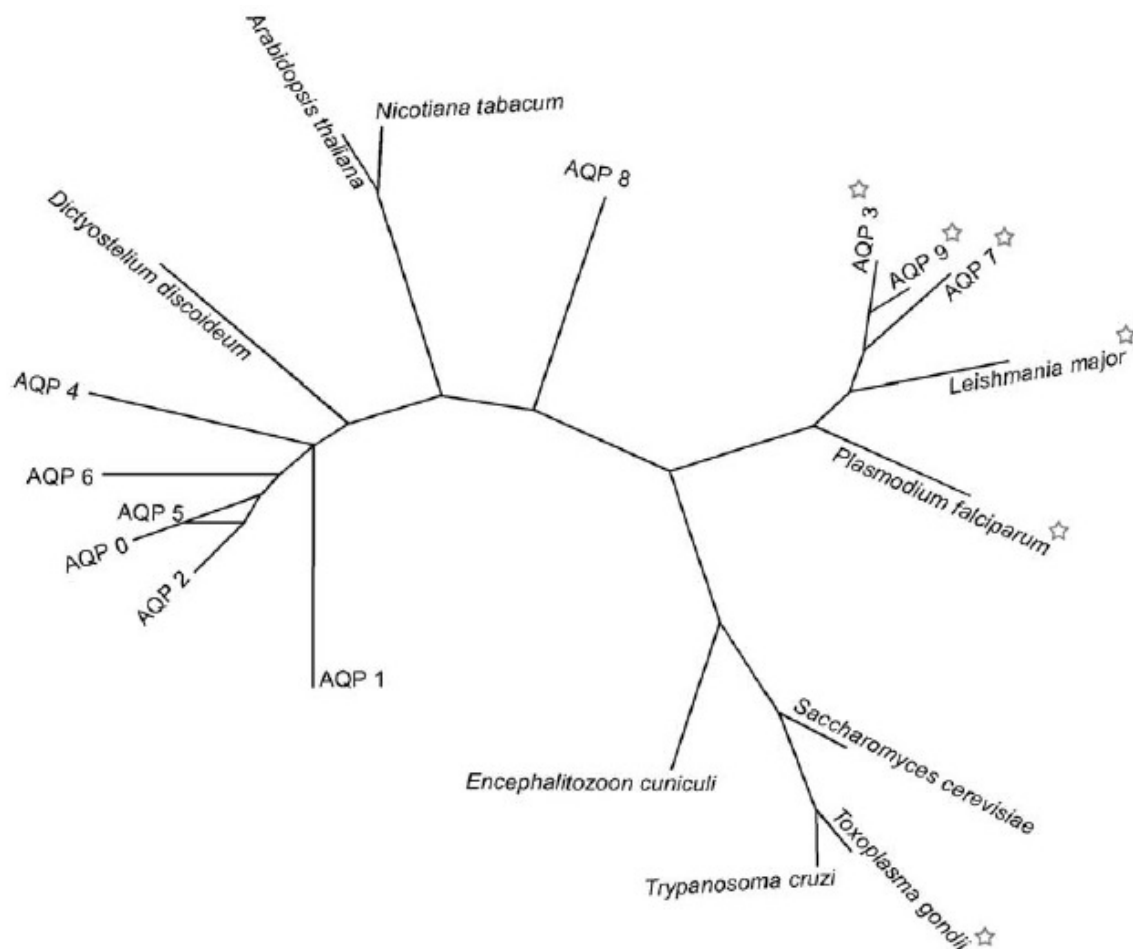


Figure 2.3. An unrooted phylogenetic tree of aquaporins (AQP) including *EcAQP*. This is based on CTREE alignment of protein sequences of *EcAQP* (GenBank accession no. NP_586002), closest BLAST match AQP A of *Dictyostelium discoideum* (BAA85158), human AQPs 0–9 (NP_036196, NP_932766, NP_000477, NP_004916, P55087, NP_001642, Q13520, NP_001161, O94778, NP_066190, respectively), plant aquaporins of *Arabidopsis thaliana* (P25818) and *Nicotiana tabacum* (CAA69353), parasitic protist aquaporins of *Leishmania major* (AAS73184), *Plasmodium falciparum* (CAC88373), *Toxoplasma gondii* (CAE46485), *Trypanosoma cruzi* (AAM76680), and AQP 2 of the yeast *Saccharomyces cerevisiae* (AAD10058). Stars indicate aquaglyceroporins.

```

EcAQP residue no.      10                      20                      30
EcAQP -----MTRETLKTLQST-----FGEMVASFVGFVAVYSALLG---
AQP1 -----MASEFKKLEWR-----AVVAEFLATTLFVVISIGSALGFKY
AQP2 -----MWELRSIAFSR-----AVFAEFLATLLFVFFGLGSAL---
DdAQP MVKVVPLRFITYDPLKDPKMIYRRPISKPVKAFKGFSEFLGTLVLYVFCGGSVCA---
          : .                               ..*::: : : :
          : .                               ..*::: : : :

          40          50          60          70          80          90
EcAQP --SALTEQSAARVIVGLTVGFGSICVVIYSFCDVTVAHFNPAITLAAILTCCKLGVLRGIGY
AQP1  PVGNNQTAVQDNVKVSLAFGLSIATLAQSVGHISGAHLNPAVTLGLLSCQISIFRALMY
AQP2  --NWPQALPSVLQIAMAFGLGIGTLVQALGHISGAHLNPAVTVACLGVGCHVSVLRAAFY
DdAQP AFAVAGDSARALLGGLIQGMALAALIWAWSGVSGCNLNPAVTLANLLSGRVGLIDSLYY
          : . : * : . : . : : : : * : : : : : . *

          100         110         120         130         140         150
EcAQP IVAQYIGFILAVCALLPCSPVGYKETLNIIRPTSPFPGDNLNVFFTEFFLTAILVHVAF
AQP1  IIAQCVGAIVATAILSGITSSLTGNSLGRNDLADGVNSGQ---GLGIEIIGTLQLVLCVL
AQP2  VAAQLLGAVAGAALLHEITPADIRGDLAVNALSNSSTAGQ---AVTVELFLTQLVLCIF
DdAQP VAAQILGCIAGAGILYGCLPNMYRIDLGVPHLAPGMNTGQ---AFLMEMMLTSLCLCVL
          : * : * : . * . * . : . * : . * : * : * :

          160         170         180         190         200         210
EcAQP ATAVNPKPKTDTEGKFVDPDEEFPVDRRITAPLCIGLTGLGFLAFLGLASSGSAFNEGLT
AQP1  ATDR--RRRDLLG-----SAPLAIGLSVALGHLLAIDYTGCGINPARS
AQP2  ASTDE--RRGENPG-----TPALSIGFSVALGHLLGIHYTGCSMNPARS
DdAQP GTSVFNVDRLNR-----IAPFAIGLALFIGVAIGNFSGCALNPFVRV
          : : : . . . * : : : : : : : : * : : * : * :

          220         230         240         250
EcAQP LAPVIMSNTWNHFWAYFAGQYLGFGVGGLLQVLVLYKLSF-----
AQP1  FGSVITHNFSNHWIFWVGPFFIGGALAVLIYDFILAPRSSDLTDRVKVWTSQGVEEYDLD
AQP2  LAPAVVTGKFDDHWVFWIGPLVGAILGSLLYNYLVFPKASLSERLAVLK-GLEPDTDWE
DdAQP LGPSIISGVWSHHVWVWLGPIVGAILAFAFYRCLQER-FDVIERPQYIAPLIDPSTAVS
          : . : : : . . * : : * : * : . : : : *

EcAQP -----
AQP1  ADDINSR--VEMKPK-----
AQP2  EREVRRRQSVELHSPQSLPRGTKA
DdAQP SY-----

```

Figure 2.4. Alignment of *EcAQP*, human AQPs 1 (accession no. NP_932766), 2 (NP_000477), and AQP A of *Dictyostelium discoideum* (BAA85158). Highlighted in black is the residue position at which the presence of a cysteine confers mercury-sensitivity to AQP 1; gray highlights are the NPA motifs thought to line the water-conducting pore of each AQP monomer. Asterisks indicate fully conserved residues; two dots, conservation of strong groups; one dot, conservation of weak groups.

2.3.4 Production of antiserum to *EcAQP*

The murine antiserum directed against pooled *EcAQP*1 and -2 recognizes the pooled full-length fusion proteins *EcAQP*1-GST and *EcAQP*2-GST (both are ~40 kDa), but not GST alone (26 kDa) (Fig. 2.5), indicating that the fusion proteins *EcAQP*1-GST and *EcAQP*2-GST were expressed in the protease-deficient *E. coli*

Rosetta strain and were purified from the GST fusion tag, and that the antiserum is specific for *EcAQP*.

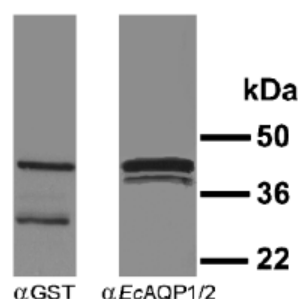


Figure 2.5. Expression of recombinant *EcAQP1*-GST and *EcAQP2*-GST. A pooled lysate of *EcAQP1* and *EcAQP2* fusion protein-expressing bacteria was subjected to SDS-PAGE, transferred to a nitrocellulose membrane, and then incubated with either monoclonal anti-GST antibody (left lane) or anti-*EcAQP1/2* murine serum (right lane). Both fusion proteins (40 kDa) and GST (26 kDa) are expressed, but only the fusion proteins and not GST is recognized by the *EcAQP1/2* antiserum. The minor band recognized by the *EcAQP1/2* antiserum is due to proteolytic degradation of the fusion proteins.

2.3.5 Immunolocalization of *EcAQP* in *Xenopus* oocytes

The antiserum stained the surface of *EcAQP*-transfected *X. laevis* oocytes (Fig.

2.6, arrows), indicating that *EcAQP* is expressed heterologously.

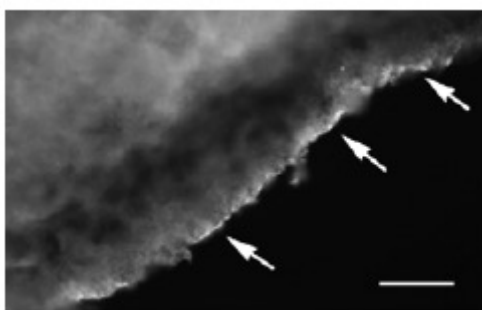


Figure 2.6. Heterologous expression of *EcAQP* in *Xenopus laevis* oocytes. Antiserum to *EcAQP1/2* stains the surface of *EcAQP*-transfected oocytes. Arrows point to immunolabel located at the edge of the oocyte. Scale bar = 50 μm .

2.4

DISCUSSION

Hundreds of AQPs or putative AQPs have been identified, from each of the three domains of life. Aquaporins are thought to exist natively as a homotetramer, with each 26–34 kDa monomer forming its own pore (Verkman and Mitra, 2000). The expected molecular weight of the *EcAQP* protein is approximately 26.8 kDa; thus it is within the range for an AQP monomer. An ‘hourglass model’ has been posited for the shape of the monomer (Jung et al., 1994), in which six transmembrane domains surround the pore, formed in part by two NPA motifs. These characteristics are also predicted for *EcAQP* (Fig. 2.4). In addition, the BLAST similarity searches strongly suggest that *EcAQP* is a member of the AQP protein family.

The significantly increased permeability of *EcAQP*-injected *Xenopus* oocytes as compared to controls (Fig. 2.1, inset) provides further evidence that the AQP-like gene within the *Enc. cuniculi* genome (Katinka et al., 2001) is indeed an aquaporin. Aquaporins of selected other protistan parasites have a measured P_f of 32 (*T. cruzi*; (Montalvetti et al., 2004), 40 (*T. gondii*; (Pavlovic-Djuranovic et al., 2003), and 276 $\mu\text{m/s}$ (*Plasmodium falciparum*; (Hansen et al., 2002). The *EcAQP* P_f (87 $\mu\text{m/s}$) is similar to those of human AQPs 3, 2, and 5 (80, 100 and 100 $\mu\text{m/s}$, respectively, (Yang and Verkman, 1997), which are considered to be in the high range for human aquaporins (King et al., 2004). However, because of differing levels of expression attributable to, among other factors, different amounts of cRNA injected by each investigator, and their varying translational and post-translational processing efficiencies, these comparisons are not strictly quantitative. The restriction of antiserum staining to

the surface of transfected oocytes is in accord with the expected localization of an AQP.

Aquaporins are divided into two phylogenetically and functionally distinct groups (reviewed in Heymann and Engel, 1999): the classic, or orthodox AQPs, which are permeable to water, and the aquaglyceroporins, which are also permeable to glycerol and other small solutes. Neither the presence nor absence of solute conductivity by *EcAQP* can be predicted based on the phylogeny in Fig. 2.3, as it clusters with neither group among the human AQPs, and branches closely with non-human AQPs of both types. However, its lack of solute conductivity, $3 \times 10^{-4} \text{ d(V/V0) \cdot s}^{-1}$, not significant relative to water-injected controls, and approximately an order of magnitude lower than the reported swelling rates of $\sim 2 \times 10^{-3} \text{ d(V/V0) \cdot s}^{-1}$ for the *T. gondii* (Pavlovic-Djuranovic et al., 2003) and *P. falciparum* aquaglyceroporins (Hansen et al., 2002), is perhaps not surprising in light of the fact that *EcAQP* shares highest identity (24%) among the human AQPs with orthodox AQP 2. *EcAQP* also branches closely with a yeast AQP (*S. cerevisiae* AQP 2; Laize et al., 2000) (Fig. 2.3), which is consistent with recent data on the fungal origins of the phylum Microsporidia (reviewed in Lee et al., 2008).

Mercury-inhibition of osmotic permeability is a hallmark of many aquaporins (Yang, 2000) and the observation that germination of spores of the microsporidian *Anncaliia* (syns. *Brachiola*, *Nosema*) *algerae* was inhibited by treatment with mercury salts (Frixione et al., 1997) was interpreted as circumstantial evidence for microsporidian AQPs. It is also possible, however,

that the inhibitory effect of mercury on germination observed by Frixione et al. (1997) is attributable to modification of other cysteine-containing microsporidian proteins. For example, Hayman et al. (2001) identified two I spore proteins with N-terminal cysteine-rich motifs, whose functions are as yet unknown. General cytotoxic effects of mercury may also be partially or wholly responsible for the observed inhibition of germination.

Pre-treatment of *EcAQP*-expressing oocytes with HgCl_2 did not inhibit swelling (Fig. 2.2). Nonetheless, this does not preclude the classification of *EcAQP* as an AQP, as several AQPs have documented mercury-insensitivity, e.g. the prototypical mercurial-insensitive AQP 4 (Yang et al., 1995). Cysteine residue 189 (C189), which is close in primary sequence to the second of the NPA motifs which have been postulated to line the aqueous pore (Jung et al., 1994), has been shown by site-directed mutagenesis to be the mercury-sensitive residue of AQP 1 (Preston et al., 1993) and site-directed mutagenesis to cysteine of any of four amino acids near the first NPA motif or one amino acid near the second NPA was found to confer mercury-sensitivity to AQP4 of *Rattus norvegicus* (Shi and Verkman, 1996). Alignment of *EcAQP* and AQP 1 amino acid sequences (Fig. 4) demonstrates that the *EcAQP* amino acid near the second NPA corresponding to the C189 of AQP 1 is glycine (i.e. *EcAQP* G203), as well as a lack of any cysteine residues in the immediate vicinity of the first NPA motif. The absence of these cysteines may explain the apparent mercury-insensitivity of *EcAQP*. Among human AQPs, the mercury-insensitive AQP 4 is the second-closest match (22% identity) to *EcAQP* according to BLAST analysis.

In the future, it may be interesting to examine whether mercury-sensitivity could be conferred upon *EcAQP* by site-directed mutagenesis of G203 to a cysteine residue.

In conclusion, the functional swelling assay, immunolocalization of *EcAQP* to the surface of transfected *Xenopus* oocytes, and amino acid sequence analysis provide evidence that this putative AQP-like sequence identified in the *Enc. cuniculi* genome (Katinka et al., 2001) may indeed be considered an AQP. As the germination of microsporidian spores is believed to depend on the rapid influx of water (reviewed in Keohane and Weiss, 1999), it is hoped that further study of microsporidian AQPs and potential inhibitors of these proteins (e.g. gold and silver salts (Niemi et al., 2002)) may yield novel therapeutic agents for human infections with these opportunistic pathogens.

CHAPTER 3

**Proteomics-based identification and
characterization of novel proteins of
the infectious apparatus of
*Encephalitozoon cuniculi***

3.1 INTRODUCTION

The spore wall, polar tube, and other specialized organelles such as the polaroplast and posterior vacuole play critical roles in the infectious process of the microsporidia (Xu and Weiss, 2005; Wittner and Weiss, 1999). In a resting spore, the polar tube lies coiled within the cell; at this stage it is solid and is thus referred to as a polar filament (Lom and Vavra, 1963; Takvorian and Cali, 1986). Upon an appropriate species-specific environmental stimulus (Undeen and Epsky, 1990), an increasing internal osmotic pressure develops and causes the polaroplast and posterior vacuole to swell and the polar filament to erupt from the anterior, thinnest point of the spore wall. During this process, the polar filament everts, becoming a hollow polar tube through which the sporoplasm passes.

In the resting spore, the polar filament extends in a straight fashion from the anchoring disk at the anterior end of the spore through the region of the polaroplast before assuming a coiled conformation in the sporoplasm (Fig. 666). The number of coils is characteristic of the species. In cross-section the polar filament is composed of three to twenty concentric layers of electron-dense and – lucent material, resembling somewhat the annular rings of a tree trunk (Lom, 1972; Vavra and Larsson, 1999). The central core is filled with an electron-dense particulate material (Kudo and Daniels, 1963; Vavra and Larsson, 1999) which in view of the two- to three-fold increase in length of the extruded polar tube relative to polar filament has been suggested to be unpolymerized polar tube protein (Weidner, 1972, 1976, 1982; Frixione et al., 1992). The polar tube also exhibits deformability in that its diameter may increase two- to four-fold to

0.4 μm to accommodate passage of the sporoplasm during the last stages of spore germination (Ohshima, 1937; Lom and Vavra, 1963; Weidner, 1972; Frixione et al., 1992).

The spore wall plays a key role in the infectious process, as it must not only withstand environmental degradative stresses in the resting spore, but also resist the increasing turgor pressure during germination until the moment of rupture (Frixione et al., 1997). The spore wall throughout the phylum has been shown to consist of two layers easily distinguishable by transmission electron microscopy (TEM), the electron-lucent endospore and the electron-dense exospore (Vavra and Larsson, 1999). At the apical end of the spore whence the polar filament ruptures, the endospore is thinner and more electron-dense. The fine structure of each layer varies according to the species and is best appreciated by high-resolution TEM. In *Enc. cuniculi*, the exospore was demonstrated to consist of three layers of different electron densities (Bigliardi et al., 1996). The microsporidian endospore is rich in the polysaccharide chitin, which has been suggested to be a component of a microfibrillar network that is seen in the spore wall in some TEM preparations (Bigliardi et al., 1996; Prigneau et al., 2000).

Investigations of the molecular composition of both the polar tube and spore wall have been facilitated by the immunodominance of component proteins in natural infections and parasite lysate immunizations. Polyclonal and monoclonal antibodies isolated from sera of infected or immunized animals have led to the identification of polar tube (PTPs) and spore wall proteins (SWPs) from

human-infecting microsporidia of the family Encephalitozoonidae via immunohistochemical techniques (Beckers et al., 1996; Lujan et al., 1998; Visvesvara et al., 1994). For example, a 51-kDa protein (SWP1) staining the exospore of *Enc. cuniculi* was identified with the aid of a monoclonal antibody and the gene was cloned by immunoscreening an expression library (Bohne et al., 2000). Homologs of this protein have been identified in *Enc. hellem* (Bohne et al., 2000) and *Enc. intestinalis* (Hayman et al., 2001). Using proteomic techniques, two endospore-associated proteins, SWP3/EnP2 and EnP1, were discovered in *Enc. cuniculi* (Xu et al., 2006; Peuvel-Fanget et al., 2006). EnP1 was later localized to the exospore as well, and found to mediate adherence to host cells (Southern et al., 2007). Similar techniques were used to localize a putative chitin deacetylase to the *Enc. cuniculi* plasma membrane–endospore interface, suggesting a role in microsporidian endospore development (Brosson et al., 2005).

With the exception of the putative chitin deacetylase (Brosson et al., 2005), SWPs and PTPs identified thus far have no conserved functional domains or homology to known proteins (Bohne et al., 2000; Xu et al., 2006) and only limited similarity to each other (discussed in Xu et al., 2006). The first two Encephalitozoonidae spore wall proteins SWP1 and SWP2 (Bohne et al., 2000; Hayman et al., 2001) are both cysteine-rich and show conservation in their N-terminii, but SWP3 of *Enc. cuniculi* is dissimilar to these proteins (Xu et al., 2006), and the three PTPs of *Enc. cuniculi* differ in molecular weight and amino acid composition. While immunohistochemical data suggests structural roles for

all of these proteins, little is known about how they accomplish their specific functions. In addition, it is possible that other, perhaps lower-abundance component proteins of the spore wall and polar tube await discovery.

A so-called “shotgun” proteomic strategy in which proteins are identified from complex biological mixtures by liquid chromatography coupled to tandem mass-spectrometry (LC-MS/MS) was adopted in this portion of the work to search for novel components of the infectious apparatus of *Encephalitozoon cuniculi*. The chief advantages of such an approach over traditional molecular biological methods are that many unanticipated proteins may be identified simultaneously without the need for purpose-engineered antibodies and other specific detection reagents, and that the limit of detection is much lower (Han et al., 2008). As more and more full and partial genomes have become available, proteomic techniques have been applied to the study of other pathogenic protists. Examples of insights yielded by recent studies include the description of developmental and surface protein expression patterns, interactions with the host immune system, and drug-induced changes in protein expression of *Plasmodium falciparum*, the causative agent of malaria (Florens et al., 2002, 2004; Lasonder et al., 2002; Doolan et al., 2003; Makanga et al., 2005); identification of the contents of secretory and invasion-related organelles of *Toxoplasma gondii*, a close relative of malaria parasites and a widespread opportunistic pathogen of humans and other mammals (Bradley et al., 2005; Hu et al., 2006); delineation of stage-specific metabolism of *Trypanosoma cruzi*, the causative agent of Chagas’ disease (Roberts et al., 2009); and characterization of global proteomic

differences between *Entamoeba histolytica*, the causative agent of amoebic dysentery, and its non-pathogenic relative *Entamoeba dispar* (Leitsch et al., 2006).

Due to the emerging nature of these pathogens, proteomics-driven investigations of the microsporidia have been sparse, but the recent sequencing of the *Enc. cuniculi* genome by Vivares and colleagues (Katinka et al., 2001) has inaugurated a new era in which these approaches are beginning to come into focus. Utilization of this genome data has enabled the compilation of a list of highly abundant proteins in *Enc. cuniculi* (Brosson et al., 2006), and the identification of new spore wall proteins of *Nosema bombycis*, a silkworm-pathogenic species (Wu et al., 2008, 2009). In this portion of the work, the inferior solubility of the microsporidian polar tube and spore wall is harnessed to identify via mass spectrometry novel components of the infectious apparatus of these organisms. The work described herein represents the first large-scale proteomics-based immunohistochemical survey of hypothetical gene products conducted in *Enc. cuniculi*.

3.2

MATERIALS AND METHODS

3.2.1 Culturing of microsporidia to maximize spore yield and ensure purity

Continuously *Enc. cuniculi*- or *hellem*- infected rabbit kidney cell line RK13 (American Type Cell Culture Collection, Manassas, VA.) cultures were maintained in minimum essential medium (MEM) supplemented with fetal bovine serum concentration and 1% penicillin-streptomycin (Invitrogen, Carlsbad, CA) at 37°C and 5% CO₂ as previously described (Keohane et al., 1996). A reduced serum concentration of 7% (relative to the standard 10%) was used to slow the rate of host cell growth relative to the parasite, which increases parasite yield per flask. Culture supernatants including spores and dead, infected host cells were collected twice weekly and replaced with fresh medium. To purify spores, culture supernatants were centrifuged at 2500 X g and the pellets washed three times in PBS. Host cell debris and non-spore material were solubilized by incubation with 1% sodium dodecyl sulfate (SDS) in Dulbecco's modified phosphate-buffered saline (DPBS) at 37°C and removed by three DPBS washes and centrifugations.

In order to confirm the species identity of the microsporidian parasite being propagated in culture and to guard against cross-contamination by other species being propagated in the laboratory, infected host cultures were tested periodically by PCR. Infected culture monolayers were rinsed with PBS and dissociated from the flask by treatment with trypsin for 3 minutes. The trypsin was inactivated by the addition of culture medium. The monolayer was dissociated by repeated rinsing with culture medium, and centrifuged at 1000 X g. Genomic DNA was purified from the cell pellet with the QIAfilter DNeasy kit (Qiagen, Valencia, CA) according to manufacturer directions and quantified by

absorbance at 260 nm using a Nanodrop spectrophotometer. Diagnostic species-specific primers against microsporidian rRNA genes were used to confirm identity of the parasite to the species level. PCR was performed using 45 μ L PCR Supermix (Invitrogen), 2.5 μ L 25 mM MgCl₂, 0.5 μ L 55 ng/ μ L purified DNA or H₂O (control reaction), and 1 μ L 10 μ M each primer (forward and reverse primers for ribosomal *Enc. cuniculi* (De Groote et al., 1995; Visvesvara et al., 1994) were ECUNF 5' ATGAGAAGTGATGTGTGTGCG 3' and ECUNR 5' TGCCATGCACTCACAGGCATC 3', respectively. DNA was initially denatured for 5 min at 94 °C followed by 35 amplification cycles (1 min denaturation at 94 °C, 1 min annealing at 55 °C, 45 s extension at 72 °C) and 7 min final extension at 72 °C. PCR products were subjected to agarose gel electrophoresis and examined by ethidium bromide staining.

3.2.2 Fractionation of spores

Polar tube and spore wall proteins were fractionated from whole, purified *Enc. cuniculi* spores as previously described (Weidner, 1976; Keohane et al., 1994; 1996, 1998, 1999). Briefly, culture-purified spores were resuspended in 1 mL DPBS in a 2.0-mL screw-capped plastic bead-beater tube (Sarstedt, Newton, NC) half-filled with mechanically disrupted by beating with 400-600 μ m acid-washed glass beads (Sigma) for three two-minute pulses in a Mini Beadbeater (Biospec Products, Bartlesville, OK). Spores were cooled on ice for one minute between pulses. Glass beads were removed from the spore homogenate by puncturing the bottom of the bead-beater tube with a 23-gauge needle, placing

the tube in a 10 x 13 mm glass tube, and centrifuging at 1000 x *g* for 10 min. The clear buffer overlaying the pellet was used to wash the glass beads and the centrifugation procedure was repeated 2x. The pellet of disrupted spores was transferred to a low-retention microcentrifuge tube (Fisher) and washed 5x with 1% SDS/DPBS and three times with DPBS to remove SDS. The pellet was washed once with 9M urea and incubated with 2% dithiothreitol (DTT) in 25 mM Tris pH 7.4 with Complete Protease Inhibitor cocktail (Roche) for 2 hr at room temperature. The supernatant and pellet were separated, the pellet was washed three times in buffer by resuspension and centrifugation, and both fractions were saved at -80 °C.

3.2.3 Digestion and proteomic tandem mass spectrometry (MS/MS) analysis of spore lysate fractions

3.2.3.1 DTT-solubilized material

Residual detergent in samples can mask and confound the detection of peptides from mass spectrometric data. However, much of it can be removed from the DTT-solubilized spore supernatant material via repeated extraction with ethyl acetate (EA), in which detergent partitions out into the upper, organic layer while the sample is retained in the lower, aqueous layer (Yeung et al., 2008). Thus SDS was removed from the DTT-solubilized spore supernatant material by the addition of 10 volumes of fresh water-saturated EA followed by vigorous vortexing and removal of the upper organic layer containing EA and SDS. This

extraction procedure was repeated 6x. Residual EA was evaporated for 20 min. This material was then digested in-solution with bead-immobilized trypsin (Pierce) according to manufacturer directions overnight at 37°C in an Eppendorf Thermomixer shaker (Eppendorf, Westbury, NY). The digest was quenched by the addition of trifluoroacetic acid (TFA) to 0.15%. This material was then analyzed by nanospray liquid chromatography coupled with tandem electrospray ion-trap mass spectrometry (nanoLC–MS/MS) on a LTQ linear ion trap mass spectrometer (LTQ, Thermo, San Jose, CA) interfaced with a TriVersa NanoMate nanoelectrospray ion source (Advion BioSciences, Ithaca, NY). An Ultimate Plus nano-HPLC system with a Famous autosampler (Dionex Corporation, Sunnyvale, CA), was coupled with the TriVersa NanoMate. Peptides were loaded on a C18 μ -PrecolumnTM Cartridge (5 μ m, 100Å, 300 μ m i.d. x 5mm) from the autosampler with a 25 μ l sample loop at a flow rate of 15 μ l/min. After injection of sample, 20 μ L, and washing for 20 minutes, the precolumn was switched in line with the analytical column, a C18 PepMap100, 3 μ m, 100 Å, 75 μ m i.d. x 150 mm (Dionex Corporation, Sunnyvale, CA). Mobile phase B (80 % acetonitrile/water + 0.1 % formic acid) was increased from 2 to 55 % over 70 minutes, held for 5 minutes, increased to 95 % over 20 minutes and held at 95 % for 5 minutes. The flow rate used was 250 nL/min and mobile phase A consisted of 5% acetonitrile/water + 0.1 % formic acid. The ten most intense ions having a charge state between +2 to +4, determined from an initial survey scan from 300 -1800 m/z, were selected for MS/MS. MS/MS was performed using an isolation width of 3 m/z; normalized collision energy of 35 % and a minimum signal intensity of 500 counts. The

dynamic exclusion option is enabled. Once a certain ion is selected twice for MS/MS in 30 sec, this ion is excluded from being selected again for MS/MS during the next period of 120 sec. Dta files were created from the raw LTQ mass spectrometer LC-MS/MS data. The created dta files were then merged using the merge script tool from Matrix Science (<http://www.matrixscience.com>). The subsequent combined merge file was used to search the E_cuniculi 11 database (Oct. 13, 2004) database using the following parameters: trypsin, 2 missed cleavages; variable modifications of carbamidomethylation (Cys), deamidation (Asn and Gln) and oxidation (Met); monoisotopic masses; peptide mass tolerance of 3.0 Da; product ion mass tolerance of 0.6 Da. Proteins were considered identified having at least one bold red peptide (the most logical assignment of a peptide to a proteins and prevents duplicate homologous proteins to be reported) and having an ion score cut-off of 40 or greater. The workflow for handling the DTT-solubilized and –insoluble material is depicted in Figure 3.1.

3.2.3.2 DTT-insoluble material

Before subjecting the pellet remaining after DTT-solubilization to proteomic analysis, it was necessary to solubilize it as much as possible. In order to proteolytically digest the sample and subject it to nanoLC-MS/MS, it was first partially solubilized in 70% trifluoroacetic acid. The reducing agent Bond-Breaker™ TCEP (Tris(2-carboxyethyl)phosphine) (Pierce) was added to 50 μ M and the chemical cleavage agent cyanogen bromide was added to 20 mM.

Oxygen was displaced from the reaction by the aeration of nitrogen gas into the solution with a gel-loading pipet tip and the solution was incubated for 18 hr at room-temperature in the dark. The mixture was then evaporated overnight under nitrogen gas and the pellet was resuspended in 100 mM ammonium bicarbonate (ABC) pH 8.5 in a sonicating water bath for 30 min at RT. Urea was added to 8M and the sample was sonicated for 15 min after which point some material was still insoluble. This material was reserved and the rest of the procedure carried out on the solubilized material. Endoproteinase Lys-C (Roche) was added according to manufacturer's directions and the reaction was incubated overnight at 37°C. The urea concentration was then adjusted to 2M by the addition of 8.5M ABC and bead-immobilized trypsin (Pierce) was added. The reaction was quenched, the material was analyzed by nanoLC-MS/MS, and data was used to search the E_cuniculi 11 database (Oct. 13, 2004) as in section 3.2.3.1. The workflow for handling this material prior to LC-MS/MS is summarized in Fig. 3.1.

Fig. 3.1. Workflow for treatment of *Enc. cuniculi* lysate.

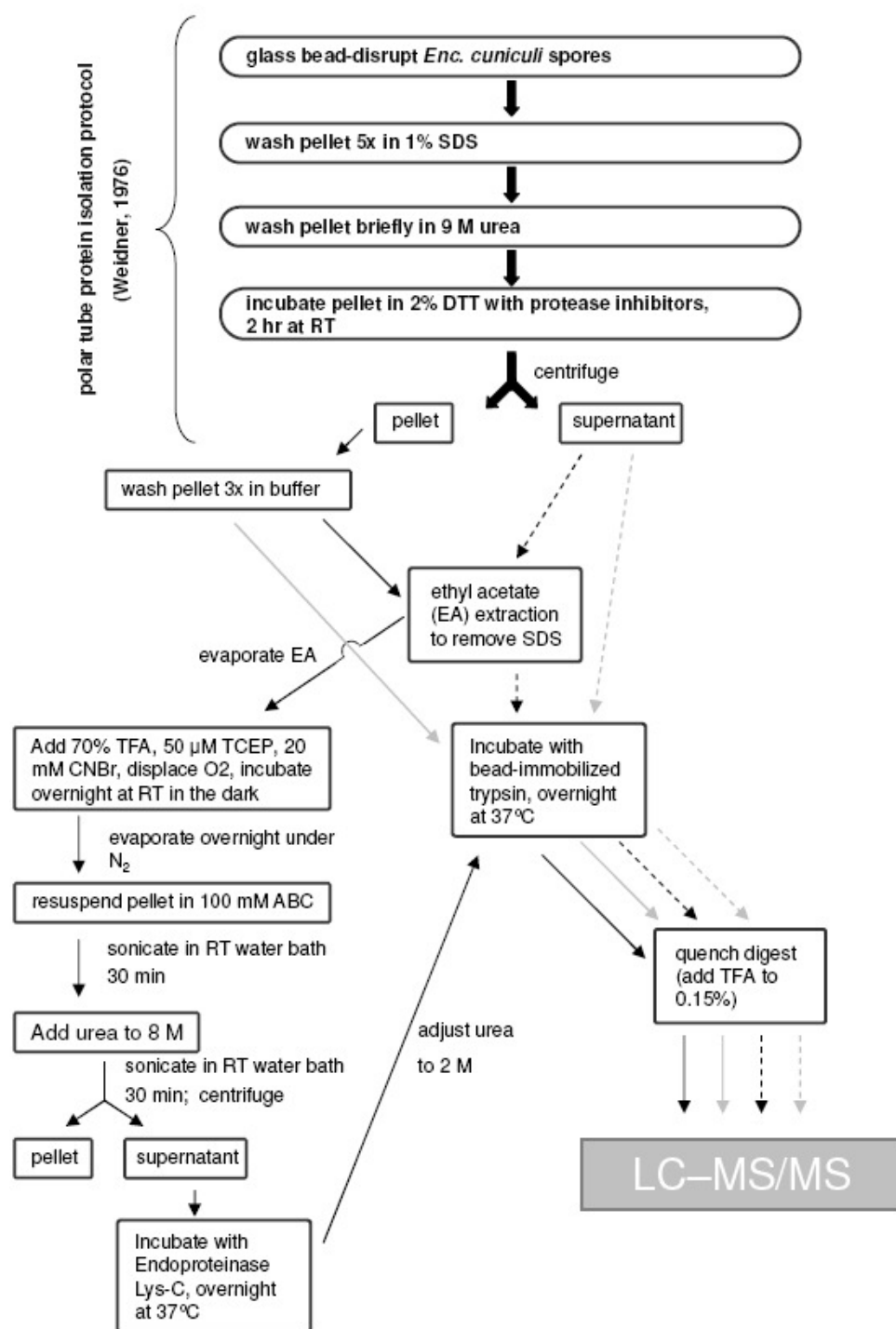


Fig. 3.1. Workflow for treatment of *Enc. cuniculi* lysate. This diagram describes how parasite lysates were fractionated, purified, and digested prior to LC-MS/MS analysis. Polar tube protein was isolated from whole spores according to Weidner (1976) (block arrows). Lysates from Experiments 1, 2, 3, and that by Y.Xu (Table 3.3) were processed according to the solid and dashed gray arrows; the lysate from preparation number 4 was processed according to the dashed black arrows, and number 5 according to solid black arrows.

3.2.4 Bioinformatic analysis of selected proteins

3.2.4.1 BLAST similarity search

It is common for biological samples to retain significant complexity even post-fractionation and consist of dozens of protein components (Liebler, 2002). Therefore it was necessary to prioritize a subset of the proteins to which the identified peptides match for further study. Identified hypothetical genes were searched for similarity to all proteins in the complete NCBI nr protein database using the BLAST algorithm (Altschul et al., 1997). Hypothetical proteins with no putative conserved domains or having similarity to known membrane or structural proteins were chosen for the generation of immunolocalization reagents. In addition, four *Enc. cuniculi* homologs (ECU01_0420, ECU04_0120, ECU07_0530, and ECU11_1210) to recently identified SWPs of the silkworm-parasitic microsporidium *Nosema bombycis* (Wu et al., 2008, 2009) were also selected for cloning and expression.

3.2.4.2 *in silico* predictions of biochemical attributes

The molecular weight (MW), isoelectric point (pI), grand average hydropathicity (GRAVY), and number of transmembrane helices for each hypothetical protein were calculated or predicted using TarO version 2.0 (url: <http://www.compbio.dundee.ac.uk/taro>) (Overton et al., 2008) and XtalPred (url: <http://ffas.burnham.org/XtalPred-cgi/xtal.pl>) (Slabinski et al., 2007). The means of expressed and non-expressed hypothetical proteins were compared by

the Student's t-test (MW, GRAVY, transmembrane helices: one-tailed; pI: two-tailed).

3.2.5 Amplification of genes from microsporidian genomic DNA and gel-purification of PCR products

PCR was performed using 45 μ L PCR Supermix (Invitrogen), 2.5 μ L 25 mM $MgCl_2$, 0.5 μ L 55 ng/ μ L purified RK13/parasite DNA, and 1 μ L 10 μ M each primer. Forward and reverse primers with 5' overhangs complementary to the pET-41 Ek-LIC vector directional cloning site (see below) and the length in base pairs of each hypothetical gene are indicated in Table 3.1. DNA was initially denatured for 5 min at 94°C followed by 5 initial amplification cycles and 30 final amplification cycles (1 min denaturation at 94°C, 1 min annealing at temperatures indicated in Table 3.1, extension at 72°C for time indicated in Table 3.1) and 7 min final extension at 72°C in a Eppendorf Mastercycler® Gradient Thermal Cycler (Eppendorf, Westbury, NY). PCR products were subjected to agarose gel electrophoresis and examined by ethidium bromide staining. Bands were excised from the gel using a clean scalpel under UV illumination. PCR products were purified from free primers, nucleotides, enzyme, buffer salts, and agarose using the silica membrane-based QIAquick Gel Extraction Kit (Qiagen, Valencia, CA). Purified PCR products were resuspended in H₂O and stored at –20°C.

Table 3.1. Primers and PCR conditions for amplification of hypothetical *Enc. cuniculi* genes

↓ locus_tag	length (base pairs)	primers (5' → 3')		annealing temp., °C (initial)	annealing temp., °C (final)	extension time, min:sec
		-forward	-reverse			
ECU01_0250	516	GAC GAC GAC AAG ATG CAC TTC AAC ATA TTT GTA G	GAG GAG AAG CCC GGT TTA TTT AGC CAG CTC AAC AG	49.0	63.0	1:00
ECU01_0420	717	GAC GAC GAC AAG ATG CCC ATG GAT AAG GAA AC	GAG GAG AAG CCC GGT TTA TTT TAC CTC CTC CAG TGC	52.3	69.0	0:54
ECU01_0440	405	GAC GAC GAC AAG ATG AGA TTA TAT AAA GCC ATG G	GAG GAG AAG CCC GGT TCA CAA CTC CTT CTT CTC TTC	50.0	63.0	1:00
ECU01_0990	3726	GAC GAC GAC AAG ATG CTG GTA GGC AAG CTG G	GAG GAG AAG CCC GGT CTA GTG GCT GCC CAA TGC T	54.0	70.0	4:30
ECU01_1070	1200	GAC GAC GAC AAG ATG ATA GGGCAA CTG AGT TT	GAG GAG AAG CCC GGT TCA TTT CTT CTC GTC GTA GC	49.7	68.9	1:35
ECU01_1240	1803	GAC GAC GAC AAG ATG ACT TTC ATA CTG CCG TC	GAG GAG AAG CCC GGT TCA CTT TCT GTG GTG GGT	48.8	66.3	2:45
ECU02_0150	663	GAC GAC GAC AAG ATG TTT GGC AGT AAA TAC TTG C	GAG GAG AAG CCC GGT TTA GTG GCA GAC TCC ACC	49.0	63.0	1:00
ECU02_1330	318	GAC GAC GAC AAG ATG TCT GTT GAA AGT ATT AAA AGG	GAG GAG AAG CCC GGT TTA TTT CCC ATT TGC ACC	50.6	68.2	0:54
ECU02_1540	1851	GAC GAC GAC AAG ATG AGG GTA TGG CTA GTT TGC	GAG GAG AAG CCC GGT TCA GAT CTC AGG AAT CCG AAG A	52.3	68.6	2:45
ECU03_0090	1869	GAC GAC GAC AAG ATG GGT GAA TGT CCC TTT CA	GAG GAG AAG CCC GGT TCA CAG AAC CTC CGC CTT	51.3	68.0	2:45
ECU03_0430	1245	GAC GAC GAC AAG ATG ATG CAG AGC ATC GAA TC	GAG GAG AAG CCC GGT TCA GTT GAA GAA GTA TAC TCT	47.3	67.3	1:45

Table 3.1. Full-length hypothetical *Enc. cuniculi* genes were amplified using primers with 5' extensions complementary to the directional cloning site of the pET-41 Ek/LIC vector (Novagen): forward primer extension 5' GACGACGACAAG 3'; reverse primer extension 5' GAGGAGAAGCCCCGGT 3'. Genes were amplified for 5 initial cycles and 30 final cycles at the listed initial and final annealing temperatures, respectively.

Table 3.1, continued. Primers and PCR conditions for amplification of hypothetical *Enc. cuniculi* genes

↓ locus_tag	length (base pairs)	primers (5' → 3')		annealing		extension time, min:sec
		•forward	•reverse	temp., °C (initial)	temp., °C (final)	
ECU03_0960	1398	GAC GAC GAC AAG ATG AAA CAG CTA GAC CTT CT GAG GAG AAG CCC GGT TCA TTT ATT TAT GCT CTC TTG		44.1	65.6	1:45
ECU03_1010	777	GAC GAC GAC AAG ATG GCA TCC AAG CAG TAC G GAG GAG AAG CCC GGT TTA ATT TTC ATC AGG ATC TCC C		51.1	69.0	1:00
ECU03_1230	990	GAC GAC GAC AAG ATG ATA AGT TCG ATC GGG TTT C GAG GAG AAG CCC GGT TTA TTG AAG ACT CTT TTC TTC AG		50.6	68.0	1:00
ECU04_0120	1476	GAC GAC GAC AAG ATG ACG GTA CGG GGC C GAG GAG AAG CCC GGT TCA AAA GTA AAA TGT TGT CGT G		53.2	71.6	1:35
ECU04_1480	654	GAC GAC GAC AAG ATG CCC TTA ATG AAG GAT GA GAG GAG AAG CCC GGT TTA TTG TGT CTT TTT CTT GAA AAT G		53.7	69.6	0:54
ECU04_1490	1644	GAC GAC GAC AAG ATG GCA AAT GAG GTT TCT AGG GAG GAG AAG CCC GGT TTA ATC TCC AAC ATA TTT GAT C		48.3	66.0	2:45
ECU05_0140	1377	GAC GAC GAC AAG ATG CAG GCA ATT TCC TCT AGC GAG GAG AAG CCC GGT TTA GCT ATT TAC TCC CTG CTC C		53.8	70.6	1:45
ECU05_0590	756	GAC GAC GAC AAG ATG AGT GCC ATT TCA AGC TTA GAG GAG AAG CCC GGT TTA CTT CTT AGA TCC TAT TTG TT		48.5	66.0	1:00
ECU05_0890	630	GAC GAC GAC AAG ATG AGG GGA GAG ATG CCG AT GAG GAG AAG CCC GGT CTA AGC CTT TGC TGC TCT CC		55.0	71.4	1:00
ECU06_0540	1167	GAC GAC GAC AAG ATG AAC TCG CTG TTT GGA AG GAG GAG AAG CCC GGT TCA GAA GCA TCC ACA GCA		49.4	68.3	1:45
ECU06_0650	372	GAC GAC GAC AAG ATG GTT AAT TCT GGA AGG CTG GAG GAG AAG CCC GGT TCA TTC GAT GGA CCT ACG G		54.2	69.9	0:54
ECU06_0660	2217	GAC GAC GAC AAG ATG GGT GGA AGA GAG CGC GAG GAG AAG CCC GGT TCA TAT GAA GCA TTT ATT TAC AG		48.8	66.3	2:45
ECU06_0720	744	GAC GAC GAC AAG ATG AAA AAC GGG ATT GAC TTC GAG GAG AAG CCC GGT TCA AAG GTC TTT ATT AGC CTG		49.9	67.3	1:00

Table 3.1, continued. Primers and PCR conditions for amplification of hypothetical *Enc. cuniculi* genes

↓ locus_tag	length (base pairs)	primers (5' → 3')	annealing temp., °C (initial)	annealing temp., °C (final)	extension time, min:sec
ECU06_1540	1500	•forward GAC GAC GAC AAG ATG CTA TCGACA TTT CTG TTC C •reverse GAG GAG AAG CCC GGT TTA AAC AAA GTT GTT GAG GTC G	49.4	68.3	1:45
ECU06_1560	2199	GAC GAC GAC AAG ATG TTT TTA GGA GAT CCG GA GAG GAG AAG CCC GGT CTA GGG TGC ATC CTT TTT GT	48.8	66.3	2:45
ECU06_1620	1720	GAC GAC GAC AAG ATG AAT CAA AGG GAT ACT CTG GAG GAG AAG CCC GGT TCA GAT CAC ACA TGG CCT	48.3	66.0	2:45
ECU07_0400	627	GAC GAC GAC AAG ATG AAG TTT AGT ACA CTC AAG C GAG GAG AAG CCC GGT TTA AGC CAG AGA CGA GTA C	50.0	63.0	1:00
ECU07_0500	567	GAC GAC GAC AAG ATG ATG GAA GAC AAG CAG G GAG GAG AAG CCC GGT TCA TAC TTT CTC GCC TTT CA	49.8	65.8	1:30
ECU07_0530	1239	GAC GAC GAC AAG ATG TAT TGT CTT CGC GC GAG GAG AAG CCC GGT TCA TGC AGA GAT TCT TGA C	48.6	68.0	1:35
ECU07_0640	606	GAC GAC GAC AAG ATG ACC TCA AGA TGC TCT GG GAG GAG AAG CCC GGT CTA TGG CCC AAA CTG CTC	50.6	67.9	1:00
ECU08_0420	1275	GAC GAC GAC AAG ATG TTT AAA CAC GAT TTT CG GAG GAG AAG CCC GGT TTA CTT CTT TTT GGG GAG AT	44.1	65.6	1:45
ECU08_0810	1305	GAC GAC GAC AAG ATG TTG TTG AAG TCG CTG G GAG GAG AAG CCC GGT CTA TTT ACA AAG ATG GGC CTT	49.8	65.8	1:30
ECU08_1020	411	GAC GAC GAC AAG ATG CTT ATC ATT AAA GGA TCA GG GAG GAG AAG CCC GGT CTA CGC CCC GTC TCT CTC	52.3	69.0	0:54
ECU08_1390	453	GAC GAC GAC AAG ATG AGG AAA ATT TAT TTA ACT ATG C GAG GAG AAG CCC GGT TCA CTT GGA ATC GTT TAT TTC	50.6	68.2	0:54
ECU08_1420	1362	GAC GAC GAC AAG ATG GCA AGC CTG GCG TAC T GAG GAG AAG CCC GGT TCA ACA GGA ATC GCC AGT GTC	55.8	71.6	1:45

Table 3.1, continued. Primers and PCR conditions for amplification of hypothetical *Enc. cuniculi* genes

↓ locus_tag	length (base pairs)	primers (5' → 3')		annealing temp., °C (initial)	annealing temp., °C (final)	extension time, min:sec
		•forward	•reverse			
ECU08_1700	783	GAC GAC GAC AAG ATG ATG AAA CAA ACT CTC CCA G GAG GAG AAG CCC GGT TTA TAC AAT AAT CTG CTC AGG ATA CC		52.1	71.2	1:30
ECU08_1730	645	GAC GAC GAC AAG ATG ATG CTT ATT GCC TTA TGC A GAG GAG AAG CCC GGT TTA AAC AAT GAG ACA GTC ACT AT		50.6	67.9	1:00
ECU08_1990	750	GAC GAC GAC AAG ATG CAT GGT TCA CTC AGC AT GAG GAG AAG CCC GGT TCA GAA AGA ACT GCC AGT TG		51.0	68.0	1:00
ECU09_0270	918	GAC GAC GAC AAG ATG AAC AAA GAG GCT TTT GA GAG GAG AAG CCC GGT CTA TCG GAA ATA ATG CTG GA		47.1	64.8	1:00
ECU09_0280	1059	GAC GAC GAC AAG ATG GAG GAT TAC ATT GGA AC GAG GAG AAG CCC GGT TTA CTT CAC CTT GTG TAT TTT AC		47.3	67.3	1:45
ECU09_0500	996	GAC GAC GAC AAG ATG AGG CTG AGC TCC ACA GAG GAG AAG CCC GGT TTA ATT GGT TCT TCC AAA AGA C		50.0	68.4	1:00
ECU09_1010	753	GAC GAC GAC AAG ATG GCG AAG AAG CAG CAG GAG GAG AAG CCC GGT TTA TTT GGA ATG GCC TTC CTC		54.2	69.9	0:54
ECU09_1080	870	GAC GAC GAC AAG ATG GAA AGA GAA GAA AAG ATC C GAG GAG AAG CCC GGT CTA GAA TAC GTC TTC TGT CCG		49.9	67.3	1:00
ECU09_1950	540	GAC GAC GAC AAG ATG GAT TGT TTG CCG AAA CAA GAG GAG AAG CCC GGT TTA ATC AGT CTT CTT GCT GCT		50.0	68.4	1:00
ECU10_1070	306	GAC GAC GAC AAG ATG ACA CAA GAA AGT ACG ATG GAG GAG AAG CCC GGT TCA GAA CAT CCC AAA GTC		48.0	67.0	0:54
ECU10_1160	3123	GAC GAC GAC AAG ATG GTT GTT AGA TGG AGG GAT G GAG GAG AAG CCC GGT TCA GGG TGT CCT GCA AGC TA		54.0	69.0	4:30
ECU10_1500	1371	GAC GAC GAC AAG ATG GAT GGA TGG TCT GGC GAG GAG AAG CCC GGT TCA ACT ACG GCT CTC CTC CT		49.4	68.3	1:45
ECU10_1620		GAC GAC GAC AAG ATG GAC GAA TTT GTT TCC CTC GAG GAG AAG CCC GGT TTA TGA AAC ACA CTT TCT ATG G		49.9	67.3	1:00

Table 3.1, continued. Primers and PCR conditions for amplification of hypothetical *Enc. cuniculi* genes

↓ locus_tag	length (base pairs)	primers (5' → 3')	annealing temp., °C (initial)	annealing temp., °C (final)	extension time, min:sec
		•forward •reverse			
ECU10_1810	1866	GAC GAC GAC AAG ATG CCC CGT AGA ACT ATG AG GAG GAG AAG CCC GGT TCA CAG AAC CTC CGC CTT	51.3	68.0	2:45
ECU11_0440	420	GAC GAC GAC AAG ATG AAA GAT CTA CTT AAA CAG AC GAG GAG AAG CCC GGT TTA CTT GAA TTT GTT CTT GTG G	50.0	63.0	1:00
ECU11_1210	888	GAC GAC GAC AAG ATG TTT CTC ATG ACA TCA ACT C GAG GAG AAG CCC GGT TTA GTA CTT GCA CTC GTC ATC	49.7	67.8	0:54
ECU11_1960	990	GAC GAC GAC AAG ATG GAA TTT GAT AGG ATA AGA G GAG GAG AAG CCC GGT TTA CTT CAG CAT GGC TAT G	46.0	63.0	1:00
ECU10_1660 (SWP1)	1353	GAC GAC GAC AAG ATG ATG AAG CTT TCA CTG C GAG GAG AAG CCC GGT TTA TGA AGA AGA TCC ACC AG	49.1	68.4	1:35

3.2.6 Cloning genes into bacterial expression vector and transformation and screening of cloning host strain

PCR products were directionally cloned into the pET-41 EK-LIC vector (EMD Biosciences, Gibbstown, NJ) as per the manufacturer. Briefly, vector-compatible overhangs on the PCR insert were generated by treating purified PCR product with T4 DNA polymerase at 22°C for 30 min, followed by inactivation of the enzyme at 75°C for 20 min. The insert was then annealed to the vector at 22°C for 5 min, and the ligation product was used to transform a chemically competent *recA endA* cloning strain of *Escherichia coli* (NovaBlue GigaSingles™ Competent Cells provided with the pET-41-EkLIC vector kit). For each hypothetical gene, five to ten colonies were screened for transformants by PCR with vector-specific primers (forward primer, STagF 5' GAACGCCAGCACATGGAC 3' ; reverse primer pET41R 5' AGGCGCGCCAAGGCCTG 3'). Plasmids were isolated from two to three PCR-positive colonies using the silica membrane-based QIAprep Spin Miniprep Kit (Qiagen, Valencia, CA) and were sequenced with the STagF primer by the Albert Einstein College of Medicine Sequencing Facility using a 3730 DNA Analyzer (Applied Biosystems, Foster City, CA). Purified plasmids were stored at -20°C.

3.2.7 Expression, detection, and purification of microsporidian proteins

5–10 ng of sequence-verified plasmid was used to transform a chemically competent protease-deficient strain of *Escherichia coli* harboring a plasmid encoding 7 tRNAs for rare codons in *E. coli* (genotype F⁻ *ompT hsdS_B*(r_B⁻ m_B⁻) *gal*

dcm pRARE2 (Cam^R), Rosetta 2™ Competent Cells, EMD Biosciences, Gibbstown, NJ). Two to three colonies of different diameters on the resulting agar plate were chosen to inoculate 2-mL Luria-Bertani broth (LB) cultures supplemented with Overnight Express™ Autoinduction System 1 (EMD Biosciences, Gibbstown, NJ) in 14-mL round-bottom polypropylene tubes (BD Falcon™ #352018, Franklin Lakes, NJ). Cultures were incubated at 30 °C or 37 °C for 20 hr with 250 rpm agitation, divided into 0.5-mL aliquots in 0.6-mL low-retention microcentrifuge tubes (Fisher), and centrifuged at 8000 rpm in a tabletop microcentrifuge to pellet the cells. The supernatants were discarded and the cell pellets frozen at –80 °C.

3.2.7.1 Evaluation of expression by SDS-PAGE and immunoblot

Expression of fusion protein was evaluated by SDS-electrophoresis of bacterial lysates followed by Coomassie staining of gels and immunoblot. Briefly, a frozen cell pellet equivalent to 75 µL of overnight bacterial culture was electrophoresed per lane in an 8% or 10% acrylamide gel. Gels were stained overnight at room temperature on an orbital shaker with the water-based Coomassie stain DyeHard™ (Crystalgen, Commack, NY) and destained with three changes of water. For immunoblots, nitrocellulose membranes were blocked in 5% non-fat dry milk (NFDM) in 0.1% Tween-20/DPBS. Immunodetection of the vector-encoded GST fusion tag was by primary antibody incubation with a 1:1000 dilution of anti-GST hybridoma supernatant (gift of Peter Davies, Albert Einstein College of Medicine) followed by secondary antibody incubation with a 1:1000

dilution of peroxidase–conjugated polyclonal goat anti-Mouse IgG (H+L) (Thermo Scientific, Rockford, IL). Immunoblots were visualized by chemiluminescence with ECL™ Western Blotting system (GE Healthcare Bio-Sciences, Piscataway, NJ).

Recombinant parasite proteins were purified from endogenous *E. coli* lysate proteins by acrylamide gel electrophoresis, visualization of protein bands by reverse zinc-staining and destaining using Zinc Stain and Destain Kit (BioRad, Hercules, CA) and excision of the band with a clean scalpel. Excised gel bands were processed immediately for immunization or stored at -80°C .

3.2.7.2 Confirmation of identity of recombinant ECU10_1500 by MALDI-TOF mass spectrometry

3.2.7.2.1 In-gel digestion

Bacterial protein lysate was subjected to SDS-PAGE electrophoresis and the gel was stained by Coomassie blue as described in section 3.2.7. The overexpressed band which unexpectedly migrated at approximately 120 kDa (see Fig. 3.5, upper panel) was excised with a clean scalpel, cut into 1 mm^3 pieces, and placed into a low retention 1.5-mL microcentrifuge tube (Fisher). A slice from a protein-free region of the gel was processed identically for use as a control. The gel pieces were incubated in 300 μL of 50 mM ammonium bicarbonate (NH_4HCO_3 , “ABC”) / 50% acetonitrile (CH_3CN , “ACN”) for 35-40 min in a shaking 35°C water bath. This step was repeated 3x to completely destain the gel. Gel pieces were dehydrated by the addition of 25 mM ACN (100 μL).

The ACN was removed by pipet and the gel was dried further in a SpeedVac concentrator (Thermo Fisher Scientific, Waltham, MA) for 3 min. The gel pieces were incubated in 100 μ L 10 mM dithiothreitol (DTT) in 25 mM ABC for 30 min at 56 °C and 15 min at RT to reduce the proteins. The DTT was removed and alkylation was accomplished by the addition of 100 μ L 55 mM iodoacetamide (“IAA”) in 25 mM ABC and incubation at 45 °C in the dark at RT. The IAA was removed and 100 μ L 25 mM ABC was added to the tube of gel pieces which was then vortexed, placed in sonicating water bath, vortexed and centrifuged. The ABC was removed and this vortex-sonication-centrifugation cycle was repeated 2x with 1:1 50 mM ABC/ACN. The solution was removed and dehydrated with ACN as before, with an additional vortex-sonication-centrifugation step prior to complete dehydration in a SpeedVac. The gel pieces were then rehydrated by the addition of 30 μ L 20 ng/ μ L sequencing grade modified trypsin (Promega, Madison, WI) in 25 mM ABC and placement of the microcentrifuge tubes on ice for 45 min. All but 2 μ L of the trypsin solution was removed and replaced with 50 μ L 25 mM ABC. Proteolytic digestion proceeded for 16 hr at 37 °C. The digest was halted by the addition of 1% trifluoroacetic acid (TFA) to a final concentration of 0.1%.

3.2.7.2.2 MALDI-TOF mass spectrometry

The digest solution was bound to a pre-equilibrated C18 ZipTip (Millipore, Billerica, MA) according to manufacturer directions and eluted with α -Cyano-4-hydroxycinnamic acid (“ α -HC”) matrix (Sigma-Aldrich, St. Louis, MO) onto a 100-

well MALDI-TOF target sample plate (Applied Biosystems, Foster City, CA).

Mass spectrometric data was collected using an AB Voyager System DE-STR MALDI-TOF mass spectrometer (Applied Biosystems, Foster City, CA). The data was acquired in reflector mode with a laser intensity of 1610. A mass range of 500 – 4000 Daltons was examined and 300 laser shots were averaged for each mass spectrum. The spectrum was internally calibrated on prominent autolysis peaks of trypsin (842.51, monoisotopic; 1045.56, monoisotopic; 2212.43, average) and the α -HC matrix trimer (568.14, monoisotopic).

3.2.7.2.3 Peptide mass fingerprinting

Monoisotopic m/z peaks from the acquired spectrum were manually identified and used to conduct a trypsin peptide mass fingerprint search of the E_cuniculi 11 (13Oct2004) database with Mascot (www.matrixscience.com, Matrix Science Inc., Boston, Mass.). The following parameters were stipulated: carbamidomethyl (fixed), deamidated (variable), Gln \rightarrow pyro-Glu, Glu \rightarrow pyro-Glu (variable), oxidation (variable), peptide mass tolerance \pm 0.5 Da, peptide charge state 1⁺, and 1 maximum missed cleavage.

3.2.8 Immunization of mice

Mice were immunized with either a slurry of crushed gel in DPBS, or with protein electroeluted from the gel mixed with Freund's Complete Adjuvant (Sigma-Aldrich, St. Louis, MO). Gel bands representing five lane-widths of an 8 x 10 cm gel were crushed with a polypropylene Kontes Pellet Pestle in accompanying

microcentrifuge tube (Fisher, Pittsburgh, PA). DPBS was added to 1 mL and the slurry was passed several times through an 18- and then 23-gauge needle. Alternatively, protein was electroeluted from freshly excised (not frozen) gel bands by electrophoresis in 0.025% SDS in standard Western Blotting Tris-Glycine buffer for 400-500 volt-hours at 4 °C in an electrophoresis-compatible dialysis cassette, the D-Tube Dialyzer (EMD Biosciences, Gibbstown, NJ). Eluate was dialyzed at 4 °C against three 1 L changes of DPBS diluted 1:1 with H₂O, evaporated by vacuum centrifugation to 0.3 mL, mixed with Freund's Complete Adjuvant at a ratio of 1:2, and emulsified for 1 min in a 1 mL syringe with a motor-driven pestle.

For each parasite protein, mice were immunized in duplicate or triplicate. Each mouse was injected intradermally (i.d.) and intraperitoneally (i.p.) using a 23-gauge needle with a total of 0.2-0.3 mL acrylamide/PBS slurry or 0.2 mL adjuvant emulsion. 0.2 mL blood was collected per mouse by retroorbital bleed four weeks post immunization. Cells were pelleted from whole blood by centrifugation at 5000 rpm for 15 min in a tabletop microcentrifuge and the sera were stored at 4 °C or -80 °C. Mice were reimmunized (boosted) with acrylamide/PBS slurry or Freund's incomplete adjuvant and blood was again collected 4 weeks post reimmunization.

3.2.9 Evaluation of sera by Immunoblot

Immunoblots against crude bacterial lysates and/or fractionated, DTT-solubilized parasite lysates were used to evaluate serum specificity. In the latter case,

membranes were blocked and antibodies diluted in 1% bovine serum albumin (BSA) + 5% NFDM (“Blotto”). Mouse sera diluted 1:500 or 1:1000 were used as primary antibody; the remainder of the immunoblotting procedure was performed as described in section 3.2.7.1.

3.2.10 Immunolocalization of hypothetical protein “hits” *in situ*

Antisera against all successfully expressed recombinant parasite proteins were tested via immunofluorescence assay (IFA) for reactivity against *Enc. cuniculi*-infected RK13 host cell culture. Antisera to recombinant hypothetical protein ECU10_1500 was also tested against *Enc. hellem*-infected RK13 host cell culture and evaluated by immunoelectron microscopy.

3.2.10.1 Immunofluorescence microscopy

Infected host cell cultures on 4-well Permanox plastic chamber slides (Thermo Fisher Science, Rochester, NY) or poly-D-Lysine + laminin-coated glass coverslips (BD, Franklin Lakes, NJ) were rinsed 2x with DPBS at RT, fixed with 2% formaldehyde/DPBS for 30 min at RT, rinsed 3x with DPBS, permeabilized in 0.2% Triton X-100/DPBS for 20 min, and blocked overnight in 3% BSA/0.2% Triton X-100/DPBS at 4°C. Subsequent steps including antibody incubations and washes were performed in 1% BSA/0.2% Triton X-100/DPBS. Fixed host cell cultures were incubated with various dilutions (between 1:100 and 1:3000) of mouse antisera to recombinant parasite proteins at 37°C for 1.5 hr in a humidity chamber, rinsed 3x, and incubated with a 1:500 dilution of goat anti-mouse IgG

conjugated to AlexaFluor 488 or 594 (Invitrogen, Carlsbad, CA) for 1 hr at 37°C, and rinsed 2x. Some cultures were incubated with 1 µg/mL 4',6-diamidino-2-phenylindole (DAPI) for 15 min at RT before the final wash. Cultures were then mounted with ProLong Antifade mounting medium (Invitrogen, Carlsbad, CA) and cured overnight in the dark. Culture slides were viewed with an epifluorescence-equipped microscope (Zeiss AxioVert 200M, Carl Zeiss, Goettingen, Germany). Images were captured with a Zeiss AxioCam monochrome digital camera (Carl Zeiss, Goettingen, Germany) and false color was assigned according to the known emission wavelength of each fluorophore. Where indicated, incremental 0.2-µm Z-stack images were captured from culture slides and deconvolved using the Iterative Maximum Likelihood algorithm in the deconvolution module of Zeiss Axiovision software.

3.2.10.2 Correlative light–immunolectron microscopy

Enc. hellem was chosen for analysis by immunoEM, as parasitophorous vacuoles were more frequently stained by ECU10_1500 antiserum than were those of *Enc. cuniculi*. Infected host cell cultures grown on treated glass coverslips were processed as in section 3.2.10.1 through incubation with mouse antiserum, inclusive. They were then rinsed 3x with 1% BSA/0.2% Triton X-100/DPBS, incubated with a 1:50 dilution of Alexa Fluor® 488 FluoroNanogold (Nanoprobes, Yaphank, NY) for 25 min at 37°C and 35 min at RT and rinsed 3x with 1% BSA/0.2% Triton X-100/DPBS. Cultures were post-fixed in 2% formaldehyde/DPBS for 3 min at RT, washed 3x in DPBS and 3x in H₂O. The

cultures were then enhanced by silver-deposition for 15 or 25 min with the LI Silver Enhancement Kit (Nanoprobes, Yaphank, NY) as per manufacturer directions and imaged using brightfield optics with a Nikon DMicrophot-FXA microscope. Images were captured using a Nikon FX-35DX digital camera controlled by Nikon Digital Sight DS-L1 software and visualization screen (Nikon Instruments, Melville, NY).

To process for immunoEM, the cultures were dehydrated in graded ethanols and embedded *in situ* in Epon resin. Glass coverslips were removed by treatment with hydrofluoric acid. Thin sections were cut with a microtome and mounted on Formvar-coated grids, stained with uranyl acetate, and observed and photographed with a JEOL 1200 EX transmission electron microscope in the Albert Einstein College of Medicine Analytical Imaging Facility.

3.3

RESULTS

3.3.1 Purity of parasites harvested from culture

Enc. cuniculi- and *Enc. hellem*- infected RK13 host cell cultures maintained in our laboratory were shown by PCR of ribosomal DNA (Fig. 3.2) to be positive and pure for each species of microsporidia.

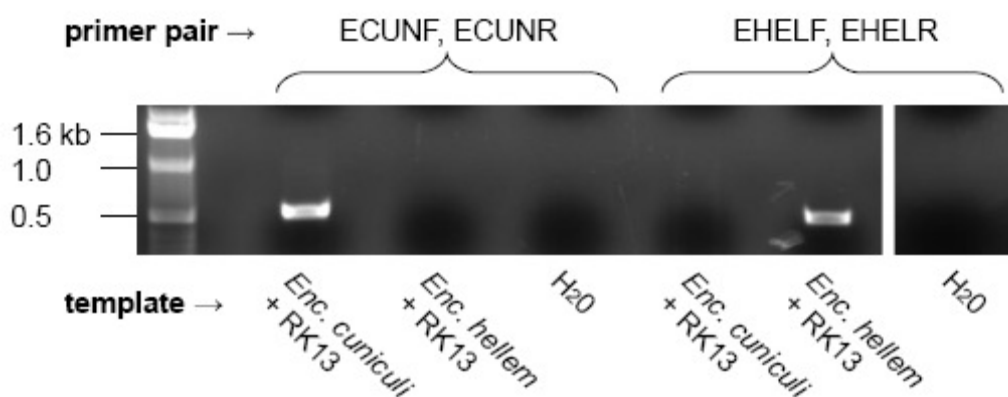


Figure 3.2. Verification of purity of microsporidia cultured *in vitro*. Expected amplicon size for *Enc. cuniculi* and *Enc. hellem* amplicons are 549 and 547 bp, respectively.

3.3.2 Results of LC-MS/MS experiments

Proteins identified by LC-MS/MS identified by MS/MS for experimental preparation numbers 4 (DTT-soluble) and 5 (DTT-insoluble) are listed in Table 3.2. Previously characterized PTPs and SWPs, other genes with assigned functions, and uncharacterized hypothetical genes were identified from each fraction. Detected peptides assigned to hypothetical proteins selected for heterologous expression in *E. coli* and/or percent coverage for these proteins are shown in Table 3.3. Peptides assigned to SWPs and PTPs are also included in Table 3.3.

Table 3.2. Proteins identified by LC-MS/MS of fractionated *Enc. cuniculi* spore lysate
 Experiment 4: DTT-soluble fraction

functional category	accession number, description
characterized polar tube proteins (PTPs)	PTP_ENCCU (O76942) Major polar tube protein precursor (Major PTP) (Q8SRT0) PTP2 (Q8SU21) PTP3
characterized spore wall proteins (SWPs)	SWP1_ENCCU (Q9XZV1) SWP 1 precursor (Q8SWL3) EnP1 (Q8SWI4) SWP3 (Q8SU65) putative chitin deacetylase
other annotated proteins	(Q8SVQ9) Zinc finger protein (Q8SQL7) Thiolttransferase (Glutaredoxin) (Q8SSL7) Phosphoacetyl-glucosamine mutase (Q8SSI6) RAN specific GTPase activating protein (Q8SRE1) Peptidyl-prolyl cis-trans isomerase (PPIase) (Rotamase) (Q8SSA1) Nucleolar protein of the GAR family (Q8SSE8) Heat-shock protein HSP90 homolog (Q8SQY5) Trptophanyl tRNA synthetase (Q8SS29) Translation elongation factor 1 alpha (Q8SR93) General Transcription Factor (Q8SQM2) 40S ribosomal protein S28 (Q8SQX3) 40S ribosomal protein S7
hypothetical proteins	(Q8STR5) Hypothetical protein ECU09_1010 (Q8SUB5) Hypothetical protein ECU10_1500 (Q8SUD4) Hypothetical protein ECU10_1070 (Q8SUM7) Hypothetical protein ECU08_1390 (Q8SUP6) Hypothetical protein ECU08_1020 (Q8SUS9) Hypothetical protein ECU08_0420 (Q8SVC2) Hypothetical protein ECU06_0650 (Q8SW99) Hypothetical protein ECU02_1330 (Q8SWJ8) Hypothetical protein ECU01_1070 (Q8SWP0) Hypothetical protein ECU01_0440 (Q8SV33) Hypothetical protein ECU07_0400

Table 3.2, continued. Proteins identified by LC-MS/MS of fractionated *Enc. cuniculi* spore lysate
 Experiment 5: DTT-insoluble fraction

functional category	accession number, description
characterized polar tube proteins (PTPs)	PTP_ENCCU (Q76942) Major polar tube protein precursor (Major PTP) (Q8SRT0) PTP2 (Q8SU21) PTP3
characterized spore wall proteins (SWPs)	SWP1_ENCCU (Q9XZV1) Spore wall protein 1 precursor (Q8SWL3) EnP1 (Q8SWI4) SWP3
other annotated proteins	(Q8SVQ9) Zinc finger protein (Q8SRL6) Required for nuclear division (Spindle POLE body DUPLICATION) (Q8SQS2) NIFS-like protein (Cysteine DESULFURASE) involved in Fe-S cluster synth. (Q8SRZ2) Vacuolar ATP synthase subunit E (Fragment) (Q8SWI8) similarity to DNA helicase (Q8SVC0) Protein kinase domain (Q8SS77) Histone H3 (Q8SQP4) Histone H4 (Q8SS29) Translation elongation factor 1 alpha (Q8SQT7) Translation elongation factor 2 (Q8SS53) 40S ribosomal protein S11 (Q8SR65) 40S ribosomal protein S23 (Q8SRN2) 40S ribosomal protein S26 (Q8SS34) 40S ribosomal protein S27 (Q8SRQ3) 60S ribosomal protein L5 (Q8SUW1) similarity to ribosomal protein L5 (Q8SSM6) 60S ribosomal protein L8 (Q8SR18) 60S ribosomal protein L44 (L42 in yeast)
hypothetical proteins	(Q8SUK1) Hypothetical protein ECU08_1730 (Q8SUK4) Hypothetical protein ECU08_1700 (Q8SUQ8) Hypothetical protein ECU08_0810 (Q8SUV9) Hypothetical protein ECU07_1550 (Q8SV27) Hypothetical protein ECU07_0500 (Q8SV33) Hypothetical protein ECU07_0400

Table 3.3. Detection of peptides for selected hypothetical genes and polar tube and spore wall proteins identified by LC-MS/MS. For each detected protein, detected peptides or amino acid sequence coverage, 95% confidence interval (where available) are indicated

Experiment no. → ↓ locus_tag	Y. Xu	1 (soluble)	1 (pellet)
ECU01_0250			
ECU01_0440			
ECU01_0990			
ECU01_1070			
ECU01_1240			KIELLR
ECU02_0150			
ECU02_1330			
ECU02_1540			
ECU03_0090	x		
ECU03_0430		MMQSIESMCLVNKK	
ECU03_0960	x		
ECU03_1010			
ECU03_1230			
ECU04_1480			
ECU04_1490	x		
ECU05_0140			
ECU05_0590			
ECU05_0890			
ECU06_0540			
ECU06_0650			
ECU06_0660	x		
ECU06_0720			
ECU06_1540	x		
ECU06_1560			
ECU06_1620		FKRLFSEK LVAIGVLESGEK LVAIGVLESGEK	
ECU07_0400			
ECU07_0500			
ECU07_0640	x		
ECU08_0420			RLGLENAR
ECU08_0810			
ECU08_1020			
ECU08_1390			
ECU08_1420			
ECU08_1700			
ECU08_1730			
ECU08_1990		VYLDGLDVVEK	
ECU09_0270			
ECU09_0280			
ECU09_0500	x		
ECU09_1010			
ECU09_1080			
ECU09_1950			
ECU10_1070			
ECU10_1160	x		
ECU10_1500		FFENLEER	
ECU10_1620			
ECU10_1810	x		
ECU11_0440			
ECU11_1960			

Table 3.3, continued. Detection of peptides for selected hypothetical genes and polar tube and spore wall proteins identified by LC-MS/MS. For each detected protein, detected peptides or amino acid sequence coverage, 95% confidence interval (where available) are indicated

Experiment no. → ↓ locus_tag	Y. Xu	1 (soluble)	1 (pellet)
ECU06_0250 (PTP1)		TSENETSPSAPAEDVGCK	
ECU06_0240 (PTP2)	x	CNLGCELK IMANLPQPK ISDVENSTSLYR SASQSDGEGTAEDAEVQQPSADGEGLE	
ECU11_1440 (PTP3)			
ECU10_1660 (SWP1)	x	VIGDLLAR TPIINMGER	NNLLGR
ECU01_1270 (SWP3)	x	EVSQWQVVR EVSQWQVVRGEDR	KIELLR
ECU01_0820 (EnP1)		NCILEPLPK AASVGGFQAATSSEK	KVEVLK NCILEPLPK AASVGGFQAATSSEK IYVEGSARPAQCSEVCIEPVER

Table 3.3, continued. Detection of peptides for selected hypothetical genes and polar tube and spore wall proteins identified by LC-MS/MS. For each detected protein, detected peptides or amino acid sequence coverage, 95% confidence interval (where available) are indicated

Experiment no. → ↓ locus_tag	2 (soluble)	2 (pellet)
ECU01_0250	GVFIDQSYPLR	
ECU01_0440	LAGYMDVTGEQNEEEKEL	
ECU01_0990		FDIVADAR
ECU01_1070		
ECU01_1240		
ECU02_0150	IPVEVYVSEAGR RIPVEVYVSEAGR	
ECU02_1330		
ECU02_1540		
ECU03_0090		
ECU03_0430		
ECU03_0960		
ECU03_1010	YKAEVVTGPEHSEVSK	
ECU03_1230		
ECU04_1480		
ECU04_1490		
ECU05_0140		
ECU05_0590	SDKEEVISGLYK	
ECU05_0890		
ECU06_0540		GIGKPR
ECU06_0650		
ECU06_0660		
ECU06_0720		
ECU06_1540		
ECU06_1560	FVNMDVNVEKIYGK	
ECU06_1620		
ECU07_0400	ETTTYVNPYEVK TTGKDTFTPEMTR TTGKDTFTPEMTRK TSGSEDAKGEESAVEGKEPEQGENDEVANPTK	
ECU07_0500		
ECU07_0640		
ECU08_0420		
ECU08_0810		
ECU08_1020		
ECU08_1390		
ECU08_1420		
ECU08_1700		
ECU08_1730	AVMSESGKPAEFKTDEVSPGVK	
ECU08_1990		
ECU09_0270	EDLVIK	
ECU09_0280		
ECU09_0500		
ECU09_1010		
ECU09_1080	KSVSGNSKATGR	
ECU09_1950	TVAESEFNKKDVISSK	
ECU10_1070		
ECU10_1160		
ECU10_1500	HVIGAACMLTQK AIQAQEPEEKDIINQK	
ECU10_1620		
ECU10_1810		
ECU11_0440		MKDLLK
ECU11_1960		LNPEDGIRILAIGEEIIR

Table 3.3, continued. Detection of peptides for selected hypothetical genes and polar tube and spore wall proteins identified by LC-MS/MS. For each detected protein, detected peptides or amino acid sequence coverage, 95% confidence interval (where available) are indicated

Experiment no. → ↓ locus_tag	2 (soluble)	2 (pellet)
ECU06_0250 (PTP1)	IAVLK TSENETSPSAPAEDVGTCK	
ECU06_0240 (PTP2)	AMIER IMANLQPK KLEGAEIMR SKIMANLQPK AVESFNKEVSK ISDVENSTSLYR ANEKAVESFNKEVSK ISDVENSTSLYRGDK AVESFNKEVSKGPSQK SASQSDGEGTAEDAQVQPSADGEGLE EGEKASQSDGEGTAEDAQVQPSADGEGLE	
ECU11_1440 (PTP3)	AVADEIKDANVR VLESTGDISEAAK LPANNGPVSNAAPAR ILTDVAASSAEDLAK AAAIAGGGQVAAQNAADR ETATSNLEVKVIPPTTSR LSQAAALKDAASMEGLDNPVVQEK	
ECU10_1660 (SWP1)	NNLLGR FKNDVR NNLLGRR QMAVFQR	AADLAALDAAEATSLAGTIR
ECU01_1270 (SWP3)	AVPIYAPSAEEVR EVSQPVVQGEDR AVPIYAPSAEEVRESISSVR	
ECU01_0820 (EnP1)	NLHLK KVEVLK CKTFPR RGEVVVR NCILEPLPK AASVGGFQAATSSEK GNNNKNCILEPLPK NGEIRGNNNKNCILEPLPK GTPMVLVDNGALAPFDPYTNTAK	GNNNKNCILEPLPK

Table 3.3, continued. Detection of peptides for selected hypothetical genes and polar tube and spore wall proteins identified by LC-MS/MS. For each detected protein, detected peptides or amino acid sequence coverage, 95% confidence interval (where available) are indicated

Experiment no. → ↓ locus_tag	3 (soluble)	3 (pellet)
ECU01_0250		
ECU01_0440		
ECU01_0990		
ECU01_1070		
ECU01_1240		
ECU02_0150		
ECU02_1330		
ECU02_1540	GDDVDEIKK	
ECU03_0090		
ECU03_0430		
ECU03_0960		
ECU03_1010		
ECU03_1230	QMGDAVR MISSIGFLPTGTSMEK	
ECU04_1480		
ECU04_1490		
ECU05_0140	NAITEAR	
ECU05_0590		
ECU05_0890	IIAEVFGDVMDGFVRK	
ECU06_0540		
ECU06_0650		
ECU06_0660		
ECU06_0720	SIMDKDWASINRGMIR	
ECU06_1540		
ECU06_1560		
ECU06_1620		
ECU07_0400		
ECU07_0500		
ECU07_0640		
ECU08_0420		
ECU08_0810		
ECU08_1020		
ECU08_1390		
ECU08_1420		KIDKIK
ECU08_1700		
ECU08_1730		
ECU08_1990		
ECU09_0270		
ECU09_0280	IKDGNAGEGTK	
ECU09_0500		
ECU09_1010		
ECU09_1080		
ECU09_1950		
ECU10_1070		
ECU10_1160	INRTLEEWLAR	
ECU10_1500		
ECU10_1620		NIEKIK
ECU10_1810		
ECU11_0440		
ECU11_1960		

Table 3.3, continued. Detection of peptides for selected hypothetical genes and polar tube and spore wall proteins identified by LC-MS/MS. For each detected protein, detected peptides or amino acid sequence coverage, 95% confidence interval (where available) are indicated

Experiment no. → ↓ locus_tag	3 (soluble)	3 (pellet)
ECU06_0250 (PTP1)		
ECU06_0240 (PTP2)		
ECU11_1440 (PTP3)	KTNALNFLSK ILTDVAASSAEDLAK	
ECU10_1660 (SWP1)		QMAVFQR
ECU01_1270 (SWP3)		
ECU01_0820 (EnP1)		

Table 3.3, continued. Detection of peptides for selected hypothetical genes and polar tube and spore wall proteins identified by LC-MS/MS. For each detected protein, detected peptides or amino acid sequence coverage, 95% confidence interval (where available) are indicated

Experiment no. → ↓ locus_tag	4 (soluble) (sequence coverage)	5 (pellet)
ECU01_0250		
ECU01_0440	14.9	
ECU01_0990		
ECU01_1070	12.5	
ECU01_1240		
ECU02_0150		
ECU02_1330	12.4	
ECU02_1540		
ECU03_0090		
ECU03_0430		
ECU03_0960		
ECU03_1010		
ECU03_1230		
ECU04_1480	38.7	
ECU04_1490		
ECU05_0140		
ECU05_0590		
ECU05_0890		
ECU06_0540		
ECU06_0650	11.4	
ECU06_0660		
ECU06_0720		
ECU06_1540		
ECU06_1560		
ECU06_1620		
ECU07_0400	37.0	FVPGPVLES LDKVAFASER
ECU07_0500		VLGAVNAVEAK
ECU07_0640		
ECU08_0420	2.83	
ECU08_0810		ALVLSLLNSIPK
ECU08_1020	19.1	
ECU08_1390	8.7	
ECU08_1420		
ECU08_1700		SAQVLVFNEEPEHK
ECU08_1730		AVMSESGKPAEFKTDEVSPGVK
ECU08_1990		
ECU09_0270		
ECU09_0280		
ECU09_0500		
ECU09_1010	4.0	
ECU09_1080		
ECU09_1950		
ECU10_1070	13.9	
ECU10_1160		
ECU10_1500	22.6	
ECU10_1620		
ECU10_1810		
ECU11_0440		
ECU11_1960		

Table 3.3, continued. Detection of peptides for selected hypothetical genes and polar tube and spore wall proteins identified by LC-MS/MS. For each detected protein, detected peptides or amino acid sequence coverage, 95% confidence interval (where available) are indicated

Experiment no. → ↓ locus_tag	4 (soluble) (sequence coverage)	5 (pellet)
ECU06_0250 (PTP1)	14.7	TSENETSPSAPAEDVGTCK
ECU06_0240 (PTP2)	49.0	KLEGAEIMR SKIMANLPQPK ISDVENSTSLYR AVESFNKEVSKGPSQK REMYFNQIGQLVGAR
ECU11_1440 (PTP3)	6.4	AQDLSSYLTK LPANNGPVSNAPAAR MAHEAEVAAASEMK SVGSSSVGAVSEEAKK AAAIAAGGGQVAAQNAADR LSQAAALKDAASMEGLDNPVVQEK
ECU10_1660 (SWP1)	5.1	TPIINMGER GNCQMCPEGTR YFEKNNLLGR
ECU01_1270 (SWP3)	9.0	EVSWQPVR AVPIYAPSAEEVR EVSWQPVRGEDR AVPIYAPSAEEVRESISSVR
ECU01_0820 (EnP1)	7.6	YLQAMNIK NCILEPLPK AASVGGFQAATSSEK YVLCVEACPFGSK AYVLYWNDHDLR GNNNKNCILEPLPK HGLFGVEFGPLDLDR K.KAYVLYWNDHDLR GTPMVLVDNGALAPFDPYTNTAK IVVNPSPSNCIPCEPECYDSSSSSECNKRR

3.3.3 Amplification of microsporidian genes

Each of the 52 genes were PCR-amplified from purified RK13 / *Enc. cuniculi* DNA as either a single (88%) or dominant band (10%) (results for a subset of the 52 genes are shown in Fig 3.3), except for ECU08_1700. The PCR reaction for this gene resulted in multiple weak PCR products (data not shown).

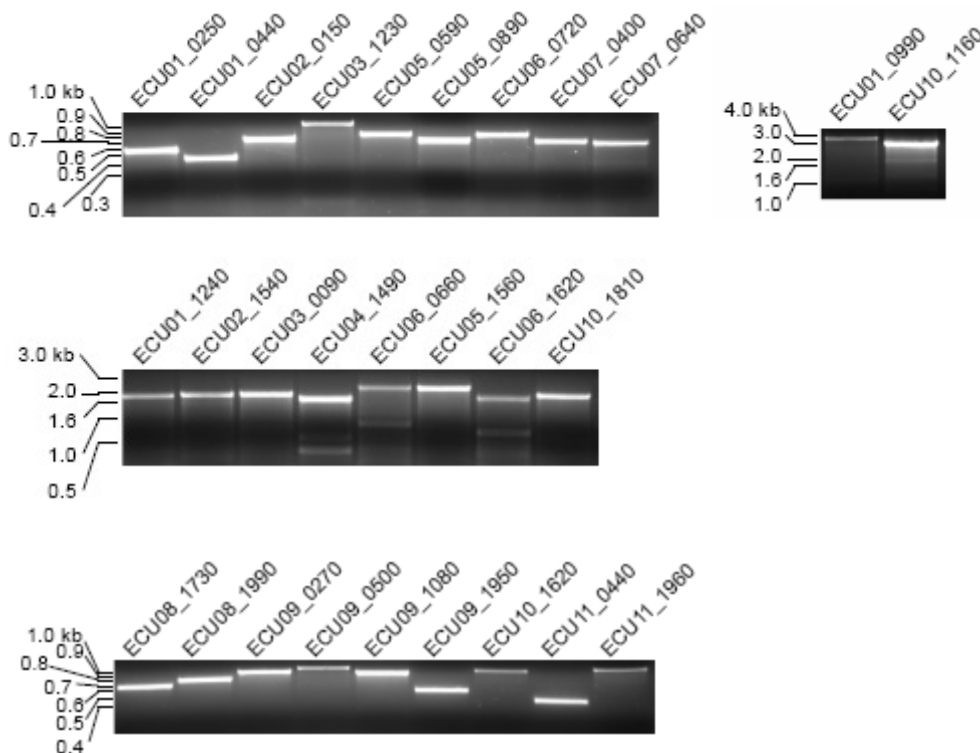


Figure 3.3 PCR-amplified hypothetical *Enc. cuniculi* genes. Typical results are shown. Nearly all genes were amplified as a single band.

3.3.4 PCR-screening and sequencing of recombinant pET-41 Ek/LIC vector colonies

Of the five to ten PCR-screened colonies for each amplified gene, 75 – 100% were observed by agarose gel electrophoresis to harbor inserts of the correct size (Fig. 3.4). Plasmids from the two to three PCR-positive colonies were

shown in all cases by nucleic acid sequencing to match the genome reference sequences and to be in-frame with the vector sequence tags (data not shown).

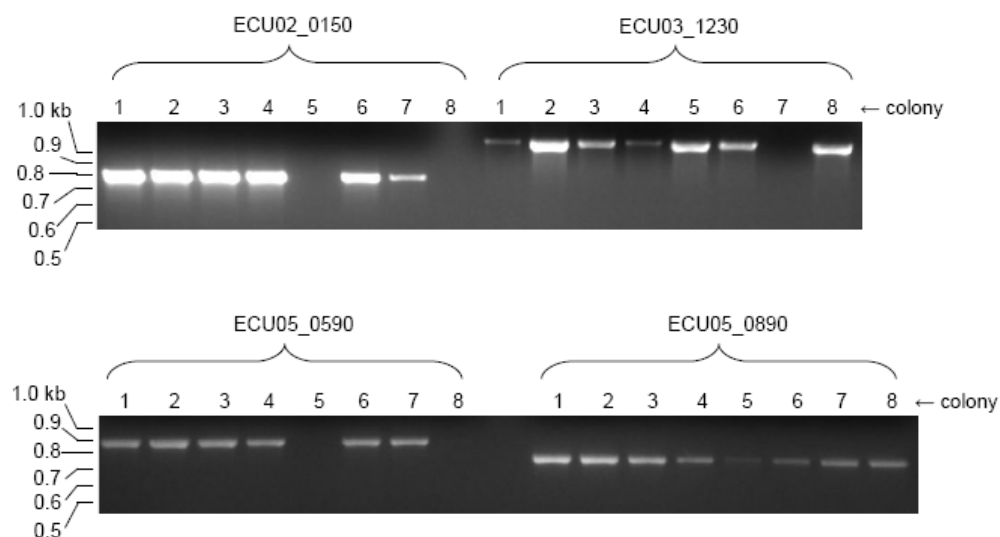


Figure 3.4. Screening of transformed *E. coli* colonies for *Enc. cuniculi* inserts.

3.3.5 Evaluation of heterologous expression of proteins

Heterologous expression of *Enc. cuniculi* proteins was evaluated by Coomassie stain of SDS-polyacrylamide gels and immunoblot. Recombinant ECU10_1500 was additionally evaluated by MALDI-TOF mass-spectrometry.

3.3.5.1 SDS-PAGE and immunoblots

39 of the 52 (75%) of the proteins, as well as spore wall protein 1 (SWP1, ECU10_1660) were visibly expressed as prominent bands by Coomassie gel staining (Fig. 3.5). These proteins were confirmed by immunoblot to be in frame with the vector-encoded GST fusion tag (representative immunoblots, Fig. 3.6).

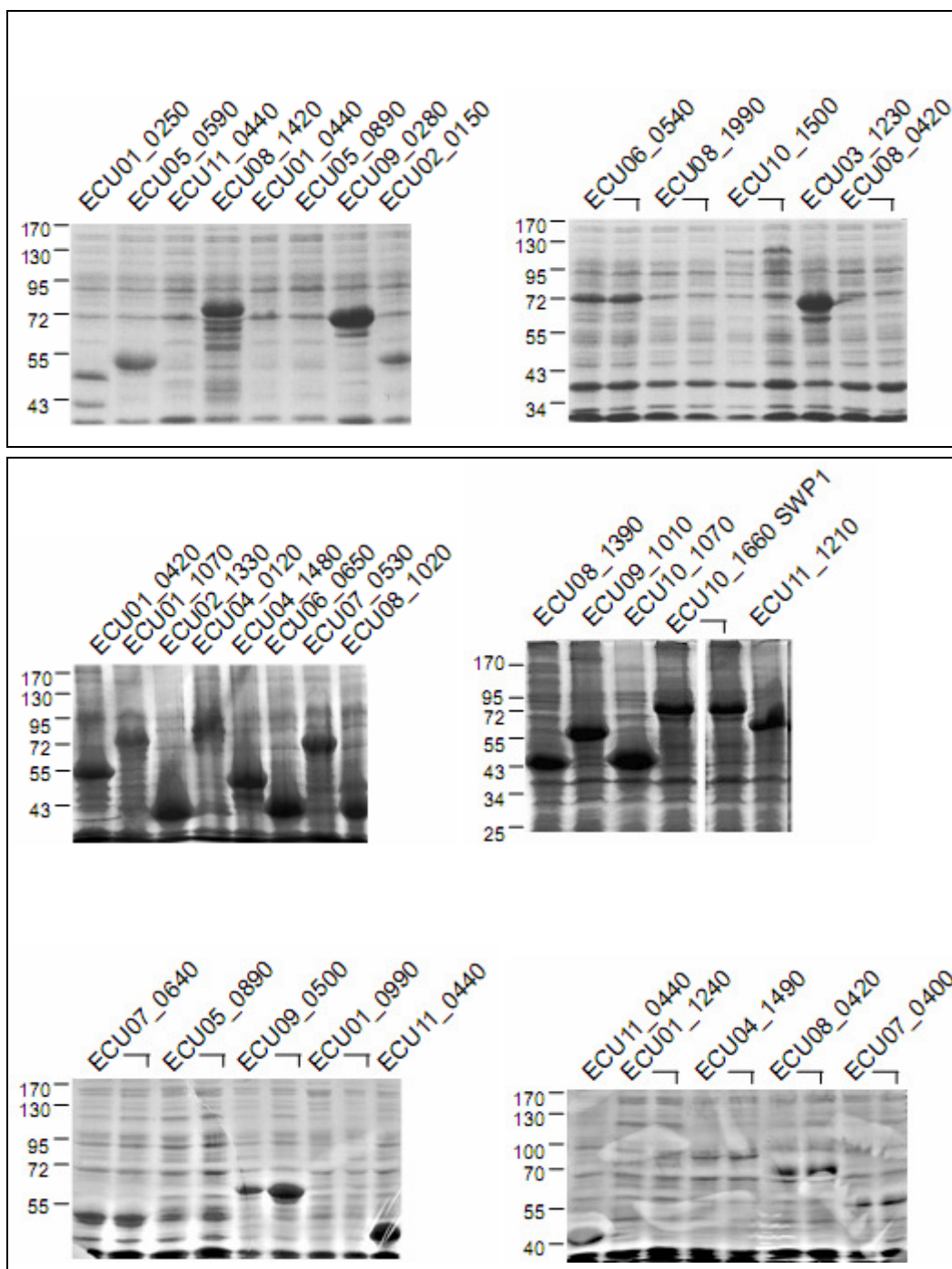


Figure 3.5 Representative results of expression of *Enc. cuniculi* genes evaluated by SDS-PAGE. Representative Coomassie-stained gels are shown of candidate *Enc. cuniculi* genes expressed heterologously in *E. coli* induced at 30°C (upper panel) or 37°C (lower panel). Expression of many target proteins is evident as visibly overexpressed bands.

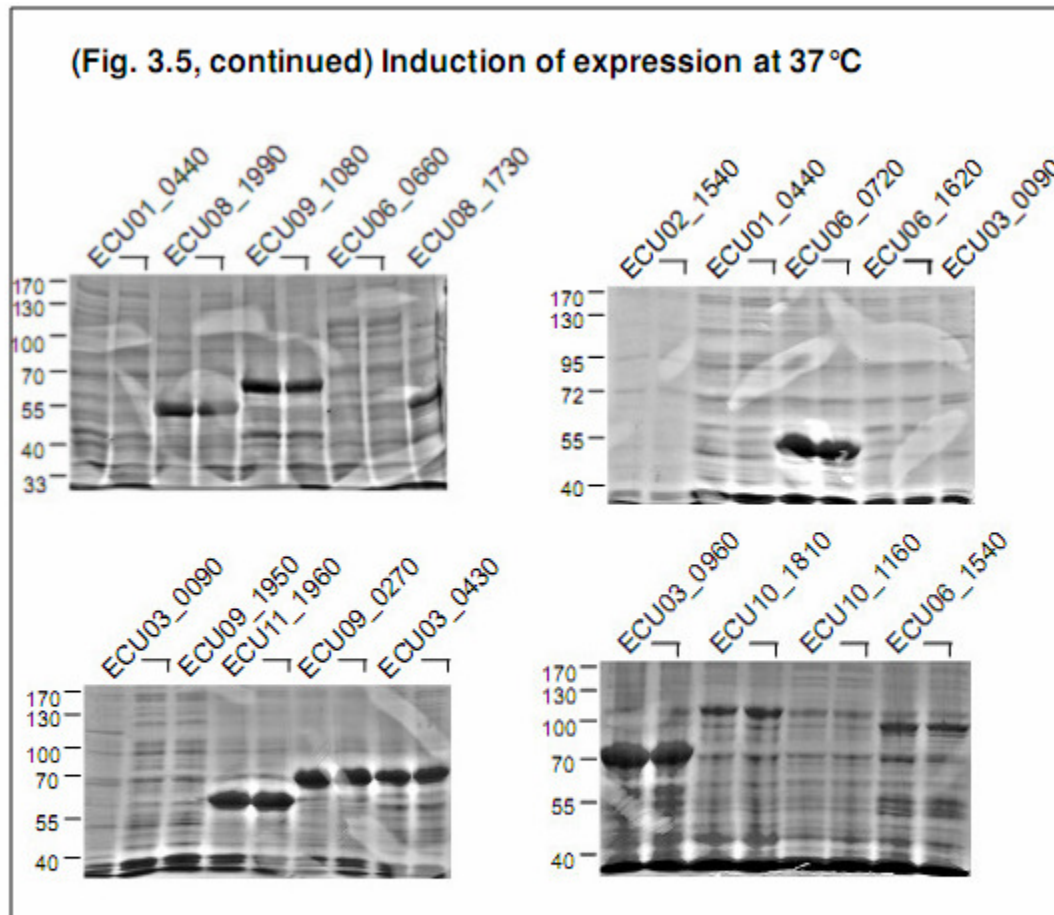


Figure 3.5, continued. Representative results of expression of *Enc. cuniculi* genes evaluated by SDS-PAGE. Representative Coomassie-stained gels are shown of candidate *Enc. cuniculi* genes expressed heterologously in *E. coli* induced 37 °C. Expression of many target proteins is evident as visibly overexpressed bands.

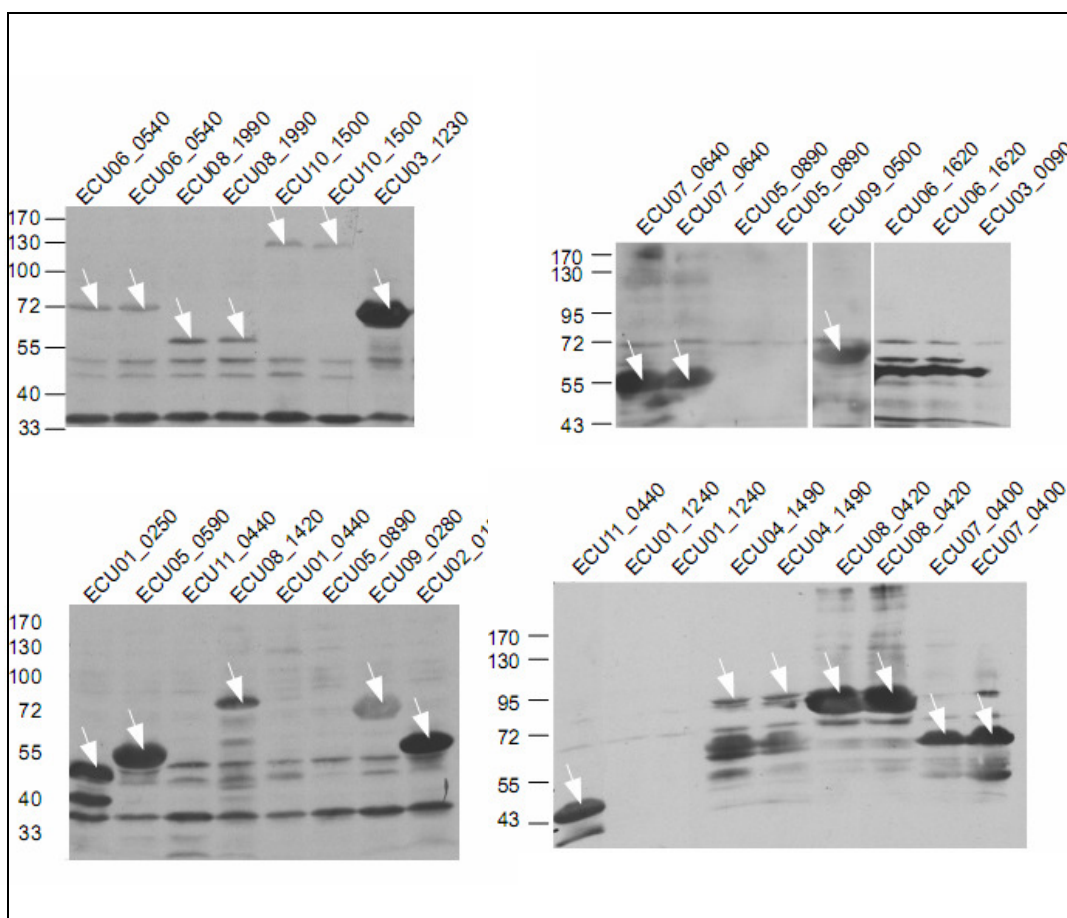


Figure 3.6. Representative results of expression of *Enc. cuniculi* genes evaluated by immunoblot. Hypothetical genes heterologously expressed in *E. coli* were evaluated for expression via immunoblot with antibody specific for GST fusion tag. Arrows indicate overexpressed *Enc. cuniculi* – GST fusion proteins.

3.3.5.2 MALDI-TOF mass spectrometry/peptide mass fingerprinting of recombinant ECU10_1500

The acquired mass spectrum is shown in Fig. 3.7. Ten manually identified monoisotopic peaks were shown to match tryptic peptides of hypothetical protein ECU10_1500 (Table 3-666) at $p < 0.05$ significance, corresponding to 29% sequence coverage for ECU10_1500. The assigned peptides are indicated in Table 3.4, some of which are indicated as spectral peaks in Fig. 3.7. The ions score was below the significance threshold for assignment to any other *Enc. cuniculi* protein.

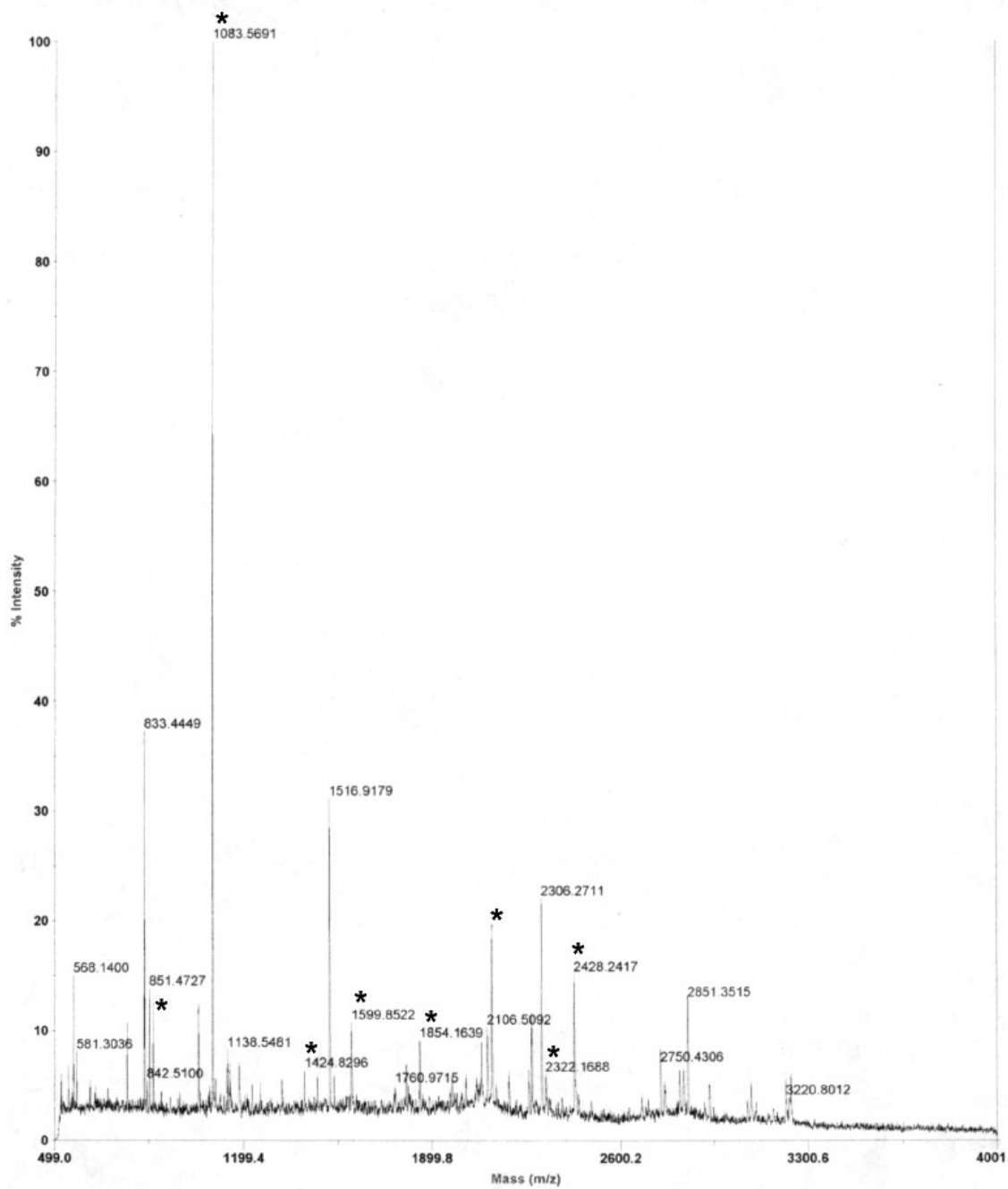


Figure 3.7. MALDI-TOF mass spectrum for ECU10_1500-GST fusion protein. Asterisks indicate peaks assigned to ECU10-1500.

Table 666. Observed peptide mass fingerprint of ECU10_1500 fusion protein.

start-end	observed	Mr (expt)	Mr (calc)	Delta	Miss	Sequence
11-32	2322.17	2321.16	2320.99	0.18	1	SSSGDEAEKVYLEMESSGSSDK
67-80	1599.85	1598.84	1598.78	0.06	0	ISTFDVYIVNENGGK
88-111	2427.40	2426.39	2426.10	0.29	0	HIGPADGIESMSSPGDSSADEVIR
217-230	1532.83	1531.82	1531.70	0.12	1	ESDIEVSKGNEDTK
277-285	1149.67	1148.66	1148.45	0.21	1	EDREMNSDR
293-308	1854.16	1853.16	1852.95	0.20	1	AIQAQEPEEKDIINQK
386-392	865.46	864.45	864.43	0.02	0	SILDFDR
406-424	2123.17	2122.16	2121.96	0.20	1	EADRDDEMIVFVEAGDVGR
439-449	1423.89	1422.88	1422.75	0.13	1	LVKFFENLEER
442-449	1083.57	1082.56	1082.50	0.06	0	FFENLEER

Table 3.4. Observed peptide mass fingerprint of expressed recombinant ECU10_1500 protein. The first column indicates the span of amino acids to which the detected peptide corresponds; the second, the observed mass-to-charge ratio (m/z); the third, the experimental m/z transformed by Mascot to a relative value; the fourth, the calculated m/z; the fifth, the difference between the relative calculated and experimental values; the sixth, the number of missed trypsin cleavages for each peptide; the seventh, the amino acid sequence of the detected peptide (fixed and variable modifications permitted in Mascot search parameters not shown).

3.3.6 *In silico* predictions of biochemical attributes

There were significant differences ($p < 0.05$) between expressed and non-expressed hypothetical *Enc. cuniculi* proteins in mean native molecular weight (37.0 vs. 59.0 kDa), pI (6.6 vs. 8.0), GRAVY score (-0.50 vs. -0.21), and number of predicted transmembrane domains (0.051 vs. 1.92). When proteins with predicted transmembrane domains were excluded, the difference in GRAVY scores between the two groups was not significant ($p = 0.22$). The native molecular weight, pI, and GRAVY score for individual proteins are depicted in Fig. 3.8.

Biochemical attributes of expressed vs. non-expressed proteins

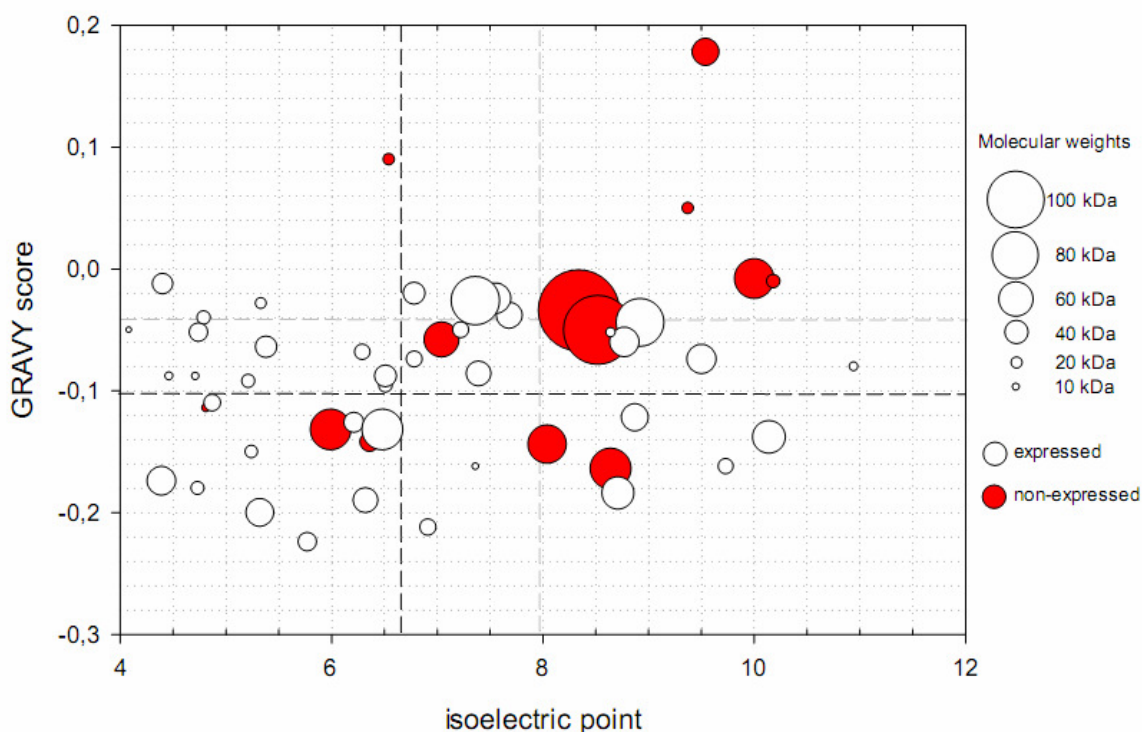


Figure 3.8. Biochemical attributes of expressed vs. non-expressed proteins. Each individual protein is plotted as a bubble sized proportionately to its molecular weight without fusion tags, on axes corresponding to its GRAVY score and pI. Mean GRAVY and pI for expressed and non expressed proteins are represented by dashed dark and light gray lines, respectively.

3.3.7 Evaluation of mouse antisera by immunoblot

16 of 17 mouse antisera tested at various dilutions by immunoblot of recombinant bacterial lysates reacted with bands of the approximate expected size of the fusion protein (Fig. 3.9, panels B, C, D, E, F, arrows). 5 of 17 antisera also reacted with bands of unexpected size or bands of smeared appearance (Fig. 3.9, panels B, C, D, E, double headed-arrows). In some cases, further dilution of the mouse antiserum and/or reduced film exposure time yielded more specific

recognition of the appropriate band (e.g., antiserum to ECU03_0430, Fig. 3.9, panel B vs. F; ECU06_0720, panel D vs. B; ECU05_0140, panel E vs. C). 6 and 5 of 14 antisera tested by Immunoblot of fractionated, DTT-solubilized *Enc. cuniculi* lysate reacted with bands of the approximate expected size of the fusion protein (Fig. 3.9, panel A, arrows) or of an unexpected size (Fig. 3.9, panel A, double-headed arrows), respectively.

Fig. 3.9. Immunoblots of mouse antisera to hypothetical *Enc. cuniculi* proteins

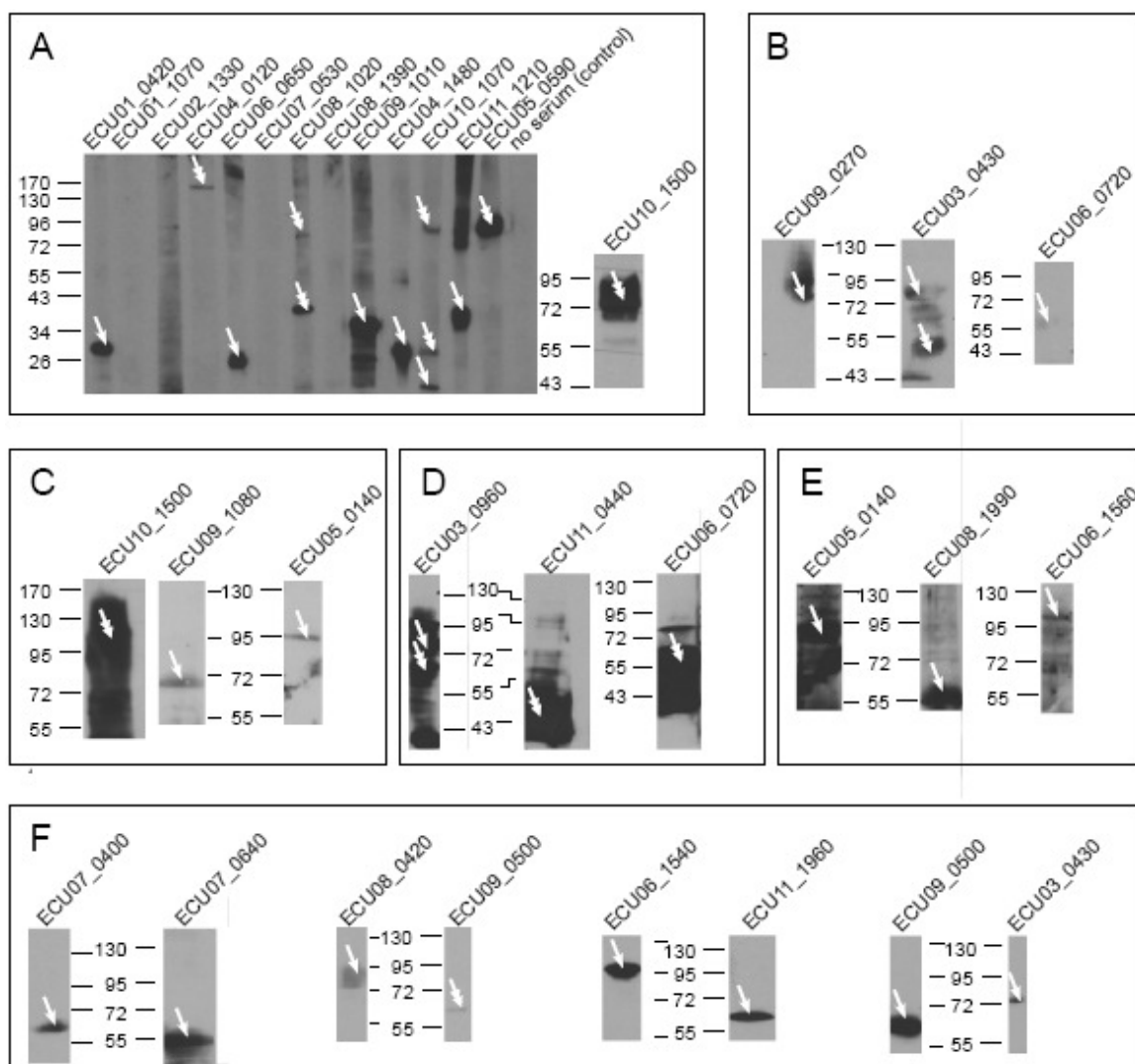


Fig. 3.9. Immunoblots of mouse antisera to hypothetical *Enc. cuniculi* proteins. Lysates from polar tube protein preparations (panel A) or of recombinant parasite protein-expressing *E. coli* (panels B, C, D, E, F) were immunoblotted against mouse antisera. Arrows indicate bands of approximate expected size; double-headed arrows indicate bands of unexpected size or smeared appearance. The concentration of mouse sera and film development times used in immunoblots in each panel are: panel A, large immunoblot at left, 1:500, 2 min; panel A, small immunoblot at right, 1:2500, 5 min; panel B, 1:100, 2 min; panel C, 1:1000, 7 min; panel D, 1:100, overnight; panel E, 1:1000, overnight; panel F, 1:1000, 30 min.

3.3.8 *In situ* immunolocalization of hypothetical proteins

3.3.8.1 Immunofluorescence microscopy

36% (14 of 39) of the antisera produced against hypothetical *Enc. cuniculi* proteins strongly stained parasites or structures within the parasitophorous vacuole by immunofluorescence (Figs. 3.10-3.26). An equal number (14 of 39) of the antisera exhibited high levels of background and/or stained host cell cultures and parasites non-specifically (representative sera, Fig. 3.27-3.29). The remainder (11 of 39) showed no reactivity by immunofluorescence (representative serum, Fig. 3.30). Although *Enc. cuniculi* is similar in size to bacteria which usually renders determination of subcellular localization at the light level impossible, the characteristic positions of different developmental forms inside the parasitophorous vacuole (e.g., early proliferative stages which are adherent to the parasitophorous vacuole membrane vs. sporogonic stages which tend to be dispersed in the lumen) (Cali and Takvorian, 1999) aids in interpretation of developmental expression patterns. In addition, counterstaining with DAPI allows staining patterns relative to the nucleus to be interpreted. Thus three tentative categories of parasite-staining sera were discerned based on staining pattern by light microscopy: nuclear/perinuclear; cytoplasmic; other intracellular; peripheral (visually consistent with periphery of cytoplasm, integral to the plasma membrane, or forming spore wall); or vacuolar (i.e., in the lumen of the parasitophorous vacuole).

3.3.8.1.1 Nuclear/perinuclear hypothetical proteins

Antisera to hypothetical genes ECU07_0400, ECU03_1010, ECU05_0140, ECU08_0420, ECU02_0150, ECU03_0430, and ECU09_1080 stained the nuclear or perinuclear region of parasites. Hypothetical proteins ECU07_0400, ECU03_1010, ECU05_0140, ECU08_0420, ECU02_0150, ECU03_0430, and ECU09_1080 have a similar localization to DAPI, as evidenced by the spatial coincidence of blue and green fluorescence in the digitally merged micrographs (Figs. 3.10-3.16, arrows, bottom panels). Nuclear regions of parasites in the central area of the vacuole as well as at or near its periphery (Figs. 3.10-3.16, arrows) were stained, suggesting that these proteins are expressed by *Enc. cuniculi* at various developmental stages during proliferative and sporogonic phases of the life cycle. The peripheral staining of extravacuolar forms by antiserum to ECU08_0420 (Fig. 3.13, curved arrows, top and bottom panels) is likely an artifact, as mild reactivity to spore walls has also been occasionally observed in normal serum of non-immunized mice (data not shown), and the staining of this structure by antiserum to ECU08_0420 is of weak intensity compared to its nuclear staining pattern and to the staining pattern by identically produced antiserum to *Enc. cuniculi* spore wall protein 1 (Fig 3.22C).

3.3.8.1.2 Cytoplasmic proteins

The hypothetical protein ECU04_1480 localizes most intensely to developmental forms at the inner periphery of the parasitophorous vacuolar membrane (Fig. 3.17, arrows, bottom panel), suggesting that this protein is most highly expressed

specifically by proliferative stages of the parasite. The area of staining is also noticeably larger than that of DAPI (Fig. 3.17, arrowheads, top and middle panels), suggesting that this protein is not restricted to the perinuclear region and is found throughout the cytoplasm.

The product of hypothetical gene ECU07_0640 is also distributed throughout the cytoplasm (Fig. 3.18, arrows, top and bottom panels), but appears to be more concentrated in the nuclear or perinuclear region (Fig. 3.18, arrowheads, top and bottom panels). In contrast, while ECU09_0270 also appears to be cytoplasmic, its distribution is more generalized (Fig. 3.19, arrows, top and bottom panels). This antiserum also stains a nearby region of the host cell cytoplasm with the same intensity (Fig. 3.19, arrowhead, bottom panel). The ECU09_1010 protein has a complementary distribution pattern to that of ECU07_0640, as it is more intensely expressed at the peripheral rather than the central or perinuclear region of the cytoplasm (Fig. 3.20, arrows, top and bottom panels).

3.3.8.1.3 Other intracellular proteins

The antiserum to hypothetical protein ECU09_02780 stains small, discrete, punctuate structures close to the nucleus (Fig. 3.21A, white boxes, top and bottom panels) which frequently appear in groups of three (Fig. 3.21B, arrows, top and bottom panels).

3.3.8.1.4 Peripheral proteins

Antiserum to ECU10_1070 stains the periphery of parasites that appear to be undergoing cytokinesis (Fig. 3.22A, arrows). The antiserum does not stain the periphery of mature, released spores as antiserum to Spore Wall Protein 1 does (Fig. 3.22C, arrows), although the latter also stains the periphery of developing forms (Figure 3.22C, arrowhead). The occurrence of nuclei in pairs but separated by the deposition of ECU10_1070 protein is evident in the deconvolved image (Fig. 3.22B, arrows).

3.3.8.1.5 Vacuolar

Antiserum to ECU10_1500 stains structures of filamentous appearance in the lumen of the parasitophorous vacuole of *Enc. cuniculi* (Figs. 3.23 and 3.24) and *Enc. hellem* (Figs. 3.25 and 3.26). These structures appear as small coils (arrows, Figs. 3.23, 3.24-3.26) or longer filaments (arrowheads, Figs. 3.24-3.26), sometimes within the same vacuole. In deconvolved images, these filamentous structures seem to pass around rather than through developing parasites (circles, Fig. 3.25). A montage of a rotated 3D reconstruction of a deconvolved stack of images (Fig. 3.26) suggests that the longer filaments seen in epifluorescence micrographs (arrowheads, arrowheads, Figs. 3.24-3.26) may actually be part a larger coil (Fig. 3.26, arrowheads), and that the protein forms a branching network (branch points, Figs. 3.25, 3.26, double-headed arrows) within the lumen of the parasitophorous vacuole.

3.3.8.1.6 Non-specific and non-reactive antisera

The remaining 25 antisera produced against hypothetical *Enc. cuniculi* proteins either were extremely weakly specific for parasites (Figs. 3.27, 3.28), showed either high background or cross-reactivity with host cells (Figs. 3.29), or were non-reactive (Fig. 3.30) by immunofluorescence. It should be noted that antisera to all four proteins selected for expression on the basis of sequence similarity to hypothetical spore wall proteins of *Nosema bombycis* (Wu et al., 2008, 2009) fall into this category.

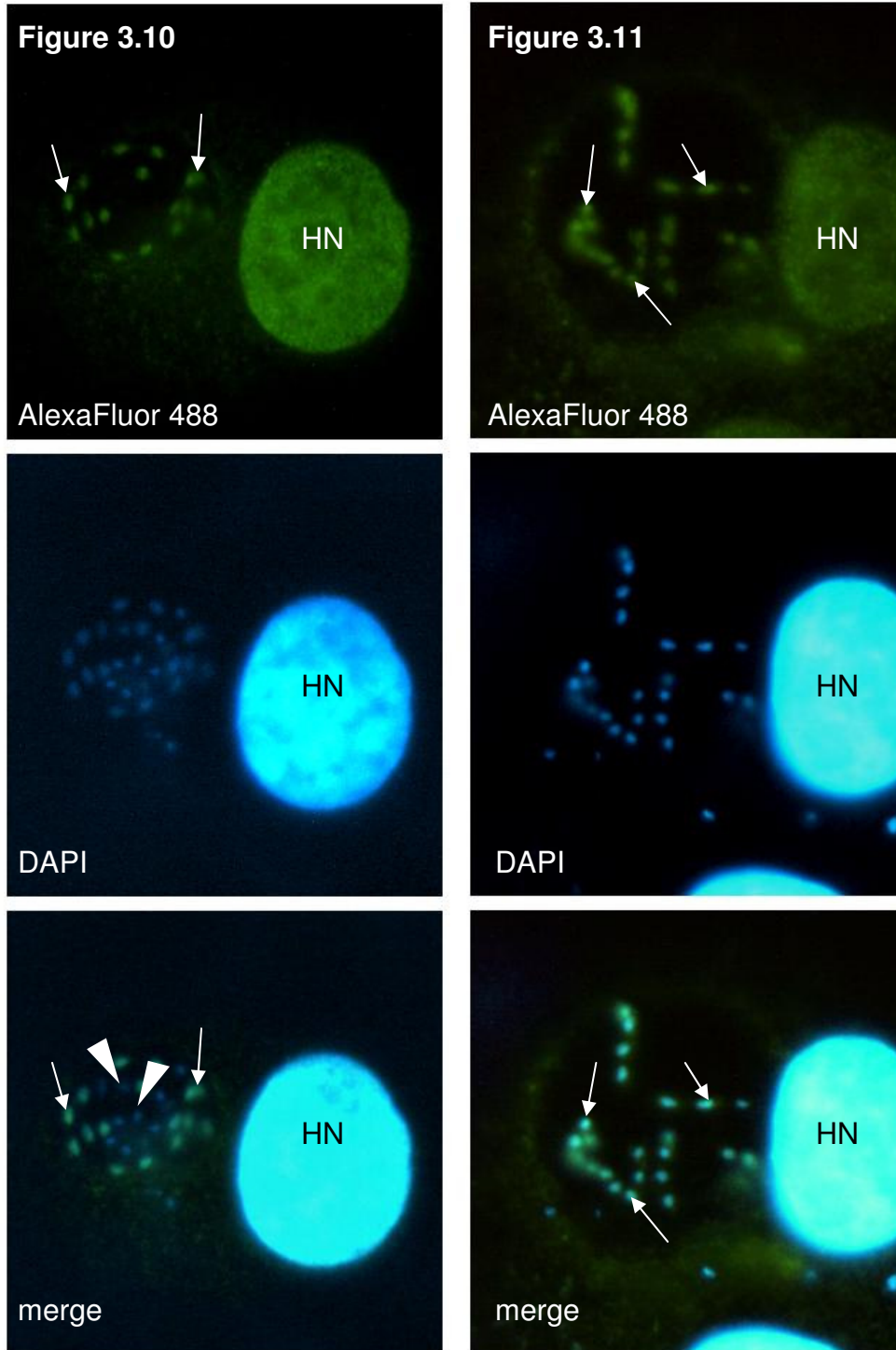


Fig. 3.10 Immunofluorescence localization of ECU07_0400. This protein localizes to the parasite nucleus (arrows) and is possibly expressed in a stage-specific manner (note lack of staining of some parasite nuclei, arrowheads). Some antiserum cross reactivity occurs with the host cell nucleus (HN).

Fig. 3.11 Immunofluorescence localization of ECU03_1010. This protein localizes to the parasite nucleus (arrows). Some antiserum cross reactivity occurs with the host nucleus (HN).

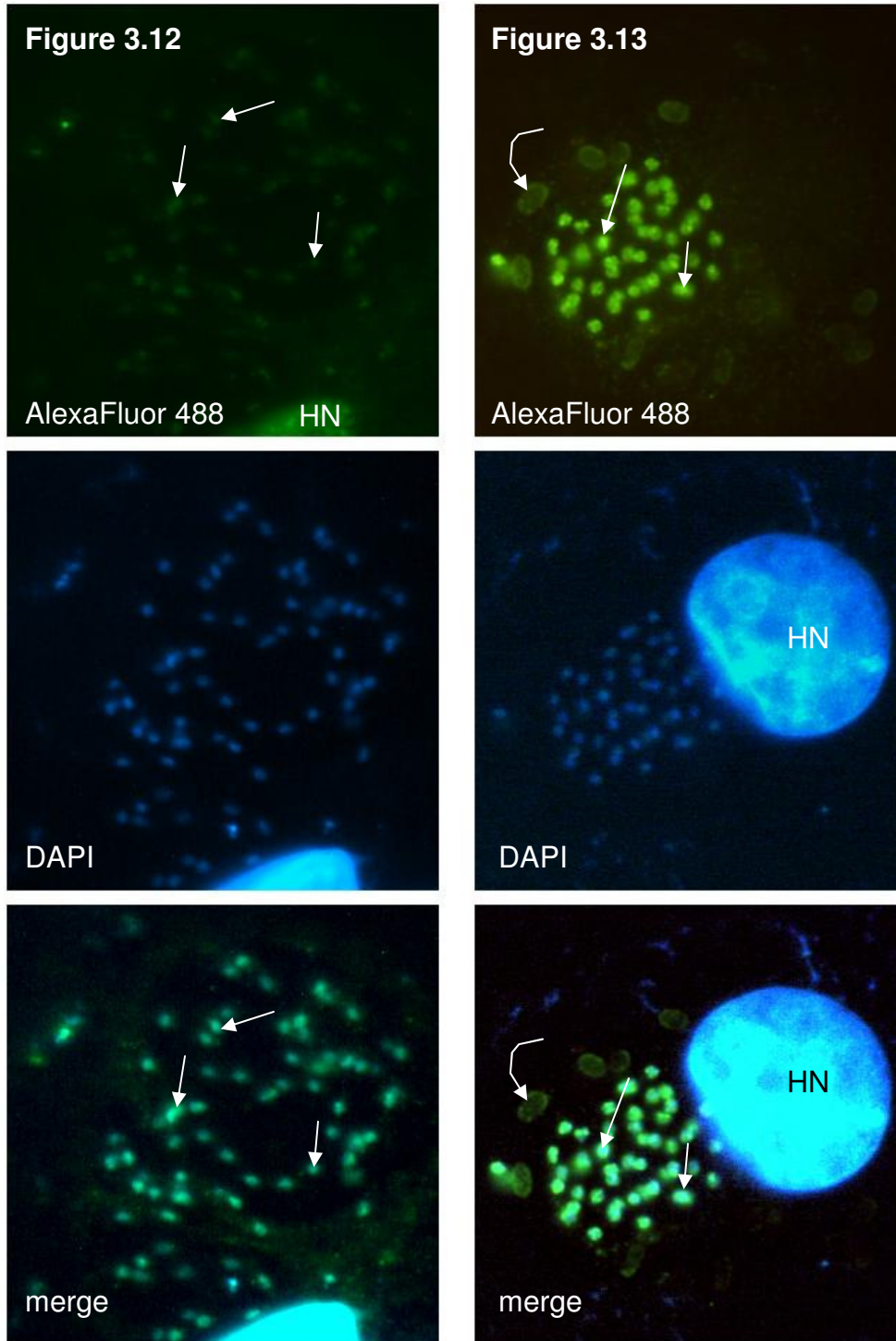


Figure 3.12 Immunofluorescence localization of ECU05_0140. This protein localizes to the parasite nucleus (arrows). Some antiserum cross reactivity occurs with the host cell nucleus (HN).

Figure 3.13 Immunofluorescence localization of ECU08_0420. This protein localizes to the parasite nucleus (straight arrows). Weak staining of spore walls (curved arrows) is likely artifactual, as this is sometimes seen with normal antiserum (data not shown). HN, host cell nucleus.

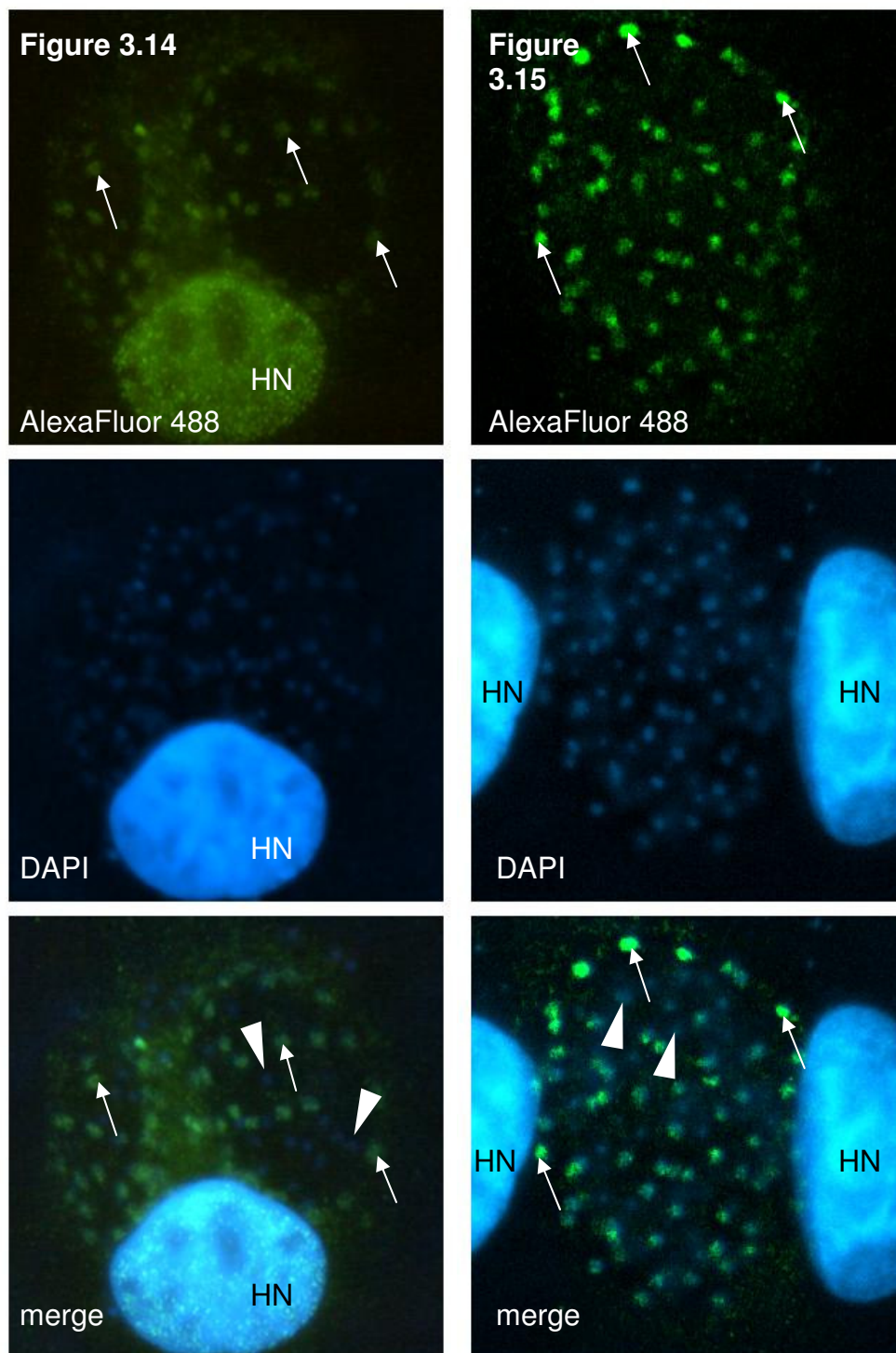


Figure 3.14 Immunofluorescence localization of ECU02_0150. This protein localizes to the parasite nucleus (arrows) and is possibly expressed in a stage-specific manner (note lack of staining of some parasite nuclei, arrowheads). Some antiserum cross reactivity occurs with the host cell nucleus (HN).

Figure 3.15 Immunofluorescence localization of ECU03_0430. This protein localizes to the parasite nucleus (arrows) and is possibly expressed in a stage-specific manner (note lack of staining of some parasite nuclei, arrowheads). HN, host cell nucleus.

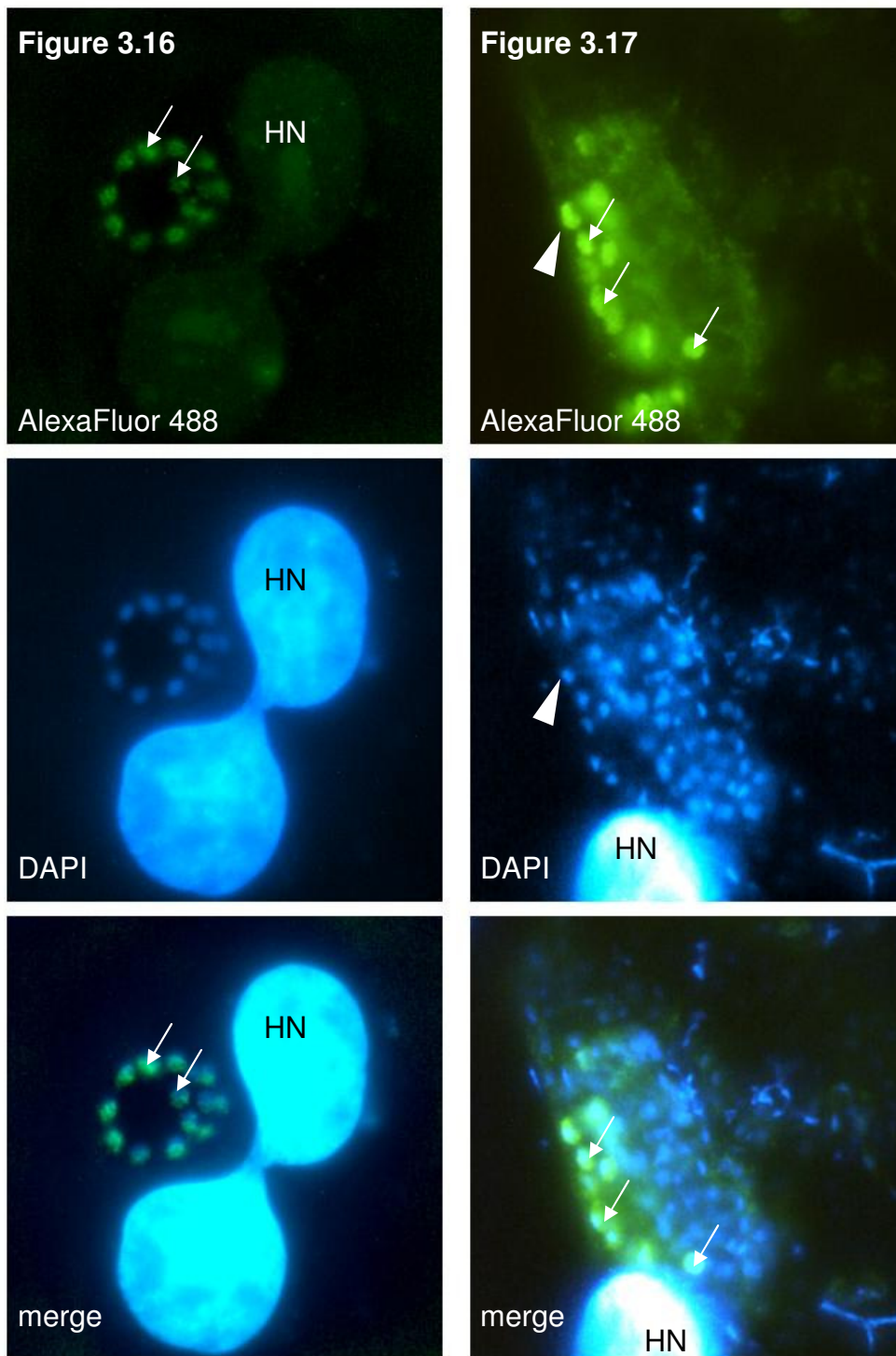


Figure 3.16 Immunofluorescence localization of ECU09_1080. This protein localizes to the parasite nucleus (arrows). Mild antiserum cross reactivity occurs with the host cell nucleus (HN).
Figure 3.17 Immunofluorescence localization of ECU04_1480. The protein localizes most intensely to developmental forms at the inner periphery of the parasitophorous vacuolar membrane (arrows), suggesting that this protein is most highly expressed specifically by proliferative stages of the parasite. The area of staining is also noticeably larger than that of DAPI, suggesting that this protein is not restricted to the perinuclear region and is found throughout the cytoplasm. HN, host cell nucleus.

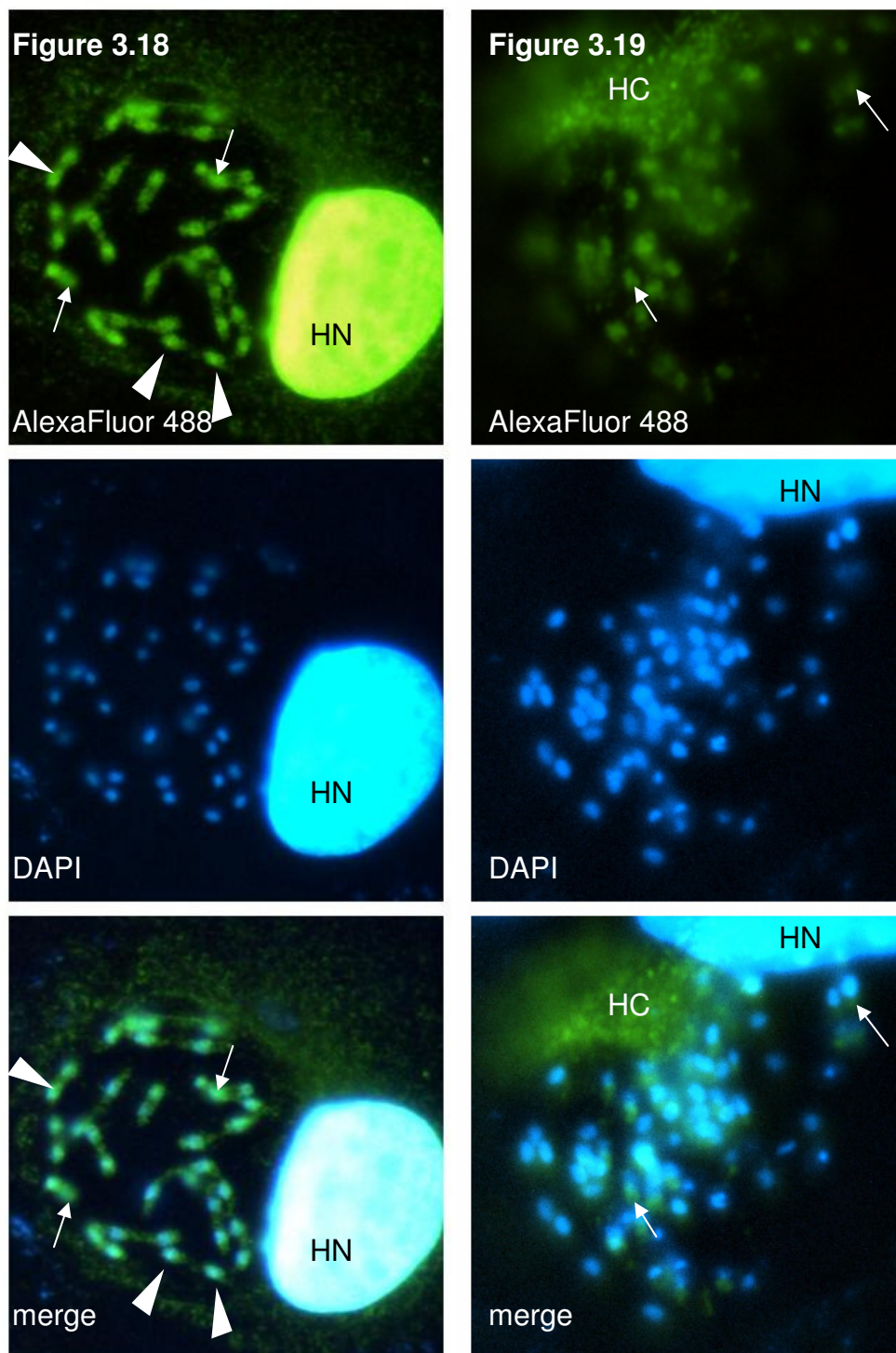


Figure 3.18 Immunofluorescence localization of ECU07_0640. This protein is distributed throughout the cytoplasm (arrows), but appears to be more concentrated in the nuclear or perinuclear region (arrowheads). Some antiserum cross reactivity occurs with the host cell nucleus (HN).

Figure 3.19 Immunofluorescence localization of ECU09_0270. This protein has a generalized cytoplasmic distribution (arrows). Some antiserum cross reactivity occurs with the host cell cytoplasm (HC). Host cell nucleus, HN.

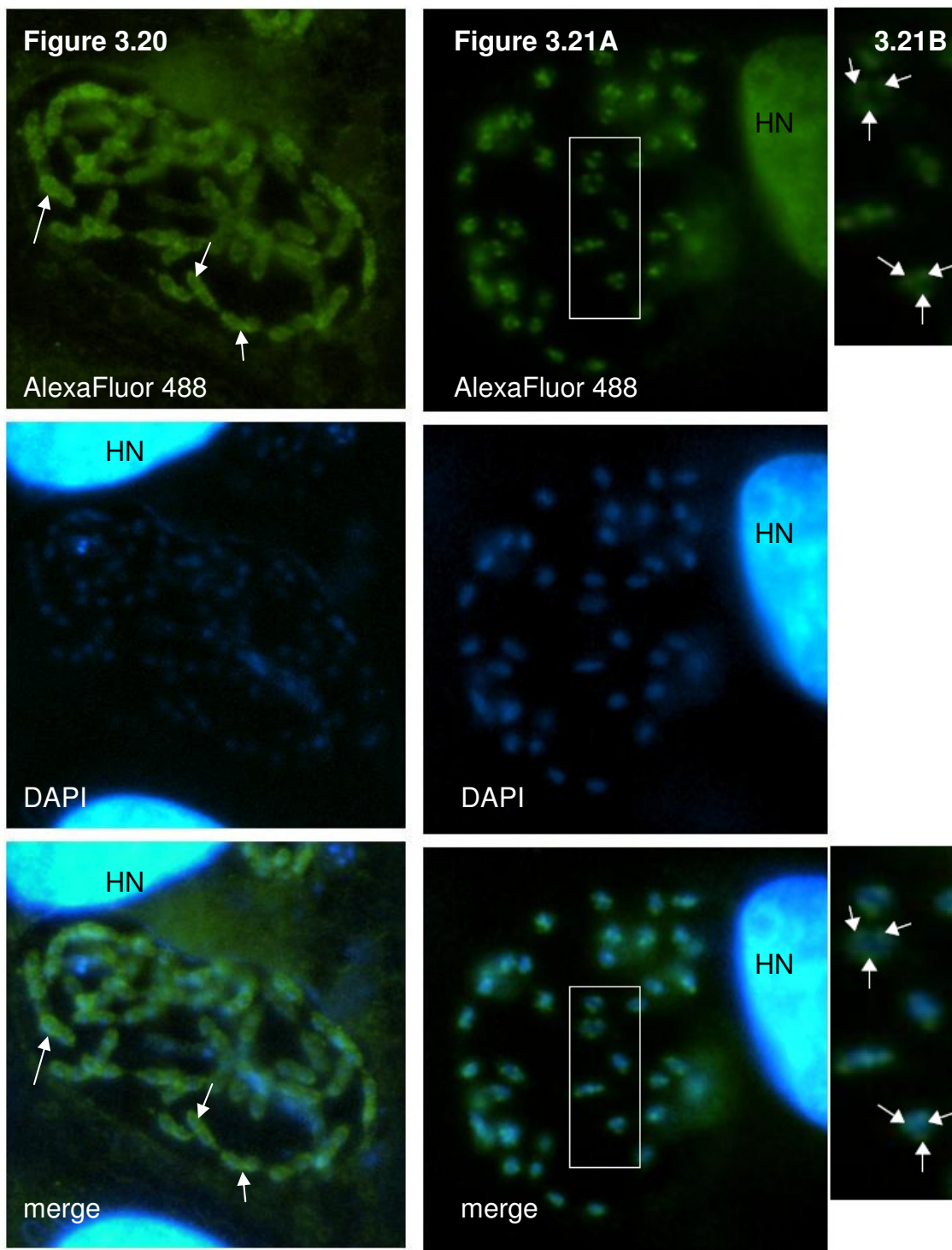


Figure 3.20 Immunofluorescence localization of ECU09_1010. This protein is distributed throughout the cytoplasm but is slightly more abundant at the periphery of developing parasites (arrows). HN, host cell nucleus.

Figure 3.21 Immunofluorescence localization of ECU09_0280. This protein is localized to small, discrete, punctuate structures close to the nucleus (Fig. 3.21A, white boxes, top and bottom panels) which frequently appear in groups of three (Fig. 3.21B, arrows, top and bottom panels). This localization pattern is consistent with a mitochondrial location for this protein. Some antiserum cross reactivity occurs with the host cell nucleus (HN).

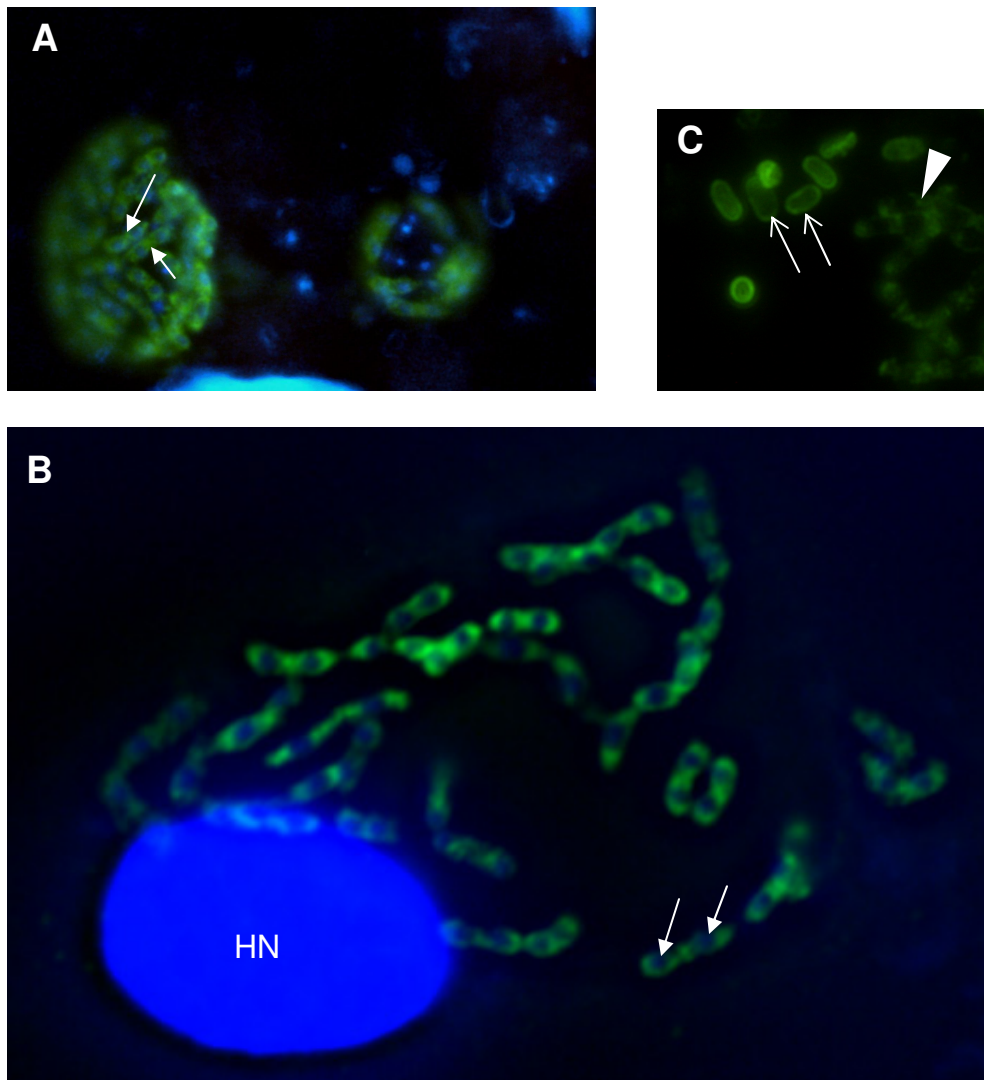


Fig. 3.22 Immunofluorescence localization of ECU10_1070 and comparison to SWP1. Nuclei were counterstained with DAPI (blue). (A) The protein encoded by ECU10_1070 is localized to a thick layer at the periphery of developing parasite stages floating in the lumen of the parasitophorous vacuole (arrows). (B) The deposition of ECU10_1070 protein at the periphery of parasites floating in the lumen of the parasitophorous vacuole and its expression by dividing parasites, indicated by the occurrence of nuclei in pairs (arrows), suggest that this protein is developmentally regulated and expressed specifically by sporonts. (C) In contrast to ECU10_1070, spore wall protein 1 (SWP1) is deposited at the periphery of mature spores (arrows) but is less abundant at the periphery of developing forms (arrowhead).

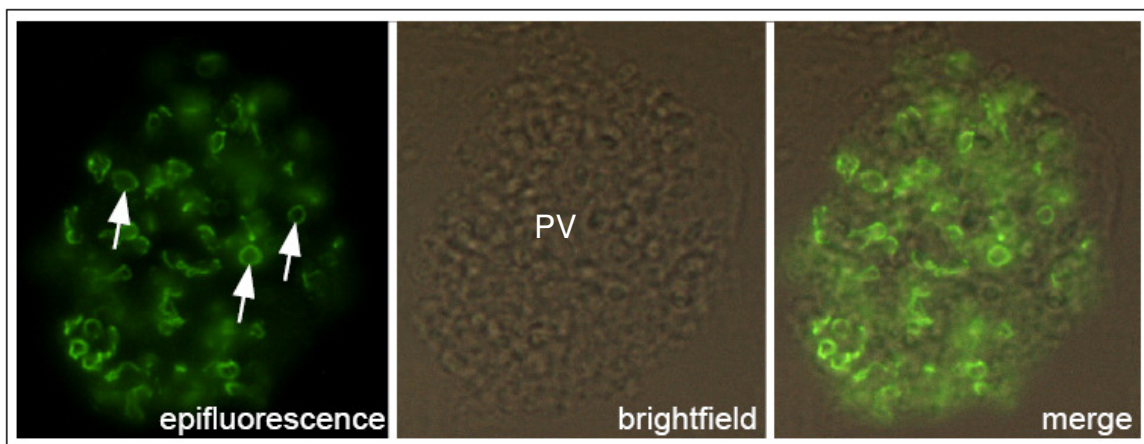


Figure 3.23 Immunofluorescence localization of ECU10_1500 in *Enc. cuniculi*. This protein localizes to novel structures of filamentous appearance (arrows) in the lumen of the parasitophorous vacuole (PV) which sometimes appear as small coils.

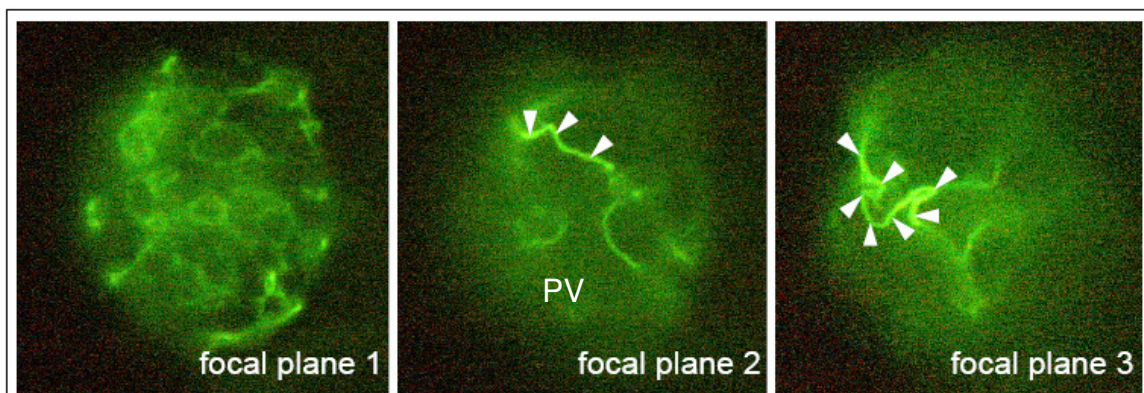


Figure 3.24 Immunofluorescence localization of ECU10_1500 in *Enc. cuniculi*: three focal planes of the same parasitophorous vacuole. The structures formed by the ECU10_1500 protein sometimes extend much of the length of the parasitophorous vacuole (PV) as long filamentous structures (arrowheads) in the lumen of the parasitophorous vacuole (PV).

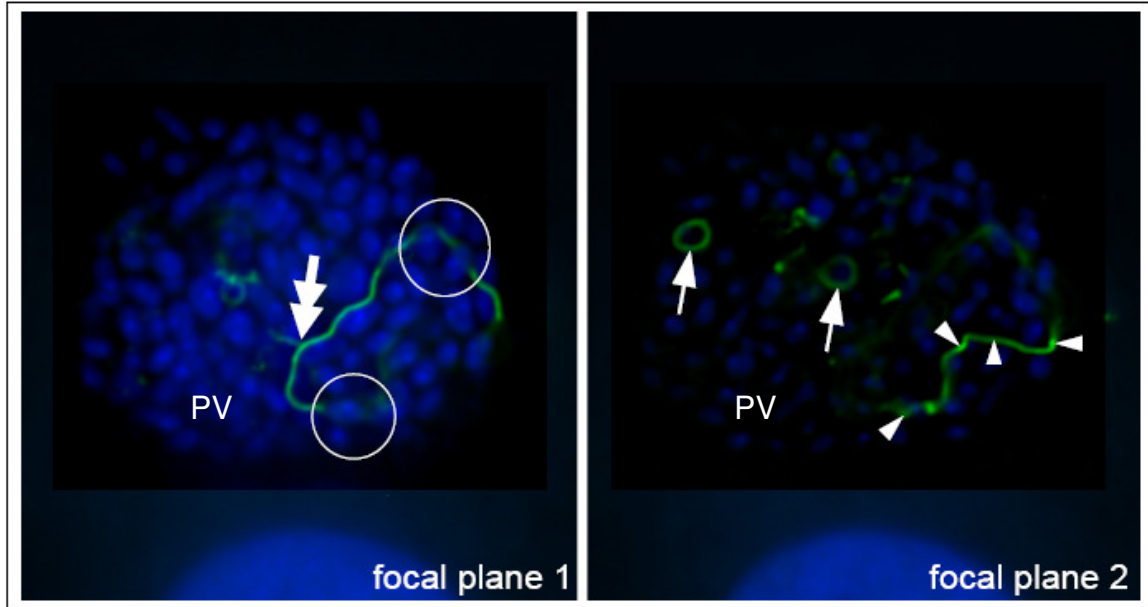


Figure 3.25 Immunofluorescence localization of ECU10_1500 in *Enc. hellem*: deconvolved Z-stack. The antiserum to ECU10_1500 cross-reacts with *Enc. hellem* parasitophorous vacuoles (PV), staining structures of similar appearance as in *Enc. cuniculi*. Nuclei were counterstained with DAPI. The filamentous structures stained by antiserum to this protein form small circles (single-headed arrows) and longer, extended forms (arrowheads) which appear to pass around rather than through parasites (circles) within the lumen of the PV. The filamentous structures can be seen to branch (double-headed arrow).

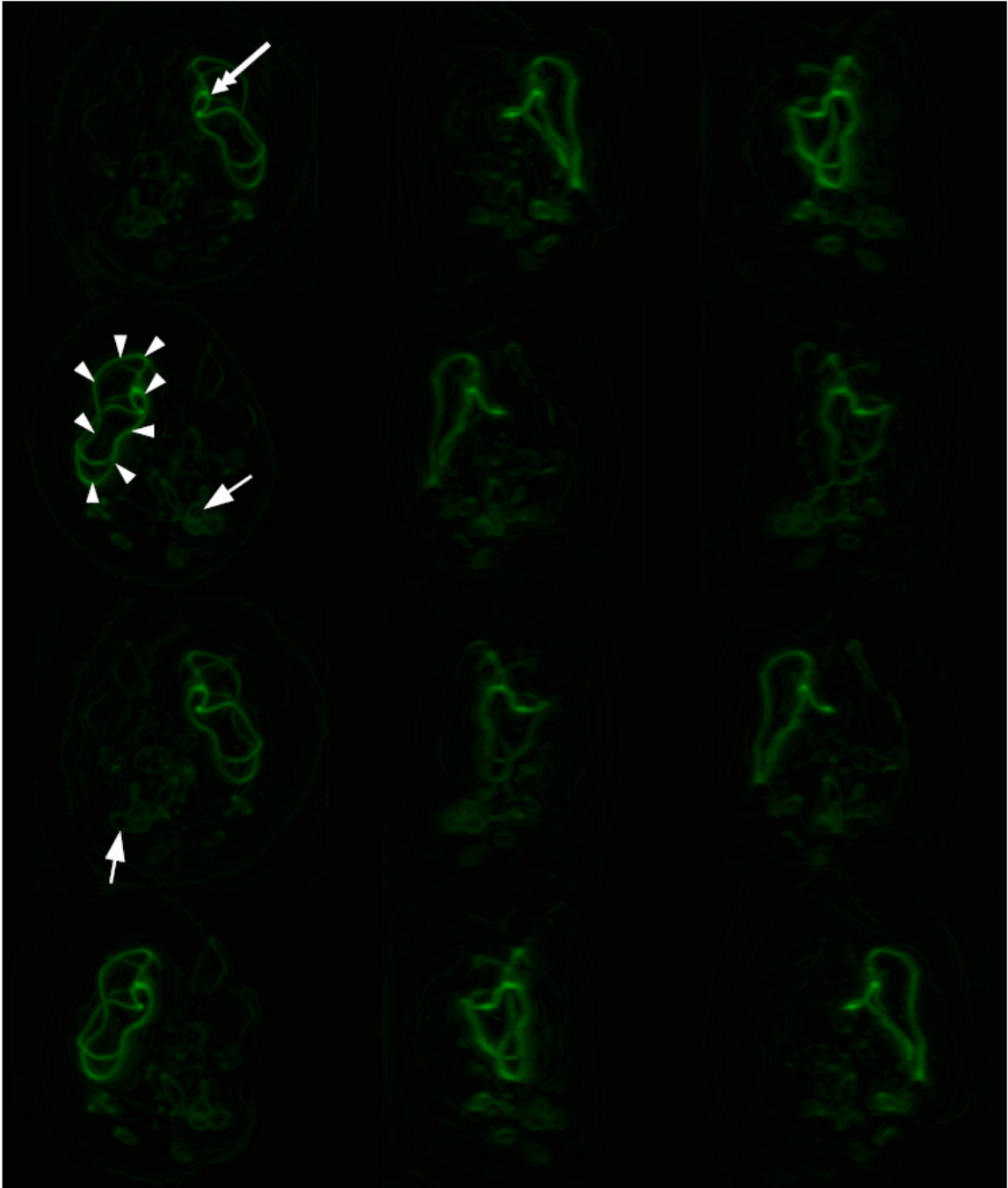
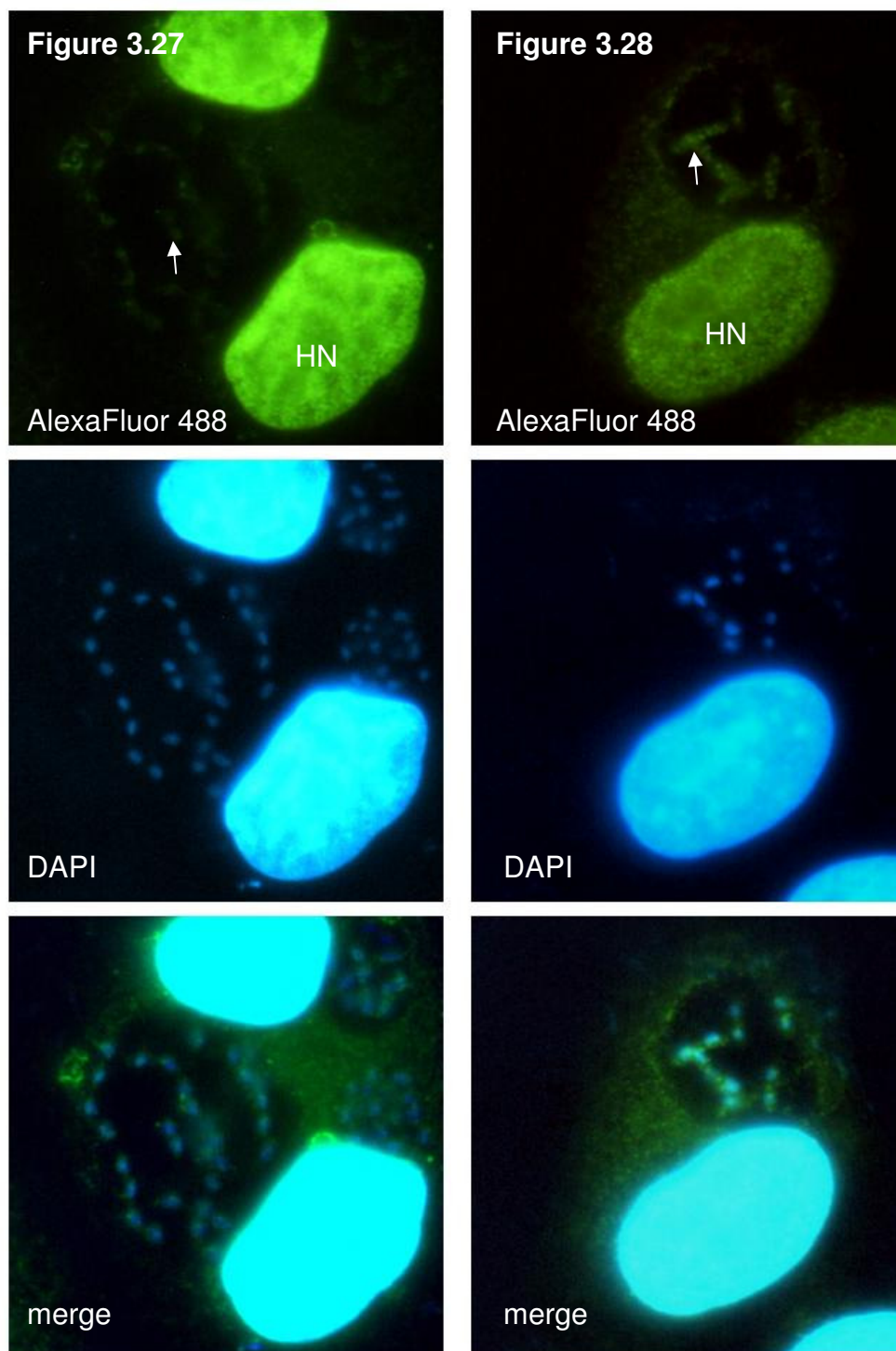


Figure 3.26 Immunofluorescence localization of ECU10_1500 in *Enc. hellem*: Rotated montage of a 3D-reconstruction of a deconvolved Z-stack. A montage of a rotated 3D reconstruction of a deconvolved stack of images suggests that the longer filaments seen by epifluorescence microscopy may actually be part a larger coil (arrowheads), and that the protein forms a branching network (branch point: double-headed arrow) within the lumen of the parasitophorous vacuole (PV) that contains a large network, smaller coils may also be seen (single-headed arrows).



Immunofluorescence localization of ECU06_1560 (Fig. 3.27) and ECU09_0500 (Fig. 3.28). Parasites are only very weakly stained (arrows), suggesting very low-titer specific antibody in these sera. HN, host cell nucleus.

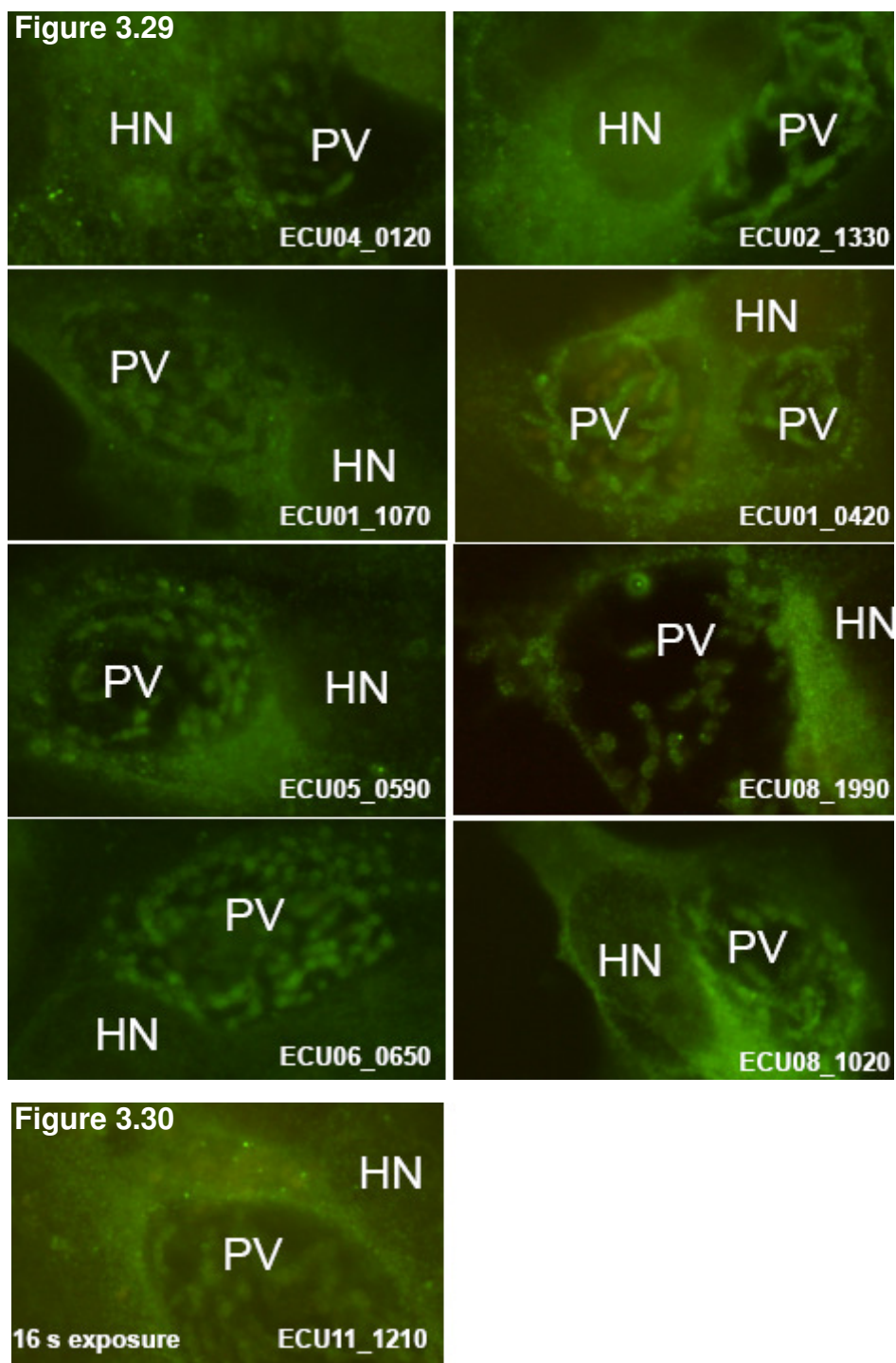


Figure 3.29. Representative nonspecific immunofluorescence staining patterns of antisera to recombinant hypothetical *Enc. cuniculi* proteins. The degree of cross-reactivity with host material precluded the use of several antisera (examples pictured here) for further immunohistochemistry. HN, host cell nucleus; PV, parasitophorous vacuole.

Figure 3.30. Representative non-reactive antiserum. Image was acquired with abnormally long exposure by digital camera (note resulting high level of background fluorescence yet low-intensity staining of cells). HN, host cell nucleus; PV, parasitophorous vacuole.

3.3.8.2 Correlative light/immunolectron microscopy

In *Enc. hellem*-infected host cell cultures stained with antiserum to ECU10_1500, silver-enhancement of gold-conjugated secondary antibody for 25 min produced a brown precipitate visible by brightfield microscopy, revealing structures of filamentous appearance consistent in appearance with those observed by immunofluorescence microscopy (Fig. 3.31, inset, upper right-hand corner, white arrows). In samples silver-enhanced for 15 min, this precipitate was visible by transmission electron microscopy as irregularly shaped round black structures 4-25 nm in diameter (Fig. 3.31, inset, bottom left corner; Figs. 3.31, 3.32, black arrows). The silver precipitate was deposited along long, narrow tracts (Figs. 3.31 and 3.32, black arrows) in the lumen of the parasitophorous vacuole, consistent with the immunostaining pattern of ECU10_1500 antiserum by light microscopy (Figs. 3.23-3.26). The precipitate appears to be deposited upon structures of filamentous or tubular appearance (Fig. 3.31, black arrowheads, Fig. 3.32, first and second insets), one of which appears to branch (Fig. 3.32, 1st inset, white arrowhead) as observed by immunofluorescence microscopy (Figs. 3.25, 3.26, white double-headed arrows). The diameter of this filamentous or tubular structure varies along its length and between filaments, ranging approximately from 80 – 140 nm. Ultrastructurally, in longitudinal section it has a slightly electron-dense core (Fig. 3.32, 2nd inset, white double-headed arrow) surrounded by an electron-lucent middle layer (Fig. 3.32, 2nd inset, black double-headed arrow) and a very fine, slightly electron-dense outer layer (Fig. 3.32, 2nd inset, black double-arrowhead). The silver precipitate is not deposited upon

cross- or longitudinal-sections of the polar filament within spores or developing stages of the parasite (Fig. 3.32, black arrowheads).

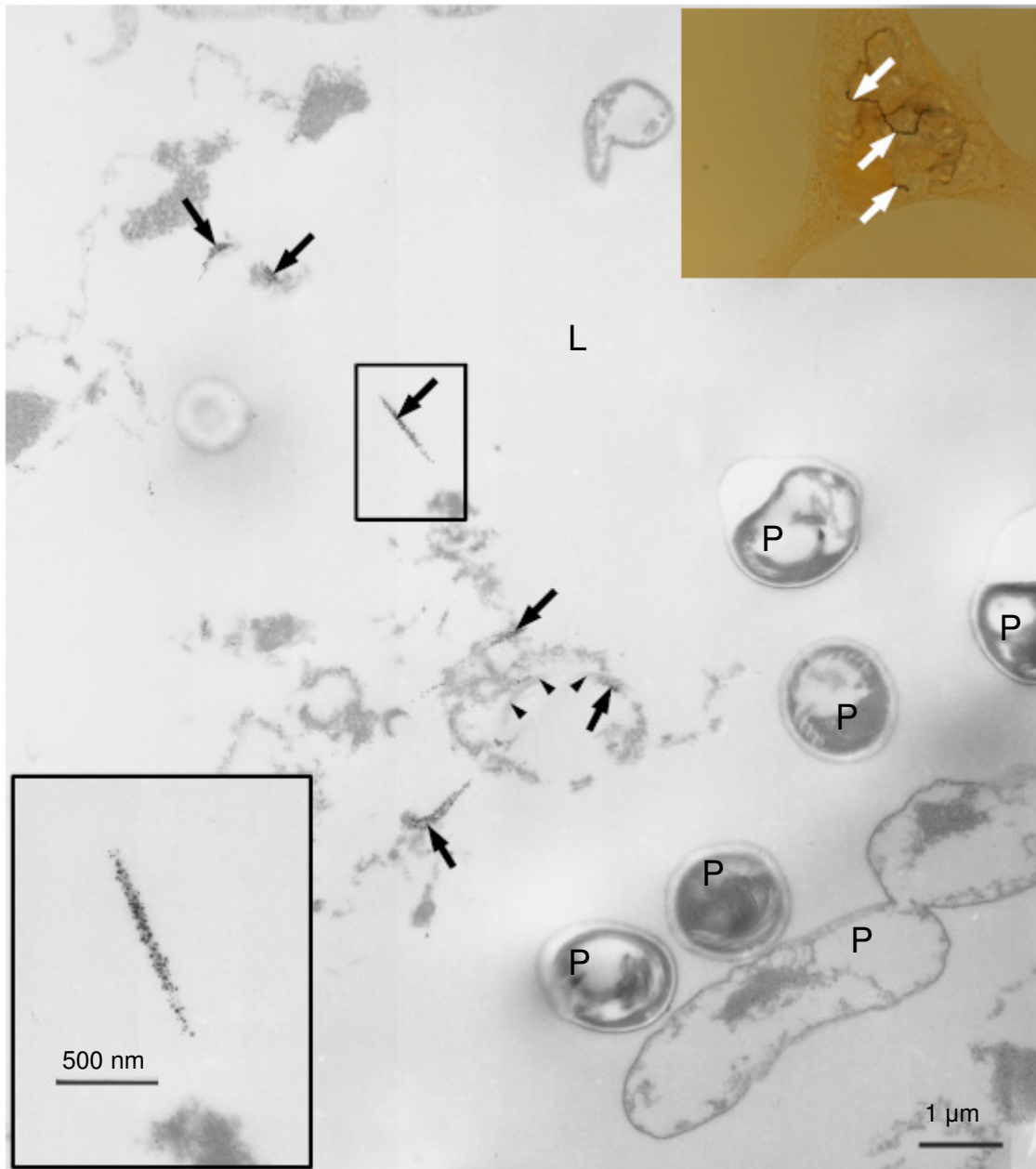


Fig 3.31 Immunolocalization of ECU10_1500 in *Enc. hellem*-infected host culture by silver-enhanced correlative light/immunoEM microscopy, plate 1. A brown precipitate visible by brightfield microscopy formed on structures of filamentous appearance (inset, upper right hand corner, white arrows) consistent in appearance with those observed by immunofluorescence. This precipitate was visible as small (4-25 nm) electron dense dots (inset, lower left corner; black arrows) on structures of filamentous or tubular appearance (arrowheads). P, parasites; L, lumen of parasitophorous vacuole.

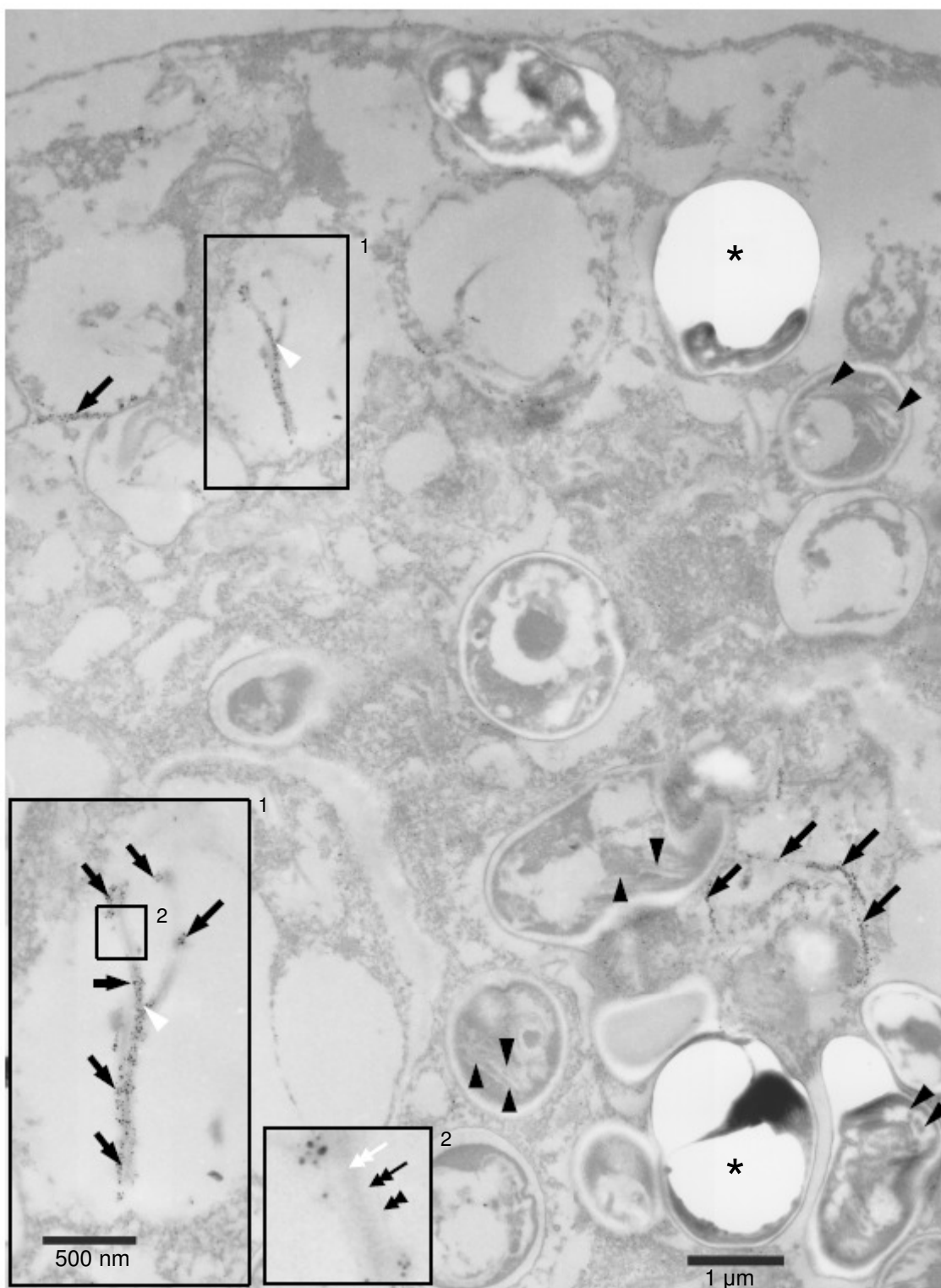


Fig 3.32 Immunolocalization of ECU10_1500 in *Enc. hellem*-infected host culture by silver-enhanced correlative light/immunoEM microscopy, plate 2. Figure legend continues on next page.

Fig 3.32, continued. ECU10_1500 is detected along long tubular or filamentous structures (black arrows) of $\sim 0.1 \mu\text{m}$ diameter in the parasitophorous vacuole and not along sections of the developing polar tube inside parasites (black arrowheads). These structures appear to branch, consistent with findings by light microscopy (white arrowhead, 1st inset). At higher magnification (1st and 2nd insets), the structure is of trilaminar appearance with an inner, slightly electron-dense core (white double-headed arrow), an electron-lucent intermediate layer (black double-headed arrow), and a very fine, slightly electron-dense outer layer (black double-arrowhead). Asterisks indicate spores or sporogonic stages dislodged during tissue processing for EM.

3.4

DISCUSSION

3.4.1 Efficacy and efficiency of methods

It was endeavored to clone, express, and generate murine antisera for the *in situ* immunolocalization of hypothetical gene products identified by mass spectrometry of fractionated of *Enc. cuniculi*. As a total of 52 hypothetical genes were identified from the five experiments (see Table 3.3), a medium-throughput approach was adopted. The efficiency of the methods employed to achieve these goals is discussed in this section.

3.4.1.1 PCR amplification of hypothetical genes of *Enc. cuniculi*

PCR conditions are critical for the production of ample quantities of error-free amplicons, and successful amplification from genomic DNA can be particularly challenging due to the complexity of the template (Sambrook and Russell, 2001). The isolation of pure genomic DNA from culture-harvested microsporidia is laborious, requiring detergent solubilization of host cell debris, mechanical disruption of spores, proteolytic digestion of protein, purification of DNA by phenol-chloroform extraction, and multiple steps of washing and centrifugation (Keohane et al., 1998). Therefore, mixed host/parasite DNA isolated from heavily infected RK13 host cell cultures by a commercially available silica membrane-based genomic DNA extraction kit was used instead as template for the amplification of microsporidian genes. However, the presence of large amounts of mammalian host DNA not only risks amplification of non-target sequences, but makes difficult the determination of the concentration of parasite DNA. The amount of mixed genomic DNA used per reaction, 27.5 ng, was

conservatively chosen to allow for 90% to be of host origin, yet still provide 10^5 - 10^6 copies of the parasite genome per reaction. Because genes were amplified using primers with vector-compatible 5' extensions, the two-stage cycling program employed accommodated annealing temperature differences between the initial, genomic DNA-primer duplex and the final, longer, amplicon-primer duplex. These PCR conditions, in addition to the frequent utilization of annealing temperatures 1-3 C° below the range of normally recommended parameters (i.e., 3-5°C below the primer-template duplex melting temperature) to spatially accommodate the grouping together of genes of similar size (within 1 kb) within one thermocycler run, and simultaneous employment of two PCR thermocyclers capable of maintaining a spatial temperature gradient, permitted the amplification of as many as twenty hypothetical genes at once. 88% of these amplicons were visible as single bands with the remaining 10% as dominant bands by agarose gel electrophoresis (representative results, Fig. 3.3). Only one hypothetical gene (ECU08_1700) failed to be amplified and resulted in multiple weak bands, none of which corresponded to the target gene. While the presence of mammalian DNA did not impede amplification of the other 52 genes (98%) in this study, it is perhaps worth attempting amplification of this gene from pure *Enc. cuniculi* DNA.

3.4.1.2 Cloning into prokaryotic vector

In order to eliminate the intermediary steps of rendering amplicons compatible to cloning and expression vectors by a second PCR reaction and/or enzymatic restriction digestion, parasite genes were amplified using primers with overhangs

complementary to a ligation-independent directional vector which was compatible with both the prokaryotic cloning and expression hosts. For each hypothetical gene, screening by vector cloning site-specific PCR of five to ten transformed colonies showed that 75-100% harbored inserts of the correct size, with most of the remainder lacking inserts altogether (representative results, Fig. 3.4); DNA sequencing confirmed that plasmids isolated from PCR-positive colonies matched their reference sequence in the *Enc. cuniculi* genome. These data suggest that in the interests of time and reagent conservation for future medium- and high-throughput projects employing the Ek/LIC vector system, transformant colony screening by PCR could be eliminated in favor of direct procession to plasmid isolation, DNA sequencing, and transformation of the expression host.

3.4.1.3 Protein expression and purification

Escherichia coli is easily the most widely employed host for the heterologous expression of eukaryotic, bacterial, archaeal, and viral proteins and is recommended by several structural genomics consortia and protein production facilities as the default host for the expression of any protein, regardless of origin (Structural Genomics Consortium et al., 2008). Because of the ease and low cost of manipulating and maintaining cultures in the laboratory, a variety of purpose-engineered host strains, vectors, expression conditions, and purification strategies have been developed for protein production in this bacterium. The host strain employed for the expression of the 52 hypothetical proteins in this study was selected on the basis of its *omp* protease deficiency, which increases

the stability and recovery of intact foreign proteins, as well as for its plasmid-encoded supply of 7 rare tRNAs to bypass the potential problem of prokaryotic–eukaryotic codon usage bias. The former attribute was particularly useful in light of the long incubation times used for expression by autoinduction.

The widely used pET vector-based system was selected for expression, as it is capable of powerfully driving expression of foreign genes by the lactose-inducible T7 promoter (Studier and Moffatt, 1986) and is compatible with a commercially available autoinduction system. In contrast to traditional induction by the lactose analog isopropyl β -D-1-thiogalactopyranoside which requires monitoring of culture cell density prior to the induction of expression, autoinduction media automatically induce expression at high culture cell density, e.g., at stationary phase. Autoinduction relies on the differential metabolization of carbon sources in the media to promote growth of cells to high density without potentially deleterious basal expression of the target gene, followed by high-level autoinduction of protein expression by lactose (Studier, 2005). The media is also enriched with magnesium and additional nitrogen sources, which promote viability at high cell densities and support increased protein synthesis, respectively (Studier, 2005; Grossman et al., 1998). Bacterial cultures and expressed transgenes are stable even several hours after full induction (Studier et al., 2005), in contrast to chemically induced cultures which are subject to loss of cell viability, target protein degradation, and selective overgrowth of non-expressor cells (Sambrook and Russell, 2001). The obviation of periodical monitoring of bacterial culture optical density was especially advantageous in this

medium-throughput expression project, where under an IPTG-induction protocol different bacterial cultures would likely have reached the appropriate cell density for induction and attained maximal transgene expression at different rates. Use of the autoinduction method permitted the simultaneous induction of expression and harvesting of cells of as many as two dozen hypothetical gene products, each in a 2-mL cell culture volume which was sufficient for the evaluation of expression and purification of protein for initial and subsequent booster immunizations of mice. In addition, in a study involving the expression of bacterial transmembrane proteins, the yield by autoinduction was found to be ten-fold higher than by IPTG induction (Chao and Fu, 2004). Thus, the superior efficacy and efficiency of autoinduction as compared to traditional IPTG induction made it a good choice for this medium-throughput expression project and likely contributed to the high success rate and efficiency of expression (39 of 52, or 75% of attempted hypothetical genes).

The choice of fusion tag for target gene expression was less straightforward, as a variety are available yet no single one has been shown to be globally superior in facilitating expression (Structural Genomics Consortium et al., 2008; Korf et al., 2005). However, the importance of this choice was not paramount for the purpose of this study, which was to produce a few hundred micrograms of each protein without regard to solubility for immunization of two to three mice. Thus the pET-41 vector which encodes glutathione-S-transferase (GST) and oligohistidine tags was chosen, as our laboratory has had previous success in inducing the prokaryotic expression of microsporidian genes fused to

GST in pGEX vectors (e.g., Ghosh et al., 2006; Xu et al., 2006) and the presence of two fusion tags for which affinity chromatography systems are available provided these as future options for protein purification. In view of the common affinity purification-related problems of poor bacterial cell lysis, failure of recombinant protein to bind to and elute from affinity purification columns, and co-purification of bacterial proteins (Structural Genomics Consortium et al., 2008; Korf et al., 2005). However, a simple “first-pass” strategy for protein purification consisting of excision of the overexpressed band from recombinant protein-expressing bacterial lysates on SDS–polyacrylamide gels was adopted. Excision of gel bands has proven to be an adequate purification strategy for the generation of murine antisera to polar tube proteins from several species of microsporidia (L.M. Weiss, unpublished observations). This strategy also permitted induction at high temperature (i.e., 37°C) without regard to solubility, which is usually encouraged by incubation below optimal physiological growth temperature (Structural Genomics Consortium et al., 2008; Korf et al., 2005) but may reduce overall expression levels. While immunization of mice with soluble protein would at least in principle increase the presence of native epitopes in the immunogen and thus successful downstream *in situ* localization of the gene product, it should be noted that in addition to the aforementioned pitfalls of affinity-based protein purification, the denaturing conditions frequently required in purification protocols (e.g., in metal affinity chromatography of oligohistidine-tagged recombinant proteins) are themselves unlikely to support folding of a target protein into its native conformation. Thus, without an automated pipetting

robot, affinity chromatography was deemed impractical for the large number of hypothetical genes for which expression was to be attempted. Nevertheless, the careful choice of expression host, vector, fusion tag, and induction conditions enabled the heterologous expression and gel-purification of 39 of 52 (75%) full-length hypothetical proteins of *Enc. cuniculi*. This success rate compares favorably with that from a compendium of eukaryotic protein expression studies maintained by the Protein Data Bank of the Protein Structure Initiative funded by the National Institute of General Medical Sciences-NIH (8,008 of 42,239, 19%) (cited in Structural Genomics Consortium et al., 2008). While the majority of studies therein likely relied on lower-temperature induction methods producing soluble protein for functional studies rather than antibody production, the autoinduction method is compatible with lower temperatures and longer incubation times (Studier, 2005) and was shown in this study of *Enc. cuniculi* to promote robust expression even at 30°C (Fig 3-44, panels F, G). The success of methods employed herein also compare favorably with that of a large-scale expression project of soluble and insoluble uncharacterized human proteins fused to GST and induced by IPTG at 30°C (29 of 55, 53%) and 20°C (24 of 38, 63%) (Korf et al., 2005).

The induction of expression of any protein is affected by its biochemical attributes, not all of which can be easily predicted, especially in heterologous contexts. However, it is well known that high molecular weight proteins are more difficult to express in *E. coli*, which is likely due to increased protein complexity and the requirement for stabilizing binding partners not present in the expression

host (Dyson et al., 2004). Korf et al. found an upper limit of approximately 80 kDa for successful expression; in this study of *Enc. cuniculi* proteins, an 83- and 84-kDa protein were expressed, but of the largest ten proteins (approximately 60–140 kDa), only 3 (30%) were expressed in contrast to the study-wide success rate of 75%. The mean molecular weight of expressed proteins was significantly less than that of non-expressed proteins (37.0 vs. 59.0 kDa, $p < 0.05$), which was quite similar to the difference found by Korf et al. (36 vs. 56 kDa). The size distribution of proteins in both the study by Korf et al. and this study are similar: 80% of the human proteins and 71% of the *Enc. cuniculi* proteins were between 20 and 70 kDa, with the average molecular weight differing only by 1 kDa (42 vs. 43 kDa, respectively).

Expressed *Enc. cuniculi* proteins were slightly more acidic than non-expressed proteins on average (pI 6.6 vs. 8.0, $p < 0.05$). A negative correlation between high pI and expression success was also demonstrated in a large-scale expression project of 1,000 proteins from the apicomplexan parasite *Plasmodium falciparum* by multivariate logistic regression to exclude confounding relationships between other biochemical attributes (Mehlin et al., 2006). Additionally, a high isoelectric point has been shown to negatively predict crystallization success (Canaves et al., 2004). The reasons for these effects by pI are not at all clear, and may be explained by unconsidered correlations of pI with other biochemical attributes. Mutually unexclusive explanations relying on fundamental biological limitations of *E. coli* are also possible.

Because proteins of hydrophobic character generally prove more difficult to express than hydrophilic proteins (Cunningham and Deber, 2007), the relationship between hydrophobicity and likelihood of expression was examined. Both overall hydrophobicity as predicted by GRAVY and number of transmembrane domains predicted by the Hidden Markov Model differed significantly ($p < 0.05$) between expressed and non-expressed proteins (-0.50 vs. -0.21 and 0.051 vs. 1.92, respectively). While none of the proteins with the six highest GRAVY values (between -0.17 and +0.89) were expressed, it is worth noting that all were predicted to have one or more transmembrane domains. When the two expressed and six non-expressed proteins with predicted transmembrane domains were excluded, the mean GRAVY values between the two groups did not differ significantly ($p = 0.22$). A lack of correlation upon multivariate analysis between GRAVY score and inducible expression has been shown in other large-scale studies (e.g., Dyson et al., 2004; Mehlin et al., 2006) and it has been suggested that this may broadly hold for non-transmembrane proteins (Dyson et al., 2004), as GRAVY calculates the mean hydrophobicity of all of the amino acid side groups with no regard to the three-dimensional confirmation of the protein (Kyte and Doolittle, 1982). Thus GRAVY is perhaps a useful predictor for inducible expression only insofar as it mirrors the number of transmembrane domains present in a protein.

The biochemical attributes of molecular weight, pI, and GRAVY for all of the proteins for which expression was attempted in this study are depicted as a 3-variable bubble plot in Fig. 3.8. Here the distributional differences in each of

these attributes between expressed and non-expressed proteins are visually apparent. The multivariate representation of each protein also suggests reasons for the success or failure of expression which would be not as readily apparent when considering each variable separately. For example, given the negative relationship between high pI and expression, it might be expected that most of the proteins with a pI greater than 9 would fail to be expressed; however, the more negative 50% of this subset (4 of 8) in terms of GRAVY score were expressed, including the protein with the highest isoelectric point in the study (pI 10.94), perhaps due in part to its small size (16 kDa). Conversely, the plot suggests that the expression-favorable attribute of small size can be trumped by a high GRAVY score or isoelectric point. Of course, there are other biochemical attributes that were not considered and are difficult to predict based on the linear amino acid sequence, which undoubtedly contributed to the failure of expression of proteins residing in generally expression-favorable quadrants of the bubble plot. Nevertheless, advance plotting of expression candidates in future medium- or large-scale expression projects may allow investigators to proceed initially with those candidates which are most likely to be expressed, or to engineer appropriate partial-length constructs which may be more amenable to heterologous expression in *E. coli* due to reduced size, lower pI, or more negative GRAVY score/fewer transmembrane domains.

3.4.1.4 Antisera production

The specificity of antisera were objectively evaluated by immunoblot prior to immunofluorescence microscopy experiments. However, positivity by immunoblot was not a good predictor of specific staining activity *in situ*, as some immunoblot-positive antisera were non-reactive for parasites (e.g., ECU11_1210, Fig. 3.30) or exhibited high levels of non-specific staining or cross-reactivity with host cells (e.g., ECU01_0420, Fig. 3.29). Conversely, antiserum to ECU10_1070 reacted fairly strongly with two larger-than-expected molecular weight bands in addition to the expected-size band (Fig. 3.9, panel A), yet displayed a very specific staining pattern by immunofluorescence microscopy (Fig. 3.22A, B). The discrepancy may be due partly to the fact that immunoblots detect denatured protein bound to nitrocellulose, while immunolocalization *in situ* depends on the recognition of three-dimensional epitopes of protein in its native conformation. In addition, aberrant migration of native and recombinant hypothetical gene products by SDS-PAGE further confounded interpretation of immunoblot results. For example, the 50 kDa native ECU10_1500 protein (82 kDa with vector-encoded fusion tags) migrated as a non-discrete band of approximately 80 kDa (Fig. 3.9, panel A) and 115 kDa (Figs. 3.5, 3.6) in native and recombinant form, respectively, yet was shown by MALDI-TOF mass-spectrometry/peptide mass fingerprinting to correspond to the appropriate gene product with 29% amino acid sequence coverage (Fig. 3.7, Table 3.4) (comparable to the average coverage of 30% of gel-excised GST-fusion proteins in a study by Korf et al., 2005). The antiserum to this gene was clearly specific for discrete structures in the

parasitophorous vacuole by immunofluorescence and transmission immunoelectron microscopy (Figs 3.23-3.26, 3.31, 3.32). Thus immunoblots were of limited utility in evaluating antisera, and poor or unexpected results should not be used to exclude antisera from downstream immunolocalization experiments in large-scale proteome projects.

The purity, quantity, and method of immunization of protein are critical for the production of polyclonal antisera (Cooper and Patterson, 2008). More than one-third of the antisera produced (14 of 39, 36%) against hypothetical *Enc. cuniculi* proteins were specific *in situ* for parasites or structures within the parasitophorous vacuole (Figs. 3.10-3.26, 3.31, 3.32), indicating that the purification and immunization methods were adequate for these antigens. Many of these antisera also demonstrated reactivity to the host cell nucleus (Figs. 3.10-3.12, 3.14, 3.18, 3.21), but spurious antibody activities are common in polyclonal sera (Cooper and Patterson, 2008) and do not necessarily detract from their utility, providing such staining does not interfere with discernment of the structure of interest. However, 64% of the antisera were either non-reactive or non-specific for parasites (Figs. 3.29, 3.30), indicating either that these hypothetical genes are not expressed by the parasite in sufficient quantities to be detected by immunolocalization techniques, or that protein preparation methods prior to immunization were inadequate for the production of quality antisera to these particular antigens. Proteins vary in their intrinsic immunogenicity, and as such there are a variety of adjuvants available for augmenting humoral responses to injected proteins in laboratory animals (Cooper and Patterson, 2008). Most of

the antisera generated in this study, including the highly specific ECU09_0270 (Fig. 3.21), ECU10_1500 (Figs. 3.23-3.26), and SWP1 (Fig. 3.22C) were produced by immunizing mice with a slurry of crushed, overexpressed protein bands excised from bacterial lysates electrophoresed through SDS-polyacrylamide gels. Polymerized acrylamide has been used as a convenient and safe adjuvant in laboratory animals for more than forty years (Weintraub and Raymond, 1963) and has been previously shown to adequately potentiate murine immune responses to parasite proteins in our laboratory (L.M. Weiss, pers. commun.). However, the weak reactivity or lack of specificity for parasites of most antisera (59%) led to the employment of Complete Freund's Adjuvant (CFA) for proteins identified in LC-MS/MS Experiment 4. CFA, an adjuvant so powerful that concerns for animal welfare preclude its use in subsequent booster immunizations, was expected to yield antisera with high titer for parasite proteins. However, this expectation was clearly met by only 3 of the 12 (25%) antisera, while 6 (50%) exhibited high levels of background or cross-reactivity with host material and 3 (25%) were completely non-reactive with infected host-cell cultures, a result inferior to that achieved using acrylamide as adjuvant wherein 41% of antisera were specific for parasites. The reason for this is unclear, and could stem from methodological shortcomings as well as endogenous expression of hypothetical genes at levels too low to be detected by immunolocalization techniques. In the former case, it is possible that CFA augmented the response to *E. coli*-derived proteins which co-migrated with overexpressed parasite proteins by SDS-PAGE or to the GST fusion tag, homologs of which are present

in the cytosol of many mammalian cells (Boyer, 1989). Conceivably, this could have produced undesirable cross-reaction with host cell material, although in view of the successful production of 14 of 39 (36%) parasite-specific antisera to proteins of various sizes, as well as the numerous antisera that were completely non-reactive, however, it seems unlikely that low-titer antibody to *E. coli* proteins or to GST is primarily responsible for cross-reaction with eukaryotic host cell material. Nonetheless, a few possibilities for troubleshooting present themselves: affinity-purify and enzymatically cleave the fusion tag from a subset of recombinant proteins, which would require significantly increasing the scale of bacterial culture from 2 mL to 50 or several hundred mL, depending on protein solubility, and attempt to renature some of these proteins under non-denaturing conditions; immunize two groups of animals simultaneously, either with acrylamide gel slurry or adjuvant of intermediate potency between acrylamide and CFA (e.g., TiterMax (Cooper and Patterson, 2008), increasing the number of booster immunizations from the current one to as many as two or three, as necessary; increase the amount of protein injected, although as little as 1 µg has been shown to be sufficient in mice (Delves, 1997) and this amount was already exceeded 10- to 50-fold for each protein; cross-link protein into multimers or to a carrier protein such as keyhole limpet hemocyanin prior to emulsification with adjuvant, as increasing protein size has been shown to increase immunogenicity (Cooper and Patterson, 2008). While all of these suggestions clearly cannot be incorporated into medium- or high-throughput projects without disproportionate effort for problematic proteins, some of them could perhaps be applied in pilot

studies to smaller subsets of proteins for which quality antisera were not obtained.

3.4.2 *In situ* immunolocalization of hypothetical proteins

A total of 39 antisera to hypothetical *Enc. cuniculi* proteins were generated on the basis of results from five independent spore fractionation experiments subjected to LC-MS/MS analysis. Different proteins were identified among the five experiments due to variations in several factors: amount of *Enc. cuniculi* lysate processed, with each lysate originating from a different batch of harvested spores; fractionation, solubilization, and purification procedures performed prior to LC-MS/MS; and statistical analysis of LC-MS/MS results. Because Experiments 4 and 5 each produced a more refined list of identified proteins which included all of the characterized PTPs, SWP1 and 2 and the endospore wall protein EnP1 (see Table 3.2), the methods therein including sample processing procedures upstream of LC-MS/MS (see Fig. 3.1) and extensive statistical analysis including confidence intervals of percent amino acid sequence coverage for each protein were deemed superior to those from prior Experiments. However, the detection of PTP-derived peptides in the insoluble pellet fraction processed in Experiment 5 (Tables 3.2, 3.3) despite that the polar tube has been reported to be completely solubilized by DTT (Weidner, 1976; Keohane et al., 1994; 1996, 1998, 1999) suggests inadequate incubation with DTT or inadequate washing of the insoluble pellet, which may have masked the detection of less abundant species. These shortcomings can be remedied by increasing incubation time or volume and adding extra washing steps prior to

extraction by EA (see Fig. 3.1), respectively. Other annotated proteins were detected in both the DTT-soluble and –insoluble fractions such as ribosomal proteins, translation factors, and nuclear proteins including histones, DNA helicase, and general transcription factors (Table 3.2) and may also have masked less abundant species. While it is theoretically possible that proteins such as these are bona-fide components of the polar tube or spore wall, it is more likely that they represent parasite-derived contaminants, as the imperfection of any cell fractionation procedure and the exquisite sensitivity of MS/MS usually lead to the detection of undesired, abundant sample-derived species such as these (e.g., Trinkle-Mulcahy et al., 2008). While it is difficult to eliminate contaminant proteins entirely, it would be worthwhile to repeat Experiments 4 and 5 to confirm these results, possibly identify new protein components, and enable statistical estimation of the number of missing components by capture-recapture analysis. For example, this analysis was employed in a proteomic survey of the *Toxoplasma gondii* apical complex and led to an estimation that ~70% of the component organelle proteins had been detected among three replicates (Hu et al., 2006).

Antisera to the four *Enc. cuniculi* proteins (ECU01_0420, ECU04_0120, ECU07_0530, and ECU11_1210) included in this study on the basis of homology to recently identified SWPs of the silkworm-parasitic microsporidium *Nosema bombycis* (Wu et al., 2008, 2009) were either non-specific or non-reactive for parasites, but it is worth noting that no peptides corresponding to these proteins were detected by LC-MS/MS. In addition, BLAST analysis reveals that

ECU04_0120 and ECU07_0530 contain a conserved domain for the DnaJ/Hsp40 chaperone and SMC (structural maintenance of chromosomes) family of proteins, respectively; thus it is conceivable that these proteins serve appropriately predictable functions in *Enc. cuniculi* rather than structural roles in the spore wall.

3.4.2.1 Nuclear/perinuclear hypothetical proteins

Fourteen of the 39 antisera (36%) exhibit parasite-specific staining activity by immunohistochemistry (Figs. 3.17-3.26; 3.31, 3.32). Seven of these stain structures of interest within parasites or the parasitophorous vacuole and are discussed in detail below. The other seven antisera appear to stain parasite nuclei indiscriminately (e.g., Figs. 3.10-3.16) or, taking account of nuclei in some regions of the parasitophorous vacuole which remain unstained, possibly in a developmental stage-specific manner (e.g., Figs. 3.10, 3.14, 3.15). In view of the MS/MS detection of nuclear proteins including histones, DNA helicase, and transcription factors, it is likely that these proteins represent genome-unannotated nuclear contaminants of the fractionated *Enc. cuniculi* lysate rather than components of the infectious apparatus. Nonetheless, it may be worthwhile to examine the immunolocalization of a representative subset of these proteins by immunoEM in order to confirm the nuclear localization and explore the possibility of stage-specific expression of these genes.

3.4.2.2 Cytoplasmic proteins

Two of the proteins which localize to the cytoplasm were revealed by BLAST algorithm (Altschul et al., 1997) to contain putative zinc-finger domains. These domains are present in a large superfamily of proteins which perform diverse roles in replication and repair, transcription and translation, metabolism and signaling, cell proliferation, and apoptosis. The domains mediate binding to a variety of targets including DNA, RNA, small molecules, and other proteins (Krishna et al., 2003). Because of the variety of roles played by zinc-finger proteins, these two proteins were selected for expression despite having conserved domains. ECU04_1480 is also significantly similar (alignment scores between 40 and 90) to zinc-finger proteins of other parasites, including: *Nosema ceranae*, a microsporidian parasite of honey bees; the kinetoplastids *Trypanosoma brucei* and *Trypanosoma cruzi*, the causative agents of African sleeping sickness and Chagas' disease, respectively; the apicomplexan *Cryptosporidium parvum*, an intestinal parasite of particular concern to immunocompromised patients; and the kinetoplastids *Leishmania major* and *Leishmania infantum*, which cause cutaneous and visceral leishmaniasis, respectively. ECU04_1480 appears to localize to both the nuclear and cytoplasmic regions of early developmental forms of *Enc. cuniculi* which grow adherent to parasitophorous vacuolar membrane (Fig. 3.17, arrows and arrowheads). The apparent stage-specific expression of this protein and its similarity to zinc-finger domain-containing proteins of other intracellular protists suggest relevance to the intracellular parasitic lifestyle, making this gene an

attractive candidate for further study. Although this gene product does not visibly accumulate in spores or mature developmental forms such as sporoblasts, it would be worthwhile to examine its localization by immunoEM to determine if its distribution is restricted to a particular intracellular compartment.

The other zinc-finger domain-containing protein which was detected, ECU09_1010 has a more diffuse distribution. It appears to be present throughout the cytoplasm, but is more concentrated at the periphery of cells (Fig. 3.20, arrows), many of which appear to be undergoing cytokinesis. No transmembrane domains were predicted by the Hidden Markov Model for this protein; thus the intense staining at the periphery of the organisms is somewhat surprising. However, considering that developing stages floating in the lumen of the parasitophorous vacuole rather than adherent to its membrane are stained, it is possible that Fig. 3.20 represents a picture of an abundantly expressed protein in the midst of being exported to the developing endospore or exospore region of the spore wall. Again, the exceedingly small size of *Enc. cuniculi* makes examination by TEM critical for defining the localization of these gene products.

The antiserum to ECU07_0640 has a complementary distribution pattern to that of ECU09_1010, in that it appears to be more concentrated in the nuclear or perinuclear region (Fig. 3.18, arrowheads, top and bottom panels) but is also present throughout the cytoplasm (Fig. 3.18, arrows, top and bottom panels) . No putative conserved domains were detected by the BLAST algorithm for this protein, but the protein exhibits slight similarity along approximately 30% of its length (BLAST score ~40) to Hsp90 co-chaperone proteins from three other

fungi. Whether or not this protein fulfills a chaperone-like role in *Enc. cuniculi* cannot be known merely from this degree of similarity and the absence of putative conserved domains. However, chaperones frequently co-purify with target proteins (Trinkle-Mulcahy et al., 2008) due to their inherent protein-binding ability, making this a possibility that should be considered; thus the ECU07_0640 protein should be accorded low-priority status for further investigation. For similar reasons, the protein ECU09_0270 should also not receive further attention at this time, as by BLAST it shows a comparable degree of similarity to transcription factors from various organisms and has a diffuse, localization pattern in the parasite nucleus and cytoplasm and significant cross-reactivity with the host cell cytoplasm (Fig. 3.19).

3.4.2.3 Other intracellular proteins

The gene product of ECU09_0280 appears to be localized to discrete small round punctuate structures which frequently appear in groups of three close to the nucleus (Fig. 3.21A, white boxes; Fig. 3.21B, arrows, top and bottom panels) but sometimes two or four. The localization pattern of this protein is reminiscent of *Enc. cuniculi* ferredoxin, an iron–sulfur cluster protein (Lange et al., 2000) that has been shown to localize to similar punctuate structures *in situ* (Williams et al., 2008). Notably, ferredoxin-stained structures also occurred most often in groups of three around each parasite nucleus. It was noted by the authors that the appearance of these ferredoxin-stained structures was consistent with that of polar vesicles, membrane-bound structures occurring in several different

microsporidia which have recently been proposed on the basis of ultrastructural data to be mitosomes (Vavra, 2005), the term given to the relic mitochondria of microsporidia (Katinka et al., 2001). ECU09_0280 has no putative conserved domains or significant similarity to characterized proteins or any other *Enc. cuniculi* proteins, but has modest similarity (BLAST score 50-65) to hypothetical proteins two other microsporidia, *Enterocytozoon bieneusi*, the most common intestinal species afflicting AIDS patients (Bryan and Schwartz, 1999) and the honey bee parasite *Nosema ceranae*. In order to confirm the mitochondrial localization of this protein, colocalization with ferredoxin by immunofluorescence microscopy and immunoEM should be performed.

3.4.2.4 Peripheral proteins

The ECU10_1070 protein is localized to a thick layer at the periphery of developing parasite stages floating in the lumen of the parasitophorous vacuole (Fig. 3.22A, arrows; Fig 3.22B). The occurrence of nuclei in pairs (Fig. 3.22B, arrows) but separated by the deposition of ECU10_1070 protein indicates that these parasites are undergoing cell division. The location of the parasites and the nuclear configuration suggest that this protein is specifically expressed by sporonts, the stage at which the commitment to spore formation begins (Cali and Takvorian, 1999). The protein does not appear to be expressed in sporoblasts, the cells which undergo metamorphosis to form spores, as the final rounds of cell division occur in sporonts and no parasites with isolated nuclei are stained. Nor does this antiserum stain the wall of mature spores, as does similarly prepared

antiserum to SWP1 (Fig. 3.22C, line arrows); note that SWP1 is also found at the periphery of developing forms (Fig. 3.22C, arrowhead). Thus it is possible that ECU10_1070 forms an early scaffold in sporogony for the deposition of SWP 1 (Bohne et al., 2000), SWP 3 (Xu et al., 2006; Peuvel-Fanget et al., 2006), or EnP1 (Peuvel-Fanget et al., 2006), the three proteins which have been shown to be components of the mature spore wall. A better appreciation of the role of ECU10_1070 presently hinges on obtaining ultrastructural data for this protein, as currently available bioinformatic data on its sequence reveals little. It is a small (11 kDa) protein with no predicted transmembrane or putative conserved domains and no significant similarity to any proteins in the National Center for Biotechnology Information (NCBI) database except for a low score match (BLAST score 51) to a component of the large ribosomal subunit of *Enterocytozoon bieneusi*, which is likely of no functional significance especially given immunolocalization data.

3.4.2.5 Vacuolar

The ECU10_1500 protein is localized to a heretofore undescribed branching network in the lumen of the parasitophorous vacuole of *Enc. cuniculi* (Figs. 3.23, 3.24). Antiserum to this protein cross-reacts with its presumable homolog in *Enc. hellem*, staining apparently identical structures (Figs. 3.25, 3.26). By light and electron microscopy, this network appears to be composed of filamentous structures roughly 100 nm in diameter (Fig. 3.32, 1st and 2nd insets). Within one parasitophorous vacuole, multiple structures of different sizes may exist, with

some appearing as small, unbranching coils and others as larger, branching networks that extend through much of the parasitophorous vacuole (Figs. 3.25, 3.26). The diameter and multilaminate ultrastructure of the filament is somewhat reminiscent of the polar tube (Fig. 3.32, 2nd insets), but antiserum to ECU10_1500 does not stain polar filaments internal to parasites or polar tubes extruded from spores (Fig. 3.32, black arrowheads), and the network formed by this protein is found strictly in the lumen of the parasitophorous vacuole. Moreover, ECU10_1500 does not exhibit sequence similarity with PTPs of any microsporidia.

Because ECU10_1500 exhibits no significant similarity to any gene in the NCBI database and possesses no conserved functional domains other than a calcium-binding motif, it is difficult to speculate on the role of the filamentous network formed by this protein. However, several intriguing possibilities present themselves from the literature. *Toxoplasma gondii* is a ubiquitous, obligate intracellular protist parasite of the Phylum Apicomplexa that also causes serious morbidity in immunosuppressed populations (Hill and Dubey, 2002). Within five minutes of invading a host cell or being phagocytosed by a macrophage, this parasite begins elaborating a network of nanotubules within the lumen of the nascent parasitophorous vacuole (Sibley et al., 1986). The ultrastructural appearance of this network is dissimilar to that formed by ECU10_1500: in cross-section, it is of membranous-vesicular appearance (Sibley et al., 1986), but is associated with several proteins derived from electron-dense granules which are thought to be involved in its formation (Mercier et al., 2002); the tubules are

hollow and somewhat smaller in diameter on average (60-90 nm) than the ECU10_1500 filaments (Sibley et al., 1995); the network fills the *Toxoplasma* parasitophorous vacuole more densely than has been observed in *Encephalitozoon* (Sibley et al., 1986, 1995); and, tubules of the network are continuous with the membrane of the parasitophorous vacuole (Sibley et al., 1995). The authors of these studies have theorized that this network may serve to maximize the surface area for nutrient acquisition from the host into the parasitophorous vacuole. While no continuity was observed between the network formed by ECU10_1500 and the parasitophorous vacuolar membrane, this possibility cannot presently be eliminated, as the silver-enhancement correlative light/electron microscopy experiments performed in this study necessarily used utilized fixatives for light-microscopy and other tissue processing techniques which represent a compromise between the preservation of ultrastructural morphology and epitopes for antigen recognition (van Tuinen, 1996). As such, the silver precipitate corresponding to ECU10_1500 was observed in very few parasitophorous vacuoles by EM, but many if not most parasitophorous vacuoles were positive by brightfield microscopy. Thus it is advisable to repeat the immunoEM experiment using different fixation conditions and embedding media to improve the morphological preservation of the sample before drawing final conclusions regarding the ultrastructure of this intravacuolar network. It is also possible that the *Encephalitozoon* filamentous network serves to structurally support the parasitophorous vacuole, which can grow to be larger than the host cell nucleus and occupy virtually the entire cytoplasm.

Interestingly, the intravacuolar network of *Toxoplasma* disassembles in the absence of Ca^{++} (Sibley et al., 1986); in view of the putative Ca^{++} -binding domains of ECU10_1500, it would be interesting to see if adding a Ca^{++} -chelator to host cell growth media decreases the abundance of the network or affects growth characteristics such as size of the parasitophorous vacuoles. However, results from such an experiment would have to be cautiously interpreted, for while no Ca^{++} -gradient is apparently maintained across the parasitophorous vacuole membrane of *Enc. hellem* (Leitch et al., 1995), this may not be the case in Ca^{++} -stressed host cell cultures. In addition, the role of cations including Ca^{++} in promoting or inhibiting spore germination is unclear (reviewed in Xu and Weiss, 2005), making the addition of Ca^{++} -chelators a potentially confounding variable in the evaluation of effects on parasite and parasitophorous vacuole growth.

3.4.3 Conclusion

In summary, this work comprises the first large-scale proteomics-based immunohistochemical survey of hypothetical gene products conducted in *Enc. cuniculi*. In an effort to find novel components of the infectious apparatus of these organisms, antisera were produced against thirty-nine of fifty-two (75%) candidate hypothetical proteins identified by LC-MS/MS of DTT-soluble and -insoluble fractions of spore lysate. The efficiency and success rate of the methods employed herein for the heterologous expression in *E. coli* compares favorably with those of other eukaryotic expression projects. As a result, novel

components of the mitosome, the developing spore wall, and a heretofore undescribed filamentous network within the parasitophorous vacuole were putatively identified *in situ*, as well as various other developmentally-expressed proteins with generalized cytoplasmic or nuclear distributions. The progress regarding the antiserum production workflow and immunolocalization data on each of the hypothetical genes selected for study is summarized in Table 3.5.

While novel components of the polar tube failed to be identified, optimization of protein expression and purification and/or murine immunization methods may produce additional candidates. However, as PTP-immunized animals have readily yielded high-titer antisera (B. Bouzahzah and F. Nagajyothi, pers. commun.) due to the extreme immunogenicity of these proteins, the possibility that the three previously characterized PTPs entirely comprise this organelle should also be considered.

CHAPTER 4

Final conclusions and future studies

The Microsporidia are a diverse and ubiquitous group of eukaryotic obligate intracellular parasites which were recognized over 100 years ago with the description of *Nosema bombycis*, a parasite of silkworms (Nageli, 1857). It is now appreciated that these organisms are related to the Fungi (Lee et al., 2008; Hibbett et al., 2007). Microsporidia infect all major animal groups most often as gastrointestinal pathogens; however, they have been reported from every tissue and organ system (Franzen and Muller, 2001), and their spores are common in environmental sources such as ditch water (see Ghosh and Weiss, 2009). Several different genera of these organisms infect humans, but the majority of cases are due to either *Enterocytozoon bieneusi* or *Encephalitozoon* species (Bryan and Schwartz, 1999; Didier and Weiss, 2006). These pathogens employ a unique infection strategy in which the contents of the spore are virtually injected into a host cell via the polar tube, an organelle that lies coiled within the resting spore but everts with a force sufficient to pierce the plasma membrane of a faraway cell. While this remarkable process has always been a primary focus in microsporidiology, many questions remain regarding the biochemical events and structural composition of the organelles that enable its occurrence. As the *Encephalitozoon cuniculi* genome has been sequenced (Katinka et al., 2001), this common human-infecting species was chosen as the model organism in which to address some of these issues.

The first half of this work provides insight regarding the biochemical mechanisms of spore germination. While the ultimate cause of polar filament eversion is not definitively known for any species, and in view of the diversity of

hosts and habitats, undoubtedly varies across the phylum, all microsporidia are believed to proximally depend on a dramatic influx of water to drive eversion of the polar filament. Ultrastructural investigations of several species demonstrated swelling and breakdown of intrasporal compartments including the posterior vacuole and polaroplasts just prior to germination (reviewed in Keohane and Weiss, 1999; Vavra and Larsson, 1999). As osmosis across the lipid bilayer is energetically limited, however, it was unclear how such a rapid influx of water might be supported, especially considering that the existence of transmembrane aquaporins (AQPs) which facilitate osmosis was unknown until the early 1990s (Preston et al., 1992). Thus the first half of this dissertation research entailed functionally testing an AQP-like protein (*EcAQP*) identified in the *Enc. cuniculi* genome (Katinka et al., 2001) in a standard heterologous *Xenopus* oocyte system (Wagner et al., 2000). The *EcAQP*-encoded protein was found to localize to the plasma membrane and confer intermediate-to-high water permeability to these oocytes (Ghosh et al., 2006 a,b). The finding that *Enc. cuniculi* encodes a functional AQP despite being one of the best eukaryotic examples of reductive genomic evolution (Texier et al., 2005) supports the notion that osmotic influx drives the germination process, especially when viewed in the context of older ultrastructural data demonstrating swelling of intracellular compartments. To gain further insight regarding how AQPs facilitate intrasporal swelling it will be necessary to localize *EcAQP in situ* by immunoEM. Whether it appears embedded in the plasma membrane, polaroplast membrane, posterior vacuole membrane, or a combination of these will be of great interest. Another

possibility is that *EcAQP* will be found in plasma membrane invaginations along the polar filament, which incidentally suggest that this organelle is actually situated outside the sporoplasm proper (Cali et al., 2002).

AQPs have been an explosive area of research since they were discovered in the early 1990s and as such, several have been identified from pathogenic protozoa in recent years (Beitz, 2005). Of particular interest, AQP-like sequences with 27 to 80% identity to *EcAQP* from four other microsporidia have now been deposited in GenBank: *Enc. hellem* (accession no. AAQ91842); *Enc. intestinalis* (accession no. AAQ23044); *Nosema ceranae* (accession no. EEQ81370); and two from *Enterocytozoon bieneusi* (accession nos. EED44283, EED44287). It is generally expected that pharmacological interference with the function of AQPs may have deleterious effects on the osmotic protection and metabolic processes of disease-causing parasites, but as most inhibitors of aquaporins such as mercury are cytotoxic, viable candidates for chemotherapy have not been forthcoming. However, potential modes of aquaporin gating or regulation are ongoing areas of research (Hedfalk et al., 2006), and coupled with the recent development of a mammalian transfection system to screen commercially available drug libraries for effects on AQP function (Solenov et al., 2004), the search for pharmacologic agents may be hastened. In a collaboration with the Department of Neuroscience at Albert Einstein College of Medicine, *EcAQP* has already been cloned into a mammalian expression vector and pilot-tested for functionality in one immortalized cell line (unpublished data).

The second half of this work endeavored to identify novel components of the infectious apparatus of *Enc. cuniculi*. As the remarkable elasticity of the polar tube and tensile strength of the spore wall are critical to later stages of the germination process which occur downstream of osmotic swelling, a better appreciation of the molecular composition of these and adjacent organelles within the spore was sought. Thus, a so-called shotgun-proteomic approach (Han et al., 2008) was employed wherein relatively insoluble fractions of spore lysate were subjected to liquid chromatography coupled to tandem mass-spectrometry (LC-MS/MS). Antisera were generated to 39 candidate genes which were then immunolocalized *in situ*, constituting the first large-scale proteomics-based immunohistochemical survey of hypothetical gene products conducted in *Enc. cuniculi*. As a result, novel components of the mitosome, the developing spore wall, and a heretofore undescribed filamentous network within the parasitophorous vacuole which is also present in sister species *Encephalitozoon hellem* were putatively identified. Preliminary ultrastructural data for this intra-vacuolar filamentous network was obtained, and continued refinement of immunoEM tissue-processing methods which simultaneously preserve morphology and cognate epitopes is in progress for the ultrastructural localization of these novel structural proteins.

While the obtainment of ultrastructural data on candidate structural proteins is a requisite early step, complementary functional studies are also essential to understand the biogenesis and functional role of complex structures.

However, in contrast to several other human-pathogenic protists for which the generation of parasite strains in which a particular gene is deleted or over-expressed is possible (e.g., *Toxoplasma*, *Plasmodium*, *Leishmania*, *Trypanosoma*), the genetic intractability of the microsporidia renders this more of a challenge. Moreover, as their life cycle includes no extracellular stage other than the thick-walled spore, and their extremely unusual genomes have not permitted the discernment of promoter sequences (Keeling and Fast, 2002), it does not seem that a transfection system is on the horizon. Thus, delineation of protein function in the microsporidia presently depends on bioinformatic analysis and classical molecular biology and biochemical experiments that do not require genetic manipulation of the parasite. In view of this limitation, perhaps the antisera which stain the intravacuolar filamentous network and the developing wall of sporonts could be used to immunoprecipitate (IP) interacting proteins from an *Enc. cuniculi* lysate, and prominent bands from samples separated by SDS-PAGE could then be subjected to MS. Subsequently, this experiment could be repeated with the same antisera on lysates of other closely related microsporidia. Using partial amino acid sequence data on presumptive homologs, perhaps full sequences could be obtained by rapid amplification of cDNA ends (RACE). An alignment of the presumptive homologs from two or more organisms may provide hints at functionality from conserved regions. Somewhat surprisingly, no novel components of the polar tube were identified in this proteomic survey of *Enc. cuniculi*. As the detection by MS of low-abundance species is frequently challenging in high-complexity mixtures such as the parasite lysates used in this

study (Han et al., 2008), a similar IP experiment may prove useful in identifying novel polar tube proteins and other low-abundance interacting partners.

BIBLIOGRAPHY

- Agre, P., Kozono, D., 2003. Aquaporin water channels: molecular mechanisms for human diseases. *FEBS Letters* 555, 72.
- Akiyoshi, D.E., Morrison, H.G., Lei, S., Feng, X., Zhang, Q., Corradi, N., Mayanja, H., Tumwine, J.K., Keeling, P.J., Weiss, L.M., Tzipori, S., 2009. Genomic survey of the non-cultivable opportunistic human pathogen, *Enterocytozoon bieneusi*. *PLoS Pathog* 5, e1000261.
- Altschul, S.F., Madden, T.L., Schaffer, A.A., Zhang, J., Zhang, Z., Miller, W., Lipman, D.J., 1997. Gapped BLAST and PSI-BLAST: a new generation of protein database search programs. *Nucl. Acids Res.* 25, 3389-3402.
- Alvarado, J.J., Nemkal, A., Sauder, J.M., Russell, M., Akiyoshi, D.E., Shi, W., Almo, S.C., Weiss, L.M., 2009. Structure of a microsporidian methionine aminopeptidase type 2 complexed with fumagillin and TNP-470. *Mol Biochem Parasitol.*
- Beckers, P.J., Derks, G.J., Gool, T., Rietveld, F.J., Sauerwein, R.W., 1996. *Encephalocytozoon intestinalis*-specific monoclonal antibodies for laboratory diagnosis of microsporidiosis. *J Clin Microbiol* 34, 282-285.
- Beitz, E., 2005. Aquaporins from pathogenic protozoan parasites: structure, function and potential for chemotherapy. *Biol Cell* 97, 373-383.
- Bergquist, N.R., Stintzing, G., Smedman, L., Waller, T., Andersson, T., 1984. Diagnosis of encephalitozoonosis in man by serological tests. *Br Med J (Clin Res Ed)* 288, 902.
- Bigliardi, E., Selmi, M.G., Lupetti, P., Corona, S., Gatti, S., Scaglia, M., Sacchi, L., 1996. Microsporidian spore wall: ultrastructural findings on *Encephalitozoon hellem* exospore. *J Eukaryot Microbiol* 43, 181-186.
- Bohne, W., Ferguson, D.J., Kohler, K., Gross, U., 2000. Developmental expression of a tandemly repeated, glycine- and serine-rich spore wall protein in the microsporidian pathogen *Encephalitozoon cuniculi*. *Infect Immun* 68, 2268-2275.
- Boyer, T.D., 1989. The glutathione S-transferases: an update. *Hepatology* 9, 486-496.
- Bradley, P.J., Ward, C., Cheng, S.J., Alexander, D.L., Coller, S., Coombs, G.H., Dunn, J.D., Ferguson, D.J., Sanderson, S.J., Wastling, J.M., Boothroyd, J.C., 2005. Proteomic analysis of rhoptry organelles reveals many novel constituents for host-parasite interactions in *Toxoplasma gondii*. *J Biol Chem* 280, 34245-34258.

- Brosson, D., Kuhn, L., Prensier, G., Vivares, C.P., Texier, C., 2005. The putative chitin deacetylase of *Encephalitozoon cuniculi*: a surface protein implicated in microsporidian spore-wall formation. FEMS Microbiol Lett 247, 81-90.
- Bryan, R.T., Schwartz, D.A., 1999. Epidemiology of Microsporidiosis. In: Wittner, M., Weiss, L.M. (Eds.), The Microsporidia and Microsporidiosis, American Society for Microbiology, Washington, D. C., pp. 502-530.
- Burri, L., Williams, B.A., Bursac, D., Lithgow, T., Keeling, P.J., 2006. Microsporidian mitochondria retain elements of the general mitochondrial targeting system. Proc Natl Acad Sci U S A 103, 15916-15920.
- Cali, A., 1991. General microsporidian features and recent findings on AIDS isolates. J Protozool 38, 625-630.
- Cali, A., Kotler, D.P., Orenstein, J.M., 1993. *Septata intestinalis* N. G., N. Sp., an intestinal microsporidian associated with chronic diarrhea and dissemination in AIDS patients. J Eukaryot Microbiol 40, 101-112.
- Cali, A., Takvorian, P., 1999. Developmental Morphology and Life Cycles of the Microsporidia. In: Wittner, M., Weiss, L.M. (Eds.), The Microsporidia and Microsporidiosis, American Society for Microbiology, Washington, D. C., pp. 85-128.
- Cali, A., Weiss, L.M., Takvorian, P.M., 2002. *Brachiola algerae* spore membrane systems, their activity during extrusion, and a new structural entity, the multilayered interlaced network, associated with the polar tube and the sporoplasm. J Eukaryot Microbiol 49, 164-174.
- Canaves, J.M., Page, R., Wilson, I.A., Stevens, R.C., 2004. Protein biophysical properties that correlate with crystallization success in *Thermotoga maritima*: maximum clustering strategy for structural genomics. J Mol Biol 344, 977-991.
- Cavalier-Smith, T., 1991. Archamoebae: the ancestral eukaryotes? Biosystems 25, 25-38.
- Cavalier-Smith, T., 2005. Economy, speed and size matter: evolutionary forces driving nuclear genome miniaturization and expansion. Ann Bot (Lond) 95, 147-175.
- Chao, Y., Fu, D., 2004. Thermodynamic studies of the mechanism of metal binding to the *Escherichia coli* zinc transporter YiiP. J Biol Chem 279, 17173-17180.
- Cooper, H.M., Patterson, Y., 2008. Production of polyclonal antisera. Curr Protoc Immunol Chapter 2, Unit 2 4 1-2 4 10.

- Cornman, R.S., Chen, Y.P., Schatz, M.C., Street, C., Zhao, Y., Desany, B., Egholm, M., Hutchison, S., Pettis, J.S., Lipkin, W.I., Evans, J.D., 2009. Genomic analyses of the microsporidian *Nosema ceranae*, an emergent pathogen of honey bees. *PLoS Pathog* 5, e1000466.
- Costa, S.F., Weiss, L.M., 2000. Drug treatment of microsporidiosis. *Drug Resist Updat* 3, 384-399.
- Cunningham, F., Deber, C.M., 2007. Optimizing synthesis and expression of transmembrane peptides and proteins. *Methods* 41, 370-380.
- de Groot, B.L., Grubmuller, H., 2001. Water permeation across biological membranes: mechanism and dynamics of aquaporin-1 and GlpF. *Science* 294, 2353-2357.
- De Groote, M.A., Visvesvara, G., Wilson, M.L., Pieniazek, N.J., Slemenda, S.B., daSilva, A.J., Leitch, G.J., Bryan, R.T., Reves, R., 1995. Polymerase chain reaction and culture confirmation of disseminated *Encephalitozoon cuniculi* in a patient with AIDS: successful therapy with albendazole. *J Infect Dis* 171, 1375-1378.
- de Jong, J.C., McCormack, B.J., Smirnoff, N., Talbot, N.J., 1997. Glycerol generates turgor in rice blast. *Nature* 389, 244.
- Delves, P.J., 1997. *Antibody Production: Essential Techniques*. John Wiley & Sons, Hoboken, NJ.
- Desportes-Livage, I., Bylen, E., 1998. Microsporidia infection in HIV - negative subjects. *Acta Protozoologica* 37, 63-70.
- Didier, E.S., Weiss, L.M., 2006. Microsporidiosis: current status. *Curr Opin Infect Dis* 19, 485-492.
- Didier, P.J., Didier, E.S., Orenstein, J.M., Shadduck, J.A., 1991. Fine structure of a new human microsporidian, *Encephalitozoon hellem*, in culture. *J Protozool* 38, 502-507.
- Doolan, D.L., Southwood, S., Freilich, D.A., Sidney, J., Graber, N.L., Shatney, L., Bebris, L., Florens, L., Dobano, C., Witney, A.A., Appella, E., Hoffman, S.L., Yates, J.R., 3rd, Carucci, D.J., Sette, A., 2003. Identification of *Plasmodium falciparum* antigens by antigenic analysis of genomic and proteomic data. *Proc Natl Acad Sci U S A* 100, 9952-9957.
- Dyson, M.R., Shadbolt, S.P., Vincent, K.J., Perera, R.L., McCafferty, J., 2004. Production of soluble mammalian proteins in *Escherichia coli*: identification of protein features that correlate with successful expression. *BMC Biotechnol* 4, 32.

- Edlind, T., Visvesvara, G., Li, J., Katiyar, S. 1994. Cryptosporidium and microsporidial beta-tubulin sequences: predictions of benzimidazole sensitivity and phylogeny. *J Eukaryot Microbiol* 41, 38S.
- Felsenstein, J., 1989. PHYLIP—phylogeny inference package (version 3.2). *Cladistics* 5, 164-166.
- Findley, A.M., Weidner, E.H., Carman, K.R., Xu, Z., Godbar, J.S., 2005. Role of the posterior vacuole in *Spraguea lophii* (Microsporidia) spore hatching. *Folia Parasitol (Praha)* 52, 111-117.
- Florens, L., Washburn, M.P., Raine, J.D., Anthony, R.M., Grainger, M., Haynes, J.D., Moch, J.K., Muster, N., Sacci, J.B., Tabb, D.L., Witney, A.A., Wolters, D., Wu, Y., Gardner, M.J., Holder, A.A., Sinden, R.E., Yates, J.R., Carucci, D.J., 2002. A proteomic view of the *Plasmodium falciparum* life cycle. *Nature* 419, 520-526.
- Florens, L., Liu, X., Wang, Y., Yang, S., Schwartz, O., Peglar, M., Carucci, D.J., Yates, J.R., 3rd, Wub, Y., 2004. Proteomics approach reveals novel proteins on the surface of malaria-infected erythrocytes. *Mol Biochem Parasitol* 135, 1-11.
- Franzen, C., Muller, A., 2001. Microsporidiosis: human diseases and diagnosis. *Microbes Infect* 3, 389-400.
- Frixione, E., Ruiz, L., Santillan, M., deVargas, L.V., Tejero, J.M., Undeen, A.H., 1992. Dynamics of polar filament discharge and sporoplasm expulsion by microsporidian spores. *Cell. Motil. Cytoskeleton* 22, 38-50.
- Frixione, E., Ruiz, L., Cerbon, J., Undeen, A.H., 1997. Germination of *Nosema algerae* (Microspora) spores: conditional inhibition by D₂O, ethanol and Hg²⁺ suggests dependence of water influx upon membrane hydration and specific transmembrane pathways. *J Eukaryot Microbiol* 44, 109-116.
- Garcia, L.S., 2002. Laboratory identification of the microsporidia. *J Clin Microbiol* 40, 1892-1901.
- Germot, A., Philippe, H., Le Guyader, H., 1997. Evidence for loss of mitochondria in Microsporidia from a mitochondrial-type HSP70 in *Nosema locustae*. *Mol Biochem Parasitol* 87, 159-168.
- Ghosh, K., Cappiello, C.D., McBride, S.M., Occi, J.L., Cali, A., Takvorian, P.M., McDonald, T.V., Weiss, L.M., 2006a. Functional characterization of a putative aquaporin from *Encephalitozoon cuniculi*, a microsporidia pathogenic to humans. *International Journal for Parasitology* 36, 57-62.

- Ghosh, K., Takvorian, P.M., McBride, S.M., Cali, A., Weiss, L.M., 2006b. Heterologous expression of an *Encephalitozoon cuniculi* aquaporin in *Xenopus* oocytes. *J Eukaryot Microbiol* 53 Suppl 1, S72-73.
- Ghosh, K., Weiss, L.M., 2009. Molecular diagnostic tests for microsporidia. *Interdiscip Perspect Infect Dis* 2009, 926521.
- Graslund, S., Nordlund, P., Weigelt, J., Hallberg, B.M., Bray, J., Gileadi, O., Knapp, S., Oppermann, U., Arrowsmith, C., Hui, R., Ming, J., dhe-Paganon, S., Park, H.W., Savchenko, A., Yee, A., Edwards, A., Vincentelli, R., Cambillau, C., Kim, R., Kim, S.H., Rao, Z., Shi, Y., Terwilliger, T.C., Kim, C.Y., Hung, L.W., Waldo, G.S., Peleg, Y., Albeck, S., Unger, T., Dym, O., Prilusky, J., Sussman, J.L., Stevens, R.C., Lesley, S.A., Wilson, I.A., Joachimiak, A., Collart, F., Dementieva, I., Donnelly, M.I., Eschenfeldt, W.H., Kim, Y., Stols, L., Wu, R., Zhou, M., Burley, S.K., Emtage, J.S., Sauder, J.M., Thompson, D., Bain, K., Luz, J., Gheyi, T., Zhang, F., Atwell, S., Almo, S.C., Bonanno, J.B., Fiser, A., Swaminathan, S., Studier, F.W., Chance, M.R., Sali, A., Acton, T.B., Xiao, R., Zhao, L., Ma, L.C., Hunt, J.F., Tong, L., Cunningham, K., Inouye, M., Anderson, S., Janjua, H., Shastry, R., Ho, C.K., Wang, D., Wang, H., Jiang, M., Montelione, G.T., Stuart, D.I., Owens, R.J., Daenke, S., Schutz, A., Heinemann, U., Yokoyama, S., Bussow, K., Gunsalus, K.C., 2008. Protein production and purification. *Nat Methods* 5, 135-146.
- Grossman, T.H., Kawasaki, E.S., Punreddy, S.R., Osburne, M.S., 1998. Spontaneous cAMP-dependent derepression of gene expression in stationary phase plays a role in recombinant expression instability. *Gene* 209, 95-103.
- Han, X., Aslanian, A., Yates, J.R., 3rd, 2008. Mass spectrometry for proteomics. *Curr Opin Chem Biol* 12, 483-490.
- Hansen, M., Kun, J.F., Schultz, J.E., Beitz, E., 2002. A single, bi-functional aquaglyceroporin in blood-stage *Plasmodium falciparum* malaria parasites. *J Biol Chem* 277, 4874-4882.
- Hartskeerl, R.A., Van Gool, T., Schuitema, A.R., Didier, E.S., Terpstra, W.J., 1995. Genetic and immunological characterization of the microsporidian *Septata intestinalis* Cali, Kotler and Orenstein, 1993: reclassification to *Encephalitozoon intestinalis*. *Parasitology* 110 (Pt 3), 277-285.
- Hayman, J.R., Hayes, S.F., Amon, J., Nash, T.E., 2001. Developmental expression of two spore wall proteins during maturation of the microsporidian *Encephalitozoon intestinalis*. *Infect Immun* 69, 7057-7066.
- Hedfalk, K., Tornroth-Horsefield, S., Nyblom, M., Johanson, U., Kjellbom, P., Neutze, R., 2006. Aquaporin gating. *Curr Opin Struct Biol* 16, 447-456.

- Henry, J.E., Oma, E.A., 1981. Pest control by *Nosema locustae*, a pathogen of grasshoppers and crickets. In: Burges, H.D. (Ed.), Microbial control of pests and plant diseases 1970–1980, Academic Press, New York, pp. 573–586.
- Heymann, J.B., Engel, A., 1999. Aquaporins: Phylogeny, Structure, and Physiology of Water Channels. *News Physiol Sci* 14, 187-193.
- Hibbett, D.S., Binder, M., Bischoff, J.F., Blackwell, M., Cannon, P.F., Eriksson, O.E., Huhndorf, S., James, T., Kirk, P.M., Lucking, R., Thorsten Lumbsch, H., Lutzoni, F., Matheny, P.B., McLaughlin, D.J., Powell, M.J., Redhead, S., Schoch, C.L., Spatafora, J.W., Stalpers, J.A., Vilgalys, R., Aime, M.C., Aptroot, A., Bauer, R., Begerow, D., Benny, G.L., Castlebury, L.A., Crous, P.W., Dai, Y.C., Gams, W., Geiser, D.M., Griffith, G.W., Gueidan, C., Hawksworth, D.L., Hestmark, G., Hosaka, K., Humber, R.A., Hyde, K.D., Ironside, J.E., Koljalg, U., Kurtzman, C.P., Larsson, K.H., Lichtwardt, R., Longcore, J., Miadlikowska, J., Miller, A., Moncalvo, J.M., Mozley-Standridge, S., Oberwinkler, F., Parmasto, E., Reeb, V., Rogers, J.D., Roux, C., Ryvarden, L., Sampaio, J.P., Schussler, A., Sugiyama, J., Thorn, R.G., Tibell, L., Untereiner, W.A., Walker, C., Wang, Z., Weir, A., Weiss, M., White, M.M., Winka, K., Yao, Y.J., Zhang, N., 2007. A higher-level phylogenetic classification of the Fungi. *Mycol Res* 111, 509-547.
- Higgins, D.G., Bleasby, A.J., Fuchs, R., 1992. CLUSTAL V: improved software for multiple sequence alignment. *Comput Appl Biosci* 8, 189-191.
- Hill, D., Dubey, J.P., 2002. *Toxoplasma gondii*: transmission, diagnosis and prevention. *Clin Microbiol Infect* 8, 634-640.
- Hirt, R.P., Logsdon, J.M., Jr., Healy, B., Dorey, M.W., Doolittle, W.F., Embley, T.M., 1999. Microsporidia are related to Fungi: evidence from the largest subunit of RNA polymerase II and other proteins. *Proc Natl Acad Sci U S A* 96, 580-585.
- Hu, K., Johnson, J., Florens, L., Fraunholz, M., Suravajjala, S., DiLullo, C., Yates, J., Roos, D.S., Murray, J.M., 2006. Cytoskeletal components of an invasion machine--the apical complex of *Toxoplasma gondii*. *PLoS Pathog* 2, e13.
- Johanson, U., Gustavsson, S., 2002. A new subfamily of major intrinsic proteins in plants. *Mol Biol Evol* 19, 456-461.
- Jung, J.S., Preston, G.M., Smith, B.L., Guggino, W.B., Agre, P., 1994. Molecular structure of the water channel through aquaporin CHIP. The hourglass model. *J Biol Chem* 269, 14648-14654.

- Kamaishi, T., Hashimoto, T., Nakamura, Y., Masuda, Y., Nakamura, F., Okamoto, K., Shimizu, M., Hasegawa, M., 1996a. Complete nucleotide sequences of the genes encoding translation elongation factors 1 alpha and 2 from a microsporidian parasite, *Glugea plecoglossi*: implications for the deepest branching of eukaryotes. *J Biochem* 120, 1095-1103.
- Kamaishi, T., Hashimoto, T., Nakamura, Y., Nakamura, F., Murata, S., Okada, N., Okamoto, K., Shimizu, M., Hasegawa, M., 1996b. Protein phylogeny of translation elongation factor EF-1 alpha suggests microsporidians are extremely ancient eukaryotes. *J Mol Evol* 42, 257-263.
- Katinka, M.D., Duprat, S., Cornillot, E., Metenier, G., Thomarat, F., Prensier, G., Barbe, V., Peyretaillade, E., Brottier, P., Wincker, P., Delbac, F., El Alaoui, H., Peyret, P., Saurin, W., Gouy, M., Weissenbach, J., Vivares, C.P., 2001. Genome sequence and gene compaction of the eukaryote parasite *Encephalitozoon cuniculi*. *Nature* 414, 450-453.
- Keeling, P.J., Luker, M.A., Palmer, J.D., 2000. Evidence from beta-tubulin phylogeny that microsporidia evolved from within the fungi. *Mol Biol Evol* 17, 23-31.
- Keeling, P.J., Fast, N.M., 2002. Microsporidia: biology and evolution of highly reduced intracellular parasites. *Annu Rev Microbiol* 56, 93-116.
- Keeling, P.J., 2003. Congruent evidence from alpha-tubulin and beta-tubulin gene phylogenies for a zygomycete origin of microsporidia. *Fungal Genet Biol* 38, 298-309.
- Keeling, P.J., Fast, N.M., Law, J.S., Williams, B.A., Slamovits, C.H., 2005. Comparative genomics of microsporidia. *Folia Parasitol (Praha)* 52, 8-14.
- Keohane, E., Takvorian, P.M., Cali, A., Tanowitz, H.B., Wittner, M., Weiss, L.M., 1994. The identification and characterization of a polar tube reactive monoclonal antibody. *J Eukaryot Microbiol* 41, 48S.
- Keohane, E.M., Orr, G.A., Takvorian, P.M., Cali, A., Tanowitz, H.B., Wittner, M., Weiss, L.M., 1996. Purification and characterization of human microsporidian polar tube proteins. *J Eukaryot Microbiol* 43, 100S.
- Keohane, E.M., Orr, G.A., Zhang, H.S., Takvorian, P.M., Cali, A., Tanowitz, H.B., Wittner, M., Weiss, L.M., 1998. The molecular characterization of the major polar tube protein gene from *Encephalitozoon hellem*, a microsporidian parasite of humans. *Mol Biochem Parasitol* 94, 227-236.
- Keohane, E.M., Weiss, L.M., 1998. Characterization and function of the microsporidian polar tube: a review. *Folia Parasitol (Praha)* 45, 117-127.

- Keohane, E.M., Orr, G.A., Takvorian, P.M., Cali, A., Tanowitz, H.B., Wittner, M., Weiss, L.M., 1999a. Analysis of the major microsporidian polar tube proteins. *J Eukaryot Microbiol* 46, 29S-30S.
- Keohane, E.M., Orr, G.A., Takvorian, P.M., Cali, A., Tanowitz, H.B., Wittner, M., Weiss, L.M., 1999b. Polar tube proteins of microsporidia of the family encephalitozoonidae. *J Eukaryot Microbiol* 46, 1-5.
- Keohane, E.M., Weiss, L.M., 1999. The structure, function, and composition of the microsporidian polar tube. In: Wittner, M., Weiss, L.M. (Eds.), *The Microsporidia and Microsporidiosis*, American Society for Microbiology, Washington, D. C., pp. 196-224.
- Khan, I.A., Moretto, M., Weiss, L.M., 2001. Immune response to *Encephalitozoon cuniculi* infection. *Microbes Infect* 3, 401-405.
- King, L.S., Kozono, D., Agre, P., 2004. From structure to disease: the evolving tale of aquaporin biology. *Nat Rev Mol Cell Biol* 5, 687-698.
- Korf, U., Kohl, T., van der Zandt, H., Zahn, R., Schleege, S., Ueberle, B., Wandschneider, S., Bechtel, S., Schnolzer, M., Ottleben, H., Wiemann, S., Poustka, A., 2005. Large-scale protein expression for proteome research. *Proteomics* 5, 3571-3580.
- Krishna, S.S., Majumdar, I., Grishin, N.V., 2003. Structural classification of zinc fingers: survey and summary. *Nucleic Acids Res* 31, 532-550.
- Kudo, R.R., Daniels, E.W., 1963. An electron microscope study of the spore of a microsporidian, *Thelohania californica*. *J. Protozool.* 10, 112-120.
- Kyte, J., Doolittle, R.F., 1982. A simple method for displaying the hydropathic character of a protein. *J Mol Biol* 157, 105-132.
- Laize, V., Tacnet, F., Ripoché, P., Hohmann, S., 2000. Polymorphism of *Saccharomyces cerevisiae* aquaporins. *Yeast* 16, 897-903.
- Lange, H., Kaut, A., Kispal, G., Lill, R., 2000. A mitochondrial ferredoxin is essential for biogenesis of cellular iron-sulfur proteins. *Proc Natl Acad Sci U S A* 97, 1050-1055.
- Lasonder, E., Ishihama, Y., Andersen, J.S., Vermunt, A.M., Pain, A., Sauerwein, R.W., Eling, W.M., Hall, N., Waters, A.P., Stunnenberg, H.G., Mann, M., 2002. Analysis of the *Plasmodium falciparum* proteome by high-accuracy mass spectrometry. *Nature* 419, 537-542.
- Lee, S.C., Corradi, N., Byrnes, E.J., 3rd, Torres-Martinez, S., Dietrich, F.S., Keeling, P.J., Heitman, J., 2008. Microsporidia evolved from ancestral sexual fungi. *Curr Biol* 18, 1675-1679.

- Leitch, G.J., Scanlon, M., Visvesvara, G.S., Wallace, S., 1995. Calcium and hydrogen ion concentrations in the parasitophorous vacuoles of epithelial cells infected with the microsporidian *Encephalitozoon hellem*. *J Eukaryot Microbiol* 42, 445-451.
- Leitsch, D., Wilson, I.B., Paschinger, K., Duchene, M., 2006. Comparison of the proteome profiles of *Entamoeba histolytica* and its close but non-pathogenic relative *Entamoeba dispar*. *Wien Klin Wochenschr* 118, 37-41.
- Liebler, D.C., 2002. Introduction to Proteomics: Tools for the New Biology. Humana Press, Totowa, NJ.
- Liman, E.R., Tytgat, J., Hess, P., 1992. Subunit stoichiometry of a mammalian K⁺ channel determined by construction of multimeric cDNAs. *Neuron* 9, 861-871.
- Lom, J., Vavra, J., 1963. The mode of sporoplasm extrusion in microsporidian spores. *Acta Protozoologica* 1, 81-89.
- Lom, J., 1972. On the ultrastructure of the extruded microsporidian polar filament. *Z. Parasitenkd.* 38, 200-213.
- Lujan, H.D., Conrad, J.T., Clark, C.G., Touz, M.C., Delbac, F., Vivares, C.P., Nash, T.E., 1998. Detection of microsporidia spore-specific antigens by monoclonal antibodies. *Hybridoma* 17, 237-243.
- Mak, D.O., Foskett, J.K., 1994. Single-channel inositol 1,4,5-trisphosphate receptor currents revealed by patch clamp of isolated *Xenopus* oocyte nuclei. *J Biol Chem* 269, 29375-29378.
- Makanga, M., Bray, P.G., Horrocks, P., Ward, S.A., 2005. Towards a proteomic definition of CoArtem action in *Plasmodium falciparum* malaria. *Proteomics* 5, 1849-1858.
- Mehlin, C., Boni, E., Buckner, F.S., Engel, L., Feist, T., Gelb, M.H., Haji, L., Kim, D., Liu, C., Mueller, N., Myler, P.J., Reddy, J.T., Sampson, J.N., Subramanian, E., Van Voorhis, W.C., Worthey, E., Zucker, F., Hol, W.G., 2006. Heterologous expression of proteins from *Plasmodium falciparum*: results from 1000 genes. *Mol Biochem Parasitol* 148, 144-160.
- Mercier, C., Dubremetz, J.F., Rauscher, B., Lecordier, L., Sibley, L.D., Cesbron-Delauw, M.F., 2002. Biogenesis of nanotubular network in *Toxoplasma* parasitophorous vacuole induced by parasite proteins. *Mol Biol Cell* 13, 2397-2409.
- Metenier, G., Vivares, C.P., 2001. Molecular characteristics and physiology of microsporidia. *Microbes Infect* 3, 407-415.

- Metge, S., Van Nhieu, J.T., Dahmane, D., Grimbert, P., Foulet, F., Sarfati, C., Bretagne, S., 2000. A case of *Enterocytozoon bieneusi* infection in an HIV-negative renal transplant recipient. *Eur J Clin Microbiol Infect Dis* 19, 221-223.
- Montalvetti, A., Rohloff, P., Docampo, R., 2004. A functional aquaporin co-localizes with the vacuolar proton pyrophosphatase to acidocalcisomes and the contractile vacuole complex of *Trypanosoma cruzi*. *J Biol Chem* 279, 38673-38682.
- Nageli, 1857. Ueber die neue Krankheit die Seiden-raupe und verwandte Organismen. *Bot. Zeitung* 15, 760-761.
- Ohshima, K., 1937. On the function of the polar filament of *Nosema bombycis*. *Parasitology* 29, 220-224.
- Overton, I.M., van Niekerk, C.A., Carter, L.G., Dawson, A., Martin, D.M., Cameron, S., McMahon, S.A., White, M.F., Hunter, W.N., Naismith, J.H., Barton, G.J., 2008. TarO: a target optimisation system for structural biology. *Nucleic Acids Res* 36, W190-196.
- Pavlovic-Djuranovic, S., Schultz, J.E., Beitz, E., 2003. A single aquaporin gene encodes a water/glycerol/urea facilitator in *Toxoplasma gondii* with similarity to plant tonoplast intrinsic proteins. *FEBS Lett* 555, 500-504.
- Pearson, W.R., Lipman, D.J., 1988. Improved tools for biological sequence comparison. *Proc Natl Acad Sci U S A* 85, 2444-2448.
- Pearson, W.R., 1990. Rapid and sensitive sequence comparison with FASTP and FASTA. *Methods Enzymol* 183, 63-98.
- Persson, B., Argos, P., 1994. Prediction of transmembrane segments in proteins utilising multiple sequence alignments. *J Mol Biol* 237, 182-192.
- Peuvel-Fanget, I., Polonais, V., Brosseau, D., Texier, C., Kuhn, L., Peyret, P., Vivares, C., Delbac, F., 2006. EnP1 and EnP2, two proteins associated with the *Encephalitozoon cuniculi* endospore, the chitin-rich inner layer of the microsporidian spore wall. *Int J Parasitol* 36, 309-318.
- Preston, G.M., Carroll, T.P., Guggino, W.B., Agre, P., 1992. Appearance of water channels in *Xenopus* oocytes expressing red cell CHIP28 protein. *Science* 256, 385-387.
- Prigneau, O., Achbarou, A., Bouladoux, N., Mazier, D., Desportes-Livage, I., 2000. Identification of proteins in *Encephalitozoon intestinalis*, a microsporidian pathogen of immunocompromised humans: an immunoblotting and immunocytochemical study. *J Eukaryot Microbiol* 47, 48-56.

- Roberts, S.B., Robichaux, J.L., Chavali, A.K., Manque, P.A., Lee, V., Lara, A.M., Papin, J.A., Buck, G.A., 2009. Proteomic and network analysis characterize stage-specific metabolism in *Trypanosoma cruzi*. *BMC Syst Biol* 3, 52.
- Sambrook, J., Russell, D.W., 2001. *Molecular cloning: a laboratory manual*. CSHL Press, Woodbury, NY.
- Sax, P.E., Rich, J.D., Pieciak, W.S., Trnka, Y.M., 1995. Intestinal microsporidiosis occurring in a liver transplant recipient. *Transplantation* 60, 617-618.
- Schreiber, R., Pavenstadt, H., Greger, R., Kunzelmann, K., 2000. Aquaporin 3 cloned from *Xenopus laevis* is regulated by the cystic fibrosis transmembrane conductance regulator. *FEBS Lett* 475, 291-295.
- Sibley, L.D., Krahenbuhl, J.L., Adams, G.M., Weidner, E., 1986. *Toxoplasma* modifies macrophage phagosomes by secretion of a vesicular network rich in surface proteins. *J Cell Biol* 103, 867-874.
- Sibley, L.D., Niesman, I.R., Parmley, S.F., Cesbron-Delauw, M.F., 1995. Regulated secretion of multi-lamellar vesicles leads to formation of a tubulo-vesicular network in host-cell vacuoles occupied by *Toxoplasma gondii*. *J Cell Sci* 108 (Pt 4), 1669-1677.
- Slabinski, L., Jaroszewski, L., Rychlewski, L., Wilson, I.A., Lesley, S.A., Godzik, A., 2007. XtalPred: a web server for prediction of protein crystallizability. *Bioinformatics* 23, 3403-3405.
- Solenov, E., Watanabe, H., Manley, G.T., Verkman, A.S., 2004. Sevenfold-reduced osmotic water permeability in primary astrocyte cultures from AQP-4-deficient mice, measured by a fluorescence quenching method. *Am J Physiol Cell Physiol* 286, C426-432.
- Southern, T.R., Jolly, C.E., Lester, M.E., Hayman, J.R., 2007. EnP1, a microsporidian spore wall protein that enables spores to adhere to and infect host cells in vitro. *Eukaryot Cell* 6, 1354-1362.
- Studier, F.W., Moffatt, B.A., 1986. Use of bacteriophage T7 RNA polymerase to direct selective high-level expression of cloned genes. *J Mol Biol* 189, 113-130.
- Studier, F.W., 2005. Protein production by auto-induction in high density shaking cultures. *Protein Expr Purif* 41, 207-234.
- Tajkhorshid, E., Nollert, P., Jensen, M.O., Miercke, L.J., O'Connell, J., Stroud, R.M., Schulten, K., 2002. Control of the selectivity of the aquaporin water channel family by global orientational tuning. *Science* 296, 525-530.

- Takvorian, P.M., Cali, A., 1986. The ultrastructure of spores (Protozoa: Microsporida) from *Lophius americanus*, the angler fish. *J Protozool* 33, 570-575.
- Takvorian, P.M., Cali, A., 1994. Enzyme histochemical identification of the Golgi apparatus in the microsporidian, *Glugea stephani*. *J Eukaryot Microbiol* 41, 63S-64S.
- Takvorian, P.M., Cali, A., 1996. Polar tube formation and nucleoside diphosphatase activity in the microsporidian, *Glugea stephani*. *J Eukaryot Microbiol* 43, 102S-103S.
- Texier, C., Brosson, D., El Alaoui, H., Metenier, G., Vivares, C.P., 2005. Post-genomics of microsporidia, with emphasis on a model of minimal eukaryotic proteome: a review. *Folia Parasitol (Praha)* 52, 15-22.
- Thompson, J.D., Higgins, D.G., Gibson, T.J., 1994. CLUSTAL W: improving the sensitivity of progressive multiple sequence alignment through sequence weighting, position-specific gap penalties and weight matrix choice. *Nucleic Acids Res* 22, 4673-4680.
- Trinkle-Mulcahy, L., Boulon, S., Lam, Y.W., Urcia, R., Boisvert, F.M., Vandermoere, F., Morrice, N.A., Swift, S., Rothbauer, U., Leonhardt, H., Lamond, A., 2008. Identifying specific protein interaction partners using quantitative mass spectrometry and bead proteomes. *J Cell Biol* 183, 223-239.
- Undeen, A.H., 1990. A proposed mechanism for the germination of microsporidian (Protozoa: Microspora) spores. *J. Theor. Biol.* 142, 223-235.
- Undeen, A.H., Epsky., N.D., 1990. In vitro and vivo germination of *Nosema locustae* (Microspora: Nosematidae) spores. *J. Invertebr. Pathol.* 56, 371-379.
- Undeen, A.H., Vandermeer, R.K., 1994. Conversion of intrasporal trehalose into reducing sugars during germination of *Nosema algerae* (Protista: Microspora) spores - a quantitative study. *Journal of Eukaryotic Microbiology* 41.
- van Gool, T., Vetter, J.C., Weinmayr, B., Van Dam, A., Derouin, F., Dankert, J., 1997. High seroprevalence of *Encephalitozoon* species in immunocompetent subjects. *J Infect Dis* 175, 1020-1024.
- van Tuinen, E.J., 1996. Immunoelectron microscopy. *Methods Mol Biol* 53, 407-422.

- Vavra, J., Larsson, J.I.R., 1999. Structure of the Microsporidia. In: Wittner, M., Weiss, L.M. (Eds.), *The Microsporidia and Microsporidiosis*, American Society for Microbiology, Washington, D. C., pp. 7-84.
- Vavra, J., 2005. "Polar vesicles" of microsporidia are mitochondrial remnants ("mitosomes")? *Folia Parasitol (Praha)* 52, 193-195.
- Verkman, A.S., Mitra, A.K., 2000. Structure and function of aquaporin water channels. *Am J Physiol Renal Physiol* 278, F13-28.
- Visvesvara, G.S., Leitch, G.J., da Silva, A.J., Croppo, G.P., Moura, H., Wallace, S., Slemenda, S.B., Schwartz, D.A., Moss, D., Bryan, R.T., et al., 1994. Polyclonal and monoclonal antibody and PCR-amplified small-subunit rRNA identification of a microsporidian, *Encephalitozoon hellem*, isolated from an AIDS patient with disseminated infection. *J Clin Microbiol* 32, 2760-2768.
- Visvesvara, G.S., 2002. In vitro cultivation of microsporidia of clinical importance. *Clin Microbiol Rev* 15, 401-413.
- Vossbrinck, C.R., Maddox, J.V., Friedman, S., Debrunner-Vossbrinck, B.A., Woese, C.R., 1987. Ribosomal RNA sequence suggests microsporidia are extremely ancient eukaryotes. *Nature* 326, 411-414.
- Wagner, C.A., Friedrich, B., Setiawan, I., Lang, F., Broer, S., 2000. The use of *Xenopus laevis* oocytes for the functional characterization of heterologously expressed membrane proteins. *Cell Physiol Biochem* 10, 1-12.
- Wasson, K., Peper, R.L., 2000. Mammalian microsporidiosis. *Vet Pathol* 37, 113-128.
- Weber, R., Bryan, R.T., 1994. Microsporidial infections in immunodeficient and immunocompetent patients. *Clin Infect Dis* 19, 517-521.
- Weidner, E., 1972. Ultrastructural study of microsporidian invasion into cells. *Z Parasitenkd* 40, 227-242.
- Weidner, E., 1976. The microsporidian spore invasion tube. The ultrastructure, isolation, and characterization of the protein comprising the tube. *Journal of Cell Biology* 71, 23-34.
- Weidner, E., 1982. The microsporidian spore invasion tube. III. Tube extrusion and assembly. *J Cell Biol* 93, 976-979.
- Weintraub, M., Raymond, S., 1963. Antiserums Prepared With Acrylamide Gel Used As Adjuvant. *Science* 142, 1677-1678.

- Weiss, L.M., Cali, A., Levee, E., LaPlace, D., Tanowitz, H., Simon, D., Wittner, M., 1992. Diagnosis of *Encephalitozoon cuniculi* infection by western blot and the use of cross-reactive antigens for the possible detection of microsporidiosis in humans. *Am J Trop Med Hyg* 47, 456-462.
- Weiss, L.M., 2001. Microsporidia: emerging pathogenic protists. *Acta Trop* 78, 89-102.
- Williams, B.A., Hirt, R.P., Lucocq, J.M., Embley, T.M., 2002. A mitochondrial remnant in the microsporidian *Trachipleistophora hominis*. *Nature* 418, 865-869.
- Williams, B.A., Cali, A., Takvorian, P.M., Keeling, P.J., 2008. Distinct localization patterns of two putative mitochondrial proteins in the microsporidian *Encephalitozoon cuniculi*. *J Eukaryot Microbiol* 55, 131-133.
- Wittner, M., Weiss, L.M., 1999. *The Microsporidia and Microsporidiosis*. American Society for Microbiology, Washington, D. C.
- Wu, Z., Li, Y., Pan, G., Tan, X., Hu, J., Zhou, Z., Xiang, Z., 2008. Proteomic analysis of spore wall proteins and identification of two spore wall proteins from *Nosema bombycis* (Microsporidia). *Proteomics* 8, 2447-2461.
- Wu, Z., Li, Y., Pan, G., Zhou, Z., Xiang, Z., 2009. SWP25, A Novel Protein Associated with the *Nosema bombycis* Endospore. *J Eukaryot Microbiol* 56, 113-118.
- Xu, Y., Weiss, L.M., 2005. The microsporidian polar tube: a highly specialised invasion organelle. *Int J Parasitol* 35, 941-953.
- Xu, Y., Takvorian, P., Cali, A., Wang, F., Zhang, H., Orr, G., Weiss, L.M., 2006. Identification of a new spore wall protein from *Encephalitozoon cuniculi*. *Infect Immun* 74, 239-247.
- Yang, B., Verkman, A.S., 1997. Water and glycerol permeabilities of aquaporins 1-5 and MIP determined quantitatively by expression of epitope-tagged constructs in *Xenopus* oocytes. *J Biol Chem* 272, 16140-16146.
- Yang, B., 2000. The human aquaporin gene family. *Current genomics* 1, 91-102.
- Yeung, Y.G., Nieves, E., Angeletti, R.H., Stanley, E.R., 2008. Removal of detergents from protein digests for mass spectrometry analysis. *Anal Biochem* 382, 135-137.

CURRICULUM VITA

Kaya Ghosh

- 1976 Born December 16 in Charleston, West Virginia
- 1994 High School Diploma
Governor Livingston Regional High School, Berkeley Heights, NJ
- 1998 Bachelor of Arts, Biological Sciences
Cornell University, Ithaca, New York
- 1998-1999 Technician, College of Veterinary Medicine
Cornell University, Ithaca, New York
- 1999 Publication: "Dominance of immunoglobulin G2c in the
antiphosphorylcholine response of rats infected with *Trichinella
spiralis*." *Infection and Immunity* 67: 4661-4667.
- 2000-2009 Graduate Student and Teaching Assistant
Department of Biological Sciences
Rutgers University, Newark, New Jersey
- 2002 Publication: "A putative serine protease among the excretory–
secretory glycoproteins of L1 *Trichinella spiralis*." *Molecular and
Biochemical Parasitology* 122: 149-160.
- 2005 Master of Science, Biological Sciences
Rutgers University, Newark, New Jersey
- 2006 Publication: "Functional characterization of a putative aquaporin
from *Encephalitozoon cuniculi*, a microsporidia pathogenic to
humans." *International Journal for Parasitology* 36: 57-62.
- 2006 Publication: "Heterologous expression of an *Encephalitozoon
cuniculi* aquaporin in *Xenopus* oocytes". *Journal of Eukaryotic
Microbiology* 53: S72-S73.
- 2006 Publication: "Microsporidia 2006: IWOP-9."
2006. *Journal of Eukaryotic Microbiology*. 2006;53 Suppl 1:S52-4.
- 2007 Student, Biology of Parasitism Summer Course
Marine Biological Laboratory, Woods Hole, Massachusetts
- 2009 Publication: "Molecular diagnostic tests for microsporidia."
Interdisciplinary Perspectives on Infectious Diseases 2009, 926521.